

Stock defined gridshells

About the computational optimization of gridshell
structures from a finite stock



MSc Thesis by N. Heijne
29-06-2023

Delft University of Technology
Faculty of Architecture and the Built Environment

Stock defined gridshells

About the computational optimization of gridshell structures from a finite stock

Author: Nick Heijne | 5432944
First mentor: Mauro Overend | *Chair of Structural Design & Mechanics*
Second mentor: Hans Hogenboom | *Chair of Design Informatics*

Abstract

The building industry is responsible for a large amount of CO₂ emissions. With an estimated 11.7 GT in 2020, the building industry emitted 36% of the worldwide CO₂ emissions (Bertin et al., 2022). This results in the need to efficiently use the current material supply. A way to achieve this is by transitioning from a linear economy to a circular economy. Within the principles of the circular economy, materials are kept in use by creating closed loops. This results in the prevention of waste. Examples of strategies that comply with the circular economy are repairing, reusing and recycling of materials or components (Brütting et al., 2019).

Recycling of steel components has become common practice over the years. Reusing steel components is less common. Reusing structural steel components can reduce overall emissions. This is because it excludes the highly impactful manufacturing phase (Yeung et al., 2016). Structural steel is suitable for reuse because members are often connected by reversible connection principles. Additionally, the steel industry has a high level of standardization and prior to reuse the structural integrity can be easier guaranteed through testing or available certification in comparison to concrete (Fivet & Brütting, 2020). When talking about the efficient use of materials also the gridshell topology is interesting to mention. Because of the double-curvature a gridshell is able to span large areas with less structural mass (Schober, 2015). Both the use of gridshell topologies and the reuse of steel are combined in this research. The question this research tends to answer is formulated as follows:

“How can computational optimization contribute to the design of gridshell structures consisting out of a finite stock of reclaimed steel beam members with the goal to improve the eco-performance calculated in embodied greenhouse gas emissions?”

From the literature different forms of structural optimization methods were found that related to the gridshell structural topology. In the literature sizing-, shape-, and topology optimization are mentioned (Li, 2018). Sizing- and topology optimization are most relevant within the scope of this research. Within this research sizing optimization is limited to stock-constrained optimization. This form of optimization optimizes according to a finite stock. Topology optimization can be divided into rationality-based optimization and structural-based optimization. Within the research of Brütting (2020) optimization of structures out of a finite stock is conducted according to the scenarios of deconstructing and reusing steel and the new production of steel. From additional research another scenario was identified. This is a scenario where a third party or a party via a material database offers their stock. Within this research this scenario is called the stockpile scenario.

Phoenix3D is a tool that is developed from the research of Brütting (2020). This tool combines both stock-constrained optimization and structural-based topology optimization. Both the scenarios of deconstruction and new production are integrated (Warmuth, 2021). Within this research the tool Phoenix3D was tested on a gridshell topology. It can be concluded that this tool is not yet suitable for this topology. The optimization finished with an unknown error message. Both the author of this research and the developer of the tool could not resolve this issue. Apart from this error message some other flaws were identified that made the tool unsuitable. One of those flaws is that Phoenix3D only accounts for steel and excludes other materials that are relevant for a gridshell. Additionally, it is only possible to add point loads to the structural analysis. With a gridshell mostly line loads are used. Lastly, the context of the deconstruction and new production scenarios are fixed. It is therefore not possible to use the tool in a different context than the one that is integrated. The above-mentioned shortcomings made it necessary to develop the in this research designed computational tool.

In this research a computational tool is designed in the visual programming environment Grasshopper. In Grasshopper the gridshell is parametrically defined. The optimization includes an optimization algorithm, in this case Galapagos, combined with an in Python coded Best-Fit algorithm. Galapagos is able to change the topology of the gridshell where the Best-Fit algorithm assigns stock according to this topology. The Best-Fit algorithm assigns stock according to the lowest greenhouse gas emissions of each individual beam member. This computational tool is tested for different cases. Stock scenarios, stock-sizes and a

real-world case study are tested and compared. Additionally, the formulation of the tool was benchmarked against Phoenix3D by testing it on a truss topology.

Looking at the results of this tool and taking optimal reuse stock conditions into account a reduction of almost 95% is possible for the emissions of the beam members. This is by comparing a gridshell designed from a single cross-section of newly produced members to a cross-section optimized gridshell from stockpile members. Results are highly dependent on the context, but in general it can be concluded that the emissions of the beam members decrease when the reuse-rate increases. The reuse-rate increases when the size of the stock increases.

The developed computational tool also includes an estimation of the emissions for glass and nodes. From the calculation of those emissions it can be concluded that the steel beam members are not the dominant factor in terms of greenhouse gas emissions. When elaborating on the emissions of the nodes it can be seen that in some cases the emissions of the nodes tend to nullify the reduction of the emissions of the beam members. This is because an assignment of a bigger cross-section results in more mass for the node. From this conclusion the following recommendations are suggested.

It is recommended to further develop the calculation methods for greenhouse gas emissions for nodes and glass and integrate them into the optimization sequence. Additionally, it is interesting to apply the in this research-developed tool to a more steel-dominant structural topology. Also, because the optimization is dependent on the stock and therefore on the context it is interesting to try out more case-studies. This will give more body to the validation of the designed computational tool in different circumstances. Computationally, it is interesting to develop the method further by storing data externally instead of in Grasshopper. This in order to prevent the software from crashing when exiting the optimization algorithm.

This thesis document is structured as follows. In the first chapter a problem statement is formulated resulting in a research question. Then the methodology of this research is elaborated on. After this first introduction the document will proceed with a literature study. This literature study maps the current knowledge and also identifies existing knowledge gaps. Based on those knowledge gaps a computational tool is developed. In the chapter after the literature research the working of this computational tool is explained. After this the results of different tests using the newly developed computational tool are presented. This document will close off with a conclusion, recommendation, discussion and reflection.

Acknowledgment

This master thesis marks the end of an exciting and instructive two-year journey. I would like to express my gratitude and appreciation to all the individuals who helped me during the time of my thesis. Without their help, knowledge and motivational words this thesis wouldn't be what it ended up being. In particular, I want to thank my parents, friends, mentors and advisers.

Firstly, I want to thank my parents for allowing me to study at TU Delft. I want to thank them for giving me the freedom to follow my own study-path. I also want to thank them for their support along the way and for their advice from a perspective not related to the built environment.

Furthermore, I want to thank my friends for their support, inspiration and motivational words. I want to thank them for reminding me that sometimes a break from work is necessary.

Lastly, I want to thank my mentors and advisers from TU Delft as well from Octatube for guiding me through this period. I want to thank them for their great advice and constructive feedback. I also want to thank them for their flexibility when things weren't going according to plan.

Contents

Abstract	3
Acknowledgment.....	5
1. Introduction.....	9
1.1 Background.....	9
1.1.1 Gridshell structures.....	9
1.1.2 Reuse in the built-environment.....	9
1.2 Problem statement.....	9
1.3 Research questions	10
1.4 Aim and restrictions	11
1.5 Research methodology	11
2. Literature research.....	13
2.1 Gridshells classification & constraints	14
2.1.1 Classification	14
2.1.2 Classification dependent.....	15
2.1.3 Constraints.....	17
2.1.4 Conclusion	18
2.2 Structural steel reuse.....	18
2.2.1 Current bottlenecks.....	18
2.2.2 Case study.....	19
2.2.3 Structural integrity.....	20
2.2.4 Eco-impact.....	22
2.2.5 Conclusion	23
2.3 Optimization in gridshells.....	25
2.3.1 Optimization in general.....	25
2.3.2 Optimization related to gridshells.....	26
2.3.3 Grasshopper optimization algorithms.....	30
2.3.4 Conclusion	31
2.4 Knowledge gaps.....	31
2.4.1 Design focus.....	32
3. Computational optimization tool	34
3.1 Overview of the computational tool.....	35
3.1 Overview of used plugins	36
3.2 Context and constraints	36
3.2.1 Load conditions.....	36
3.2.2 Support conditions	37
3.2.3 Connections	37
3.2.4 Constraints.....	37
3.3 Definition of stock.....	38

3.4 Description of scenarios	38
3.4.1 Deconstruction	38
3.4.2 New production	38
3.4.3 Stockpile	39
3.5 GHG-calculations.....	39
3.5.1 Steel beam members.....	40
3.5.2 Nodes	41
3.5.3 Glass	42
3.5.4 Remaining output.....	43
3.6 Parametric definition gridshell.....	43
3.6.1 Basic measurements and shape.....	43
3.6.2 Bubble-packing	44
3.6.3 Delaunay triangulation	44
3.6.4 Variables optimization algorithm	45
3.7 Stock assignment and optimization algorithm.....	45
3.7.1 Basic principle Best-Fit.....	45
3.7.2 Capacity check Best-Fit.....	46
3.7.3 Optimization algorithm: Galapagos	47
3.8 Finite element analysis Karamba3D.....	48
3.8.1 First finite element analysis	48
3.8.2 Second finite element analysis	49
3.9 Multiple loops with seed addition	49
3.9.1 Adding seeds	49
3.9.2 Design explorer	50
4. Optimization results.....	51
4.1 Testing different input.....	52
4.1.1 Comparison scenarios.....	52
4.1.2 Comparison stock-sizes.....	53
4.1.3 Different transport context.....	57
4.1.4 Conclusion	57
4.2 Case-study	58
4.2.1 Description of context	58
4.2.2 Conclusion	59
4.3 Benchmarking against Phoenix3D	60
4.3.1 Testing truss structure	60
4.3.2 Conclusion	61
5. Conclusion	62
5.1 Discussion	62
5.2 Conclusion & recommendations	62

5.3 Reflection.....	64
6. Figures.....	66
7. Bibliography	68
8. Appendix	74
8.1 Reclaimed steel testing.....	74
8.2 Eco-impact calculation	76
8.3 Structural optimization.....	78
8.4 Definition of stock in Excel	80
8.5 Comparison scenarios	81
8.6 Comparison stock-sizes	102
8.7 Case-study.....	106
8.8 Benchmark Phoenix3D.....	108
8.9 Grasshopper script.....	113
8.10 Pseudocode.....	121
8.11 Visualisations gridshell	123
8.12 Overview stock assignment.....	128
8.12.1 Small stock, optimized gridshell.....	128
8.12.2 Medium stock, optimized gridshell	130
8.12.3 Large stock, optimized gridshell.....	133
8.12.4 Small stock, standard gridshell	135
8.12.5 Medium stock, standard gridshell.....	139
8.12.6 Large stock, standard gridshell	142
8.12.7 Hybrid (medium) stock, optimized gridshell (case-study).....	146
8.12.8 Benchmark Phoenix3D, optimized truss, Best-Fit formulation.....	148
8.12.9 Benchmark Phoenix3D, optimized truss, Best-Fit + Node shift.....	149

1. Introduction

1.1 Background

1.1.1 Gridshell structures

The structural topology of a (grid)shell allows for an efficient span of large areas from a material perspective. Because of the double-curvature the shell is able to transfer loads within their surface without creating a bending moment. Compared to flat structures they therefore require less structural mass. Transparency within a shell can be achieved by dividing the shell surface into members. Gridshells consisting of a single-layer also transfer the loads within the surface. This needs to be achieved without too much deflection in the members. A triangulation of the surface fits this purpose. The first known transparent shell that only transferred loads in the surface itself is the Schwedler dome on the Gasometer in Vienna (fig. 1) (Schober, 2015).



Figure 1 - Schwedler dome on the Gasometer in Vienna circa. 1896 (Schober, 2015)

1.1.2 Reuse in the built-environment

In ancient times reuse was common within masonry construction. In terms of manpower it was more efficient to reuse than to produce new building materials. Likewise, with steel, the Roman empire hardly threw away any steel. All produced steel was kept in the system by reclaiming, reusing and recycling. To reduce the cost, during the end of the 19th century, steel was manufactured with additional scrap. During the 20th century the idea of steel with additional scrap was neglected because buyers didn't like the idea of second-hand material (Addis & Addis, 2006).

1.2 Problem statement

The building industry is responsible for a large amount of CO₂ emissions. With an estimated 11.7 GT in 2020, the building industry emitted 36% of the worldwide CO₂ emissions (Bertin et al., 2022). This results in the need to efficiently use the current material supply. Within the principles of the circular economy, materials are kept in use by creating closed loops resulting in the prevention of waste. Strategies for this are repairing, reusing and recycling of members (Brütting et al., 2019). Where recycling of steel components is common practice, reusing steel components is less known. Reusing structural steel components can reduce overall emissions because it excludes the highly impactful manufacturing phase (Yeung et al., 2016).

From 1925 to 1975 shell structures were a popular structural topology made out of concrete or masonry. At this time material was more expensive than labor (Chilton & Chuang, 2017). Because of developments in digital design, digital fabrication and the demand for the reduction of material usage shell structures are again an upcoming structural topology. In particular the gridshell, existing out of members and nodes

instead of a surface (Dyvik et al., 2021). Although the gridshell is a material-efficient structural topology they are currently made out of newly produced materials instead of reused or reclaimed materials.

Structural steel is suitable for reuse because members are often reversibly connected. The steel industry also has a high level of standardization and prior to reuse the structural integrity can be easier guaranteed through testing or available certification in comparison to other building materials (Fivet & Brütting, 2020).

Currently, there are some bottlenecks regarding the reuse of building components including structural steel members. One of those bottlenecks is the lack of supply and demand (Gorgolewski, 2019). This results in scraps whereby the sizes (length and cross-section) greatly differ. To make the design of structures out of reclaimed materials even more complex is the fact that a reuse rate of 100% doesn't guarantee an optimal environmental performance (Brütting et al., 2020).

The reuse of components in new structures implies a shift in the design paradigm. Instead of manufacturing for design there needs to be designed from what is manufactured (Gorgolewski, 2008). To facilitate and ease the reuse in structural design the concept of stock-constrained optimization is introduced. Stock-constrained design is the configuration of a structure from a set of a finite amount of members. A lot of research in this area is conducted by Jan Brütting. The work is mostly focused on trusses and the designs remain fairly conceptual. Node-design and cladding-design is something that is not taken into account. It is also mentioned that more research with an existing realistic stock would contribute to validating their presented principles (Brütting et al., 2020). Additionally, the constraints that are used in this research work do not directly relate to the design of gridshell structures. Finally, it is mentioned in Brütting et al. (2019) that simultaneous optimization of topology, geometry and stock assignment could potentially lead to more optimal results. In Warmuth et al. (2021) a computational tool integrated in the visual programming software Grasshopper is introduced. Here stock is assigned by either the Best-Fit formulation or the Mixed-Integer Linear Programming (MILP) formulation. What this current tool is lacking is the freedom to change the reuse scenario and the possibility to adapt to a gridshell topology.

1.3 Research questions

Based on the problem definition stated, research questions are formulated. A main research question is formulated. The main research question is formulated as follows:

“How can computational optimization contribute to the design of gridshell structures consisting out of a finite stock of reclaimed steel beam members with the goal to improve the eco-performance calculated in embodied greenhouse gas emissions?”

To answer the main research question sub-questions are formulated. The sub-questions can be divided into research questions based on current knowledge from the literature and research questions based on the design.

The following research sub-questions are formulated and are based on existing literature:

1. How can we classify gridshell structures and what are current constraints?
 - a. What is the influence of classification on node and glass design?
 - b. What are manufacturing constraints in gridshell design?
 - c. What are mechanical constraints in gridshell design?
2. How can structural steel members be reused in new structures?
 - a. What are the current bottlenecks in the reuse of structural steel?
 - b. How can the structural integrity of reused steel members be guaranteed?
 - c. How do we calculate the embodied greenhouse gas emissions of reused structural steel members?
3. What are existing computational optimization methods used in stock-constrained design?
4. What are existing computational optimization methods used in gridshell design?

The following research sub-questions are formulated and are based on the design:

5. How do the different scenarios (new production, deconstruction and stockpile) perform in terms of greenhouse gas emissions?
6. How does the stock-size of members influence the greenhouse gas emissions of the gridshell structure?

1.4 Aim and restrictions

This research aims to propose a computational tool that can help in optimizing the assignment of reclaimed beam members to decrease embodied greenhouse gas emissions. The tool will be parametrically defined with a focus on gridshell topologies. This research is restricted to optimizing the beam members of the gridshell structure. Optimization of glass and nodes are out of the scope.

1.5 Research methodology

The first phase of the research is focused on existing literature. This research is subdivided into the general topics: reuse, optimization and gridshells. Within these different topics multiple subtopics are divided. Then again those subtopics are divided into even smaller topics. The smaller topics will help answer the questions related to the broader topic. Each topic or subtopic is related to a research sub-question (see diagram 1). Resultant of the literature research is the knowledge that can be used for the final design of an optimization tool. Examples of these resultants are as follows. Within the topic “Reuse” the resultant will be a definition of a database with available stock including necessary member properties. This also results in an assessment of the feasibility of reuse. For the topic “Optimization” the resultant will be knowledge of existing methods and their underlying theory. This can be used as the basis for the design of the computational optimization tool. Within the topic “Gridshells” the resultant will be a set of constraints that will be implemented into the computational tool.

Parallel to the literature research phase, research will be conducted into the structural context and analysis of the project C30 from Octatube. This project will be used as a starting point for the optimization tool and will help present a realistic case. From this project the structural context can be formed including load cases and supports. Documentation of the structural calculations and simulations for the above-mentioned project is provided by Octatube.

The design phase includes the design of the computational optimization tool as well as the validation of the design. First, the computational optimization tool itself will be designed. The design of the tool uses all the knowledge from previous research and will be designed in Rhino3D Grasshopper from McNeel with an integration of Python. Within the topology optimization methods for gridshells there is a clear distinction between a rationalized standardized grid and a non-standard grid. After finishing the design of the tool different tests can be conducted. Tested is the difference in stock-scenarios and stock-sizes. The tool can also be compared with the existing tool Phoenix3D.

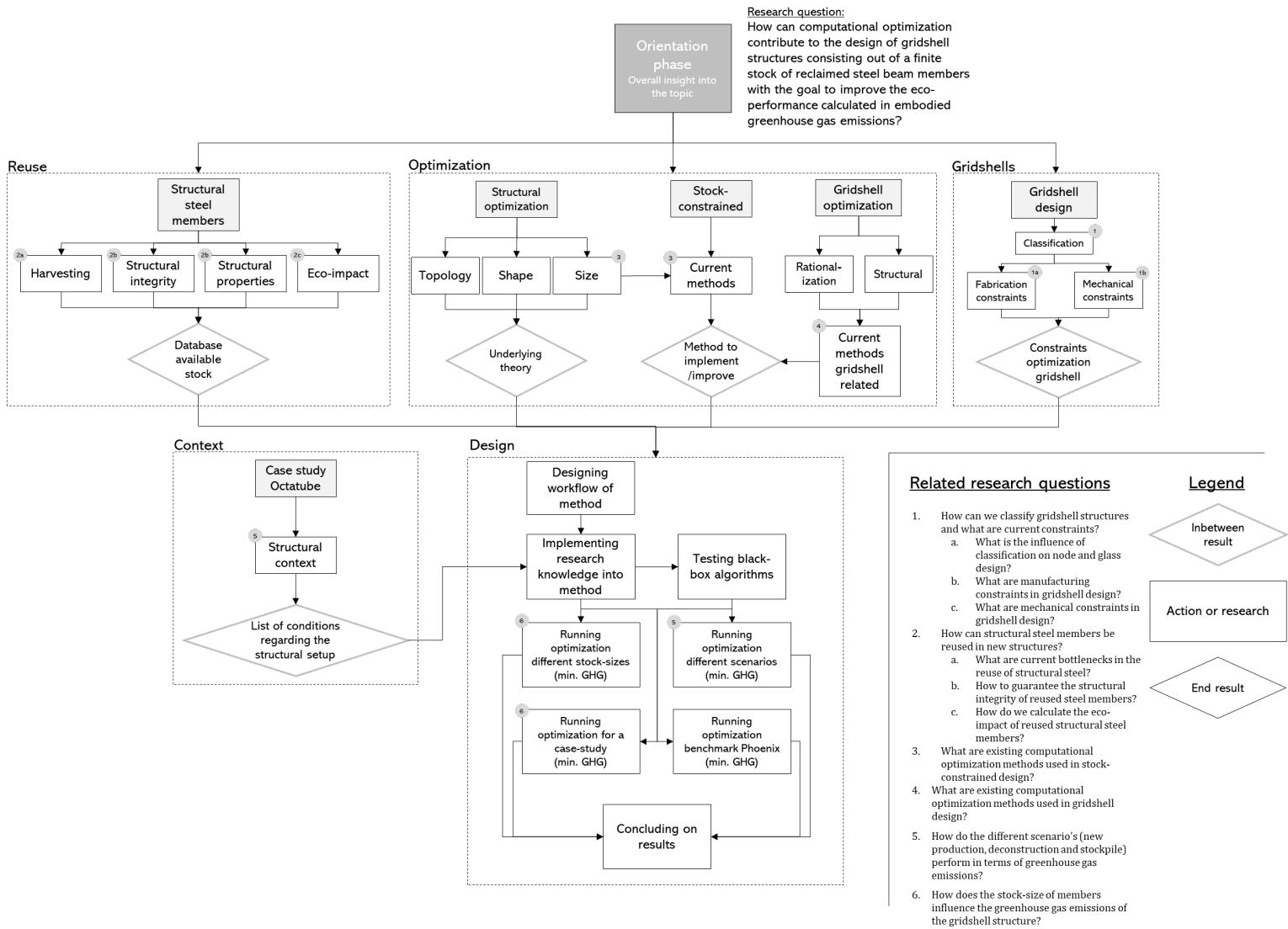


Diagram 1 – overview of the research methodology

2. Literature research

This chapter focusses on the current knowledge found in the literature. First it emphasises on the classification of gridshells and how the different elements influence each other. Secondly, reuse of steel is researched in depth. Here the current ways of providing structural integrity are presented and methods of calculating the embodied emissions in steel members is treated. The last part of this literature research is about structural optimization both in general and by taking gridshell structures into account. After the literature study the knowledge gaps are summarized and it is explained which of those are the main focus in this research.

2.1 Gridshells classification & constraints

This chapter is focused on some of the more general knowledge concerning gridshell structures. It will elaborate on the classifications of a gridshell structure as well as the constraints it has.

2.1.1 Classification

To define the influence of a gridshell topology on the design of glass and nodes first a general understanding of gridshells is needed. To get this understanding the classifications of gridshells are researched in depth. Additionally, constraints are mentioned. The constraints are related to the classification as well the node- and glass design.

Gaussian curvature

Starting with the overall shape of the gridshell. The overall shape can be determined by the Gaussian curvature. The surface is monoclastic when the Gaussian curvature equals zero (for example a cone shape), the surface is synclastic when the Gaussian curvature is larger than zero (for example an ellipsoid shape), the surface is anticlastic when the Gaussian curvature is lower than zero (for example a hyperbolic shape), and lastly, it can be a combination of the aforementioned (Gokul Santosh et al., 2022).

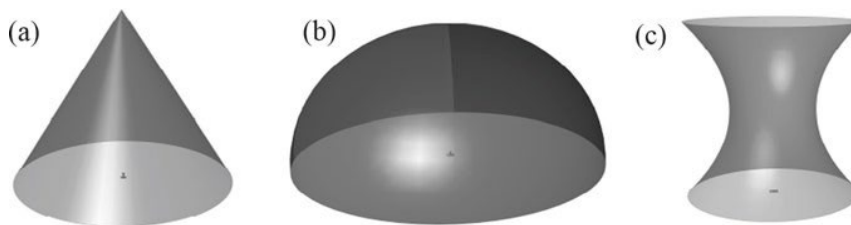


Figure 2 – a. Cone, b. Ellipsoid, c. Hyperbolic (Gokul Santosh et al., 2022)

Built-up

Another way to distinguish different types of gridshells is by the way they are built-up. The two topologies are bending active and discrete gridshells. Bending active gridshells are bent during erection and have members acting as a single element spanning the full width of the gridshell. The other topology is the discrete gridshell. Within this type the gridshell exists out of multiple (in most cases) straight members which are connected with nodes (Dyvik et al., 2021).

Grid pattern definition

How the grid pattern of a gridshell is defined can also be typical for this type of structure. There are three main definitions to distinguish (see fig. 3). First there is the diagrid definition. This pattern is built up from a sequence of two generatrix lines. Then there is the lattice shell definition. This pattern is built up by projecting a repeating pattern on a surface. Lastly, there is the geodesic dome definition. Here the surface is polyhedrally discretized (Bouleau et al., 2019). The most known grid patterns are the quadrilateral (diagrid) and the triangular (diagrid), but also the Kagome (lattice, fig. 4) grid pattern can be seen more often (Mesnil et al., 2017).



Figure 3 - diagrid, lattice and geodesic setup (Bouleau et al., 2019)

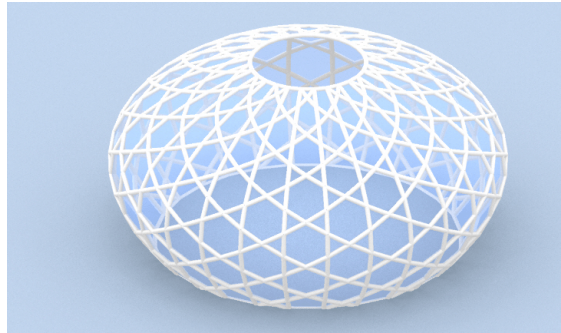


Figure 4 – example of a Kagome grid pattern (Mesnil et al., 2017)

Gridshell section

There is also a distinction to be made when looking at the cross-section of a gridshell. The cross-section of a gridshell can be subdivided into a single layer and a non-single layer cross-section. This tells if the gridshell is structurally sufficient with only one layer or if it needs additional layers to meet its structural criteria (Richardson et al., 2013). From the definition provided by Schober (2015) we only speak from a shell when the forces act within the surface only. It is therefore questionable if a gridshell with more than one layer can be called a gridshell.

Now that we have reviewed the parameters by which gridshell structures can be classified, it is also interesting for the proceedings of this research to know how these parameters influence the design of glass and nodes.

2.1.2 Classification dependent

Apart from the members a discrete gridshell also consists of cladding material (in most cases glass) and nodes. The two elements are influenced by the classifications mentioned above. One of them is the node design. It needs to be mentioned that here we refer to an individual node in a discrete gridshell as described in Dyvik et al. (2021). Also, the glass design is of importance in the design of a (transparent) gridshell structure.

Node design

A node within a gridshell is required to have certain structural properties. When forces act in-plane the node should be able to transfer axial forces. In case of a non-rigid grid pattern it should be able to transfer in-plane shear forces. When forces act out-of-plane the node should be able to transfer bending moments, contain sufficient stiffness and be able to transfer out-of-plane shear forces (van der Linden, 2015).

While the topology of the gridshell influences the design of the nodes in turn the nodes influence the overall structural capacity of the gridshell. Mostly the joint stiffness is of influence. Feng et al. (2011) concluded that the ultimate bearing capacity of a gridshell with fully rigid joints is greater than one with in-plane pin and out-plane rigid joints.

The design of the node is as mentioned above dependent on the needed stiffness of the connection between members. Apart from the stiffness the topology also influences the node design. First of all the node is influenced by the grid pattern. For example, when applying a regular quadrilateral grid pattern the members meet at the node from four sides, in comparison to six sides with a triangular grid pattern (see also fig. 5). The amount of Gaussian curvature in the overall shape also influences the node. The Gaussian curvature determines the angle at which the members will meet at the node (Stephan et al., 2004).

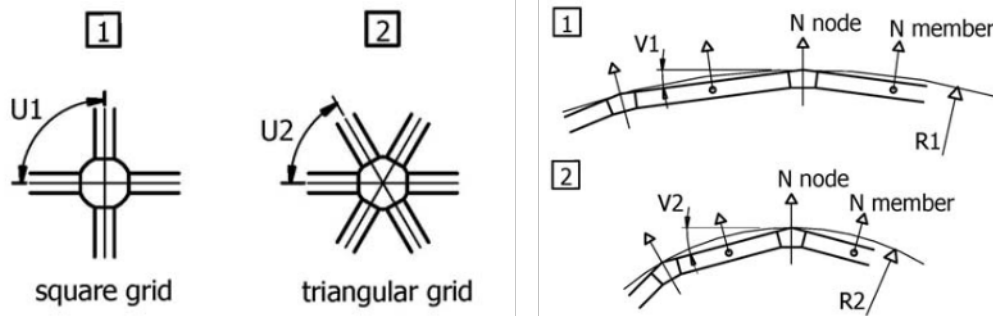


Figure 5 – influence of gridshell topology on node design (Stephan et al., 2004)

Also, the cross-section of the gridshell makes a difference in node design. According to Stephan (2022) from Novum Structures, a contractor specializing in gridshell structures, a single-layer gridshell can be divided into splice plate nodes and end-face nodes. The splice plate node is cut in at the ends of the member and is then connected to the nodes. The end-face nodes meet the member end face to end face. For a double layered gridshell a spatial node is used. With this node members can meet not only in-plane but also out of plane (see also fig. 6).

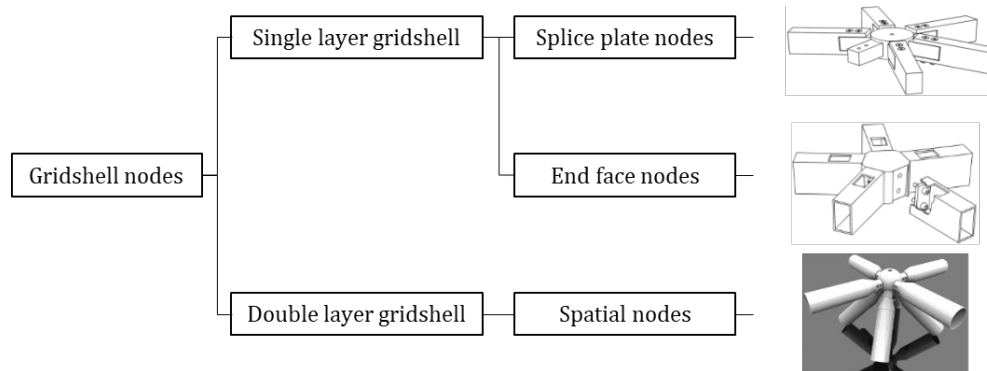


Figure 6 – different node options (Stephan, 2022)

Another way of solving the node connection is by welding. An example of this can be seen in the C30 gridshell from the company Octatube (2021). In this particular example they welded full-length ladder frames. This resulted in the assembly of viewer individual members compared to the node member principle mentioned above.

Apart from the more 'regular' ways of solving the connection between members a relatively new way is introduced with the advancements in additive manufacturing. The company Jansen (*Study Jansen VISS³, n.d.*) introduced a free-form self-supporting façade. Their VISS profiles are combined with 3D-printed steel nodes (see fig. 7). Because every node allows for the connection of members from different angles a high level of form freedom is achieved.



Figure 7 – steel printed node combined with the VISS profiles (*Study Jansen VISS³, n.d.*)

Glass design

The glass design is mostly dependent on the grid pattern. Some examples where the grid pattern defines the glass geometry can be seen in projects C30 by Octatube, the atrium roof for ETH Zurich by RUCH Metallbau and the Glass Roof Dutch Maritime Museum by NEY+partners.



Figure 8 – examples of gridshells following the gridpattern, sources: Octatube, n.d., NEY+partners, n.d., AURA Foto Film Verlag, 2022

The normal size of a glass pane is 2,5 by 3,6-meters. From this size the glass is cut into the sizes that are needed (Franco, 2022). Cutting of glass starts from this standardized size. The cutting efficiency is dependent on the geometry that needs to be cut. An efficient cutting pattern results in the reduction of waste.

It is possible to cold and hot bend glass for gridshells. Within the context of this research the scope is limited to the use of straight glass panes. This limitation is justified by the reuse of straight members in the gridshell.

2.1.3 Constraints

Optimization in structural design is often neglected. The reason for this is the complexity of generated designs resulting in a lack of manufacturability. Therefore it is important to not only take the mechanical constraints into account but also the fabrication constraints (Mesnil et al., 2017).

Mechanical constraints

Examples of mechanical constraints that are used in gridshell design are mass constraints, displacement of members and/or cladding, strength constraints (often checked by utilization) and stability constraints (Gythiel & Schevenels, 2022). It is also mentioned that a torsion-free beam layout is important (Mesnil et al., 2017). When designing a gridshell where the member-to-member connection is fixed, the mechanical constraints for the nodes also play a major role.

Fabrication constraints

Fabrication constraints of a gridshell are mostly related to the manufacturability of the glass. According to internal documentation from Octatube (received 7-4-2023) the maximum sizes and the width-to-length ratio are both dependent on the glass thickness. In general, it can be said that the more thickness the glass has the bigger the maximum sizes can be. For heat-strengthened as well tempered glass a minimum size of 200-mm by 300-mm is taken into account. The maximum sizes are dependent on the thickness but are independent of the heat treatment of the glass. Also, the nodes bring some fabrication constraints. Where the type of node is chosen according to the type of gridshell that is designed. It can be concluded that there is a limit on the capacity of the node to connect a certain amount of members.

2.1.4 Conclusion

Classifying a gridshell can be done by the amount of Gaussian curvature of the overall shape, how the gridshell is built-up, the way the grid pattern is defined and if the gridshell is single-layered or not.

Node- and glass design are both influenced by the different parameters that define the classification of the gridshell. The node within the gridshell influences the overall structural capacity of the gridshell (Feng et al., 2011) and should be structurally sufficient (van der Linden, 2015). The Gaussian curvature and the grid pattern influence the node design (Stephan et al., 2004). Different node designs exist for double-layered and single-layered gridshells (Stephan, 2022). The glass design is mostly influenced by the Gaussian curvature and the grid pattern. Different case studies show different glass geometries that follow the pattern of the grid (see fig. 8).

Important constraints that need to be taken into account in gridshell design are mechanical- and fabrication constraints (Mesnil et al., 2017). Examples of mechanical constraints are mass constraints, displacement of members and/or cladding, strength constraints (often checked by utilization) and stability constraints (Gythiel & Schevenels, 2022). An example of a manufacturing constraint is the maximum sizes and minimum corner angles in which standard glass panels can be cut.

2.2 Structural steel reuse

When looking at the distribution of structural mass in the built environment the current stock consists mostly of concrete, brick masonry and steel. Within a circular built environment buildings that reach their end-of-life phase need to be seen as material banks rather than newly generated material waste (Hopkinson et al., 2019). This brings the opportunity to dismantle and reuse. Although this sounds theoretically promising some barriers need to be overcome. This will be elaborated on further in this chapter.

Different strategies exist for the reuse of structural components. The following pathways are proposed by Brütting et al. (2019):

- At the existing site, reuse and renovation of the building structure;
- At a new site, reuse the whole system for the same purpose;
- At a new site, reuse the whole system for different purposes;
- At a new site, reuse of individual components for the same purpose;
- At a new site, reuse individual components for different purposes.

2.2.1 Current bottlenecks

Because the reuse of structural components is a relatively new practice there are currently some bottlenecks that need to be overcome. One of them is the lack of dismantlability in current buildings. This is the reason why the reuse of structural steel components is favored. Steel is often assembled with reversible connections (Fivet & Brütting, 2020; Iacovidou & Purnell 2016). Another barrier is the fact that it is hard to coordinate demand and supply. Reclaimed materials do not show up at the right time in the right amount or size. Additionally, there is a lack of certainty of structural characteristics compared to newly produced structural components. Another bottleneck is the additional time needed within the design process. Opportunities need to be taken when new components become available. This can result in late changes to the design. What also adds time to the design process is the gathering of information

about the availability of components. Lastly, there are the additional labor costs for the increased time in the design process as well as the time needed for deconstruction (Gorgolewski, 2019).

Something that could solve some of the above-mentioned bottlenecks is more insight into the material flow within the built environment. Madaster (2022) is a company that makes it possible to map this kind of information. On their platform, the user gets the possibility to create a material passport of a building. This helps gather information about the used products and their materialization. This also includes information about the level of circularity, the embodied environmental impact and the end-of-life value. Although a lot of information is gathered now, this information isn't publicly available yet. The company is looking for ways to make this information available without violating their user's privacy (S. Beeks, personal communication, 5 December 2022).

Apart from Madaster there are also platforms for the Dutch market that try to bring supply and demand together. Examples are: [matchingmaterials.com](https://www.matchingmaterials.com), marktplaats.insert.nl and www.oogstkaart.nl. When searching on those platforms (search executed on the 13th of December, 2022) the bottleneck of a lack in supply and demand can be identified. Also by looking beyond the scope of the Dutch market it is hard to find sufficient stock. Summum Engineering (n.d.) is trying to overcome this problem by configuring stock by scalping multiple databases or marketplaces. Although this could solve part of the problem it is still not sufficient in the context of this project. When looking at the current supply on individual inventories, it mostly consists of HEA and IPE steel profiles. A gridshell structure would be the chosen typology for a designer because of its transparency and minimized structural mass. The found profiles in their available sizes would be too big to achieve this. Further research resulted in finding stock beyond the building industry. This stock has its origin from the oil and gas industry. By a proof of concept this stock concluded to be suitable for building industry purposes. The next chapter shows an example of this.

2.2.2 Case study

The case study that is known for its successful reuse practice is the London Olympic Stadium. The reused steel in this project was provided by the company Cleveland Steel & Tubes Ltd. In the roof structure a total of 3,850 tonnes of steel was used whereby 2,500 tonnes (65%) consisted of surplus steel. The steel is predominantly recovered from steel mills and the oil and gas industry (Cleveland Steel & Tubes Ltd, 2022).



Figure 9 – the roof trusses of the stadium made out of reused steel (International Olympic Committee, 2013)

Additionally, the company Cleveland Steel & Tubes Ltd. has an available online stocklist. In this stocklist they distinguish certified and uncertified stock. Uncertified stock is stock where there was once a certificate, but where the certificate is not traceable anymore. With the certified stock an up-to-date certificate is available. All stock is in between the lengths of 4,5-m up to 15-m. The uncertified stock consists of circular hollow sections ranging from a diameter of 13-mm up to 2170-mm with wall thicknesses ranging from 2-mm up to 184-mm. In this case no steel grade is specified because of the lack of certification. The certified stock consists of circular hollow sections ranging from a diameter of 27-mm up to 2300-mm with a wall thickness ranging from 2,5-mm up to 50,8-mm. A lot of different grades are available. The European grades that are available are S185, S235, S275, S355, S420 and S460.

2.2.3 Structural integrity

As mentioned in the previous chapter the stock of reused steel exists out of certified supply as well as uncertified supply. With the certified stock there is no problem with reusing it. The uncertified stock therefore needs to be tested to guarantee its structural integrity. This chapter focusses on this testing procedure.

Testing

In the report ‘European Recommendations for Reuse of Steel Products in Single-Storey buildings’ by Girao Coelho et al. (2020) a full procedure is described. The full protocol is described in a diagram which can be found in Appendix ‘8.1 Reclaimed steel testing’. First, there is an overall audit and assessment of the building. After this there is a more in dept reliability assessment. Based on the class (see below) material testing is conducted. Lastly, based on the future scenario the steel will be directly reused or be stored for future use. The classes that are described in the report are A, B and C and are defined as follows.

- Class A: the most reliable class as it meets the needed performance requirements and the original certificates are available;
- Class B: the steel members meet the needed performance requirements based on comprehensive material testing (destructive and non-destructive) and are recertified by the European Product Standards;
- Class C: in principle, the most unreliable class as the steel is assigned with the most conservative grade based on age (at least >1970) and location of the building, is visually inspected for damage and defects, can only be used for non-safety critical structures.

For class C there is no testing procedure only the visual inspection takes place. For class A it can be optional to perform some non-destructive testing to confirm material properties mentioned on the certificates. For class B there is non-destructive testing and destructive testing. It is possible to use steel members without CE-certificate (Conformité Européenne), but here the structural engineer is responsible for determining the mechanical properties (den Hollander, 2018). This could also be done through destructive and non-destructive testing. The destructive tests can be performed on a sample that can represent a batch. A batch of members is formed according to the size and profile type. Examples of non-destructive testing are hardness testing, positive metal identification, instrumented indentation testing and small punch testing. Examples of destructive testing are tensile testing, chemical composition analysis, charpy impact test and metallography. For the full description of these testing procedures see Appendix ‘8.1 Reclaimed steel testing’ in figure 46. The mechanical properties that need to be determined according to the EN 1090-2 are strength (yield strength and tensile strength), elongation and heat treatment delivery conditions (Girao Coelho et al., 2020).

Estimating mechanical properties

Fujita and Kuki (2016) presented a method to determine mechanical properties such as tensile strength, yield strength and elongation based on the Vickers hardness. The flow of the estimation of mechanical properties from the Vickers hardness is illustrated in figure 10.

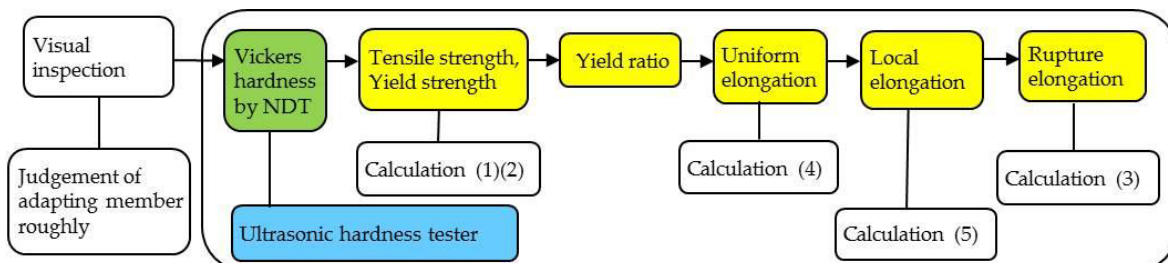


Figure 10 – the process of estimation of mechanical properties (Fujita & Kuki, 2016)

The following equations illustrated in the diagram above are used to estimate the mechanical properties.

$$T_s = 2.5 * H_v + 100$$

(1)

$$Y_s = 2.736 * H_v - 70.5 \quad (2)$$

$$\varepsilon_f = \varepsilon_u + \varepsilon_n \quad (3)$$

$$\varepsilon_u = k \left(1 - \frac{Y_s}{T_s} \right) = k(1 - Y_R) \quad (4)$$

$$\varepsilon_n = \gamma \frac{\sqrt{A_0}}{L_0} \quad (5)$$

With:

T_s = tensile strength

Y_s = yield strength

H_v = Vickers hardness

ε_f = rupture elongation

ε_u = uniform elongation

ε_n = local elongation

k = correction factor (0,6 is used in reference)

γ = coefficient indicating local elongation (0,7)

A_0 = cross-sectional area

L_0 = gauge length

Equations were later verified by applying them to a reuse case. This method is currently used to estimate the mechanical properties. The authors mention that when more data is stored in a database it will be easier to estimate the mechanical properties in the near future by statistical analysis.

Additional recommendations

The Dutch steel industry also did research into the possibilities of reusing steel (den Hollander, 2018). Their most important recommendation is that reused steel should only be used in buildings with the consequence class CC1 or CC2a. The consequence class describes the impact in case of collapse. With class CC1 the impact of the loss of life is small and economic and social consequences are negligible. Examples of class CC1 are industrial buildings with a maximum of three stories and a small capacity, greenhouses and single-family houses with a maximum of four stories. With class CC2 the impact of the loss of life is medium and economic and social consequences are considerable. Examples of class CC2 are hospitals, stores, school buildings, parking garages, public buildings and single-family houses with more than four stories. CC2a is focussed on a low-risk group, examples of these are single-family houses of more than four stories, hotels and office buildings with a maximum of four stories, school buildings with a maximum of one story, stores with a maximum of two stories, public buildings with a maximum of 2000-m² per story, industrial buildings with a maximum of two stories and parking garages with a maximum of two stories. Lastly, there is also consequence class CC3, examples of this class are: buildings with a height of >70-m, buildings with a span of >50-m, stadiums, stations, concert halls, hospitals of more than four stories, industries with dangerous chemicals and nuclear power plants. Within this class the Dutch steel industry doesn't recommend the reuse of steel.

Recommendations given by the Dutch steel industry seem to be quite conservative when taking the case study of the London Olympic Stadium into account. This case study includes a stadium and would therefore be of the class CC3. Reused steel is still used in the roof.

2.2.4 Eco-impact

The ecological impact (eco-impact) can be used to validate the use of reused members. This impact can be calculated by calculating the embodied emissions in materials or products. In this chapter a way of calculating embodied greenhouse gas emissions is illustrated.

Overview of phases

Before the processes of reusing steel can be calculated in the embodied emissions the individual phases need to be known. Yeung et al. (2016) mapped the full process of reusing as well recycling of steel products. The mapping is according to the principles of the Life Cycle assessment. In their conducted research only the downstream processes are taken into account. For example, the process of producing diesel isn't taken into account, but the burning of diesel during deconstruction is. The diagram describing the full process with all the necessary phases can be found in Appendix '8.2 Eco-impact calculation' in figure 47. Some processes are unique for each scenario (recycling or reusing). Recycling includes demolition, sorting, removal, shredding and the phases needed to reprocess the steel. Reusing includes the phases of deconstruction, transportation of reused members and cleaning.

In the case study from Colabella et al. (2017) a bending active gridshells was designed and constructed from reusing discarded skies. One of their conclusions was that the transportation phase was of major importance for the overall impact of the structure. This is endorsed in the study conducted by Brütting et al. (2020). This study is a more conceptual case but researched the influence of different phases in depth. Here it is mentioned that when a material is sourced at a distance larger than 2000-km the reuse rate drops below 50% and thus reusing members isn't clearly beneficial.

GHG calculation

In Brütting et al. (2020) a method is used to calculate the eco-impact in terms of embodied greenhouse gas (GHG) emissions. This is expressed in the units $\text{kgCO}_{2\text{eq}}$. For this method different GHG emission coefficients are calculated for every relevant phase. GHG emission coefficients are calculated with the use of the Life Cycle Assessment method.

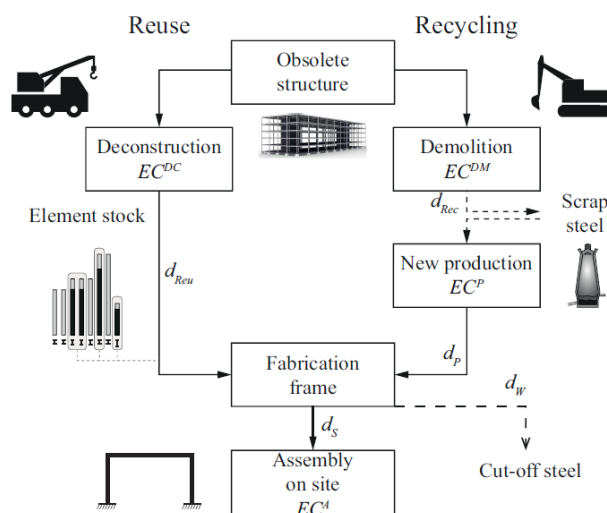


Figure 11 – phases taken into account for the calculation of GHG (Brütting, Senatore, et al., 2020)

The scenarios that are used are the reuse of structural members and the production of new structural members from recycled content. For the full breakdown of the calculation (see Appendix '8.2 Eco-impact calculation').

In Warmuth et al. (2021) an integrated stock-constrained optimization tool is developed (see '2.3.2 Optimization related to gridshells'). Here a simplified formula is used. The formula is based on the values provided by Brütting, Senatore, et al. (2020). This equation is formulated as follows:

$$GHG_{Total} = \frac{0,3546kgCO_{2eq}}{kg} * M_{Stock} + \frac{0,11kgCO_{2eq}}{kg} * M_{Reuse} + \frac{0,8973kgCO_{2eq}}{kg} * M_{New} \quad (6)$$

The values are derived from Brütting, Senatore, et al. (2020). The fixed values are derived with the following equations:

$$0,3546 = EC^{DC} + EC^T * d_{Reu} \quad (7)$$

$$0,11 = EC^A + EC^T * d_s \quad (8)$$

$$0,8973 = EC^{DM} + EC^P + EC^A + EC^T * (d_{Rec} + d_p + d_s + d_w) \quad (9)$$

EC are the embodied greenhouse gas emissions coefficients in $kgCO_{2eq}$, whereby EC^{DC} for deconstruction, EC^A for assembly, EC^{DM} for demolition, EC^P for production and EC^T for transport. d is the transport distance in kilometers, whereby d_{Reu} the distance between deconstructed building and the fabrication facility, d_s the distance between the fabrication facility and the building site, d_{Rec} the distance between deconstructed building and the recycling facility, d_p the distance between the production facility and fabrication facility and d_w the distance that needs to be traveled to get rid of cut-off waste. In the equation, M_{Stock} is used for the mass of the stock before it is cut. M_{Reuse} is the mass of the members eventually reused in the structure. Lastly, M_{New} is the mass of the members from the new production. It can be observed that the fixed values in the equation also represent the distances, which could be different depending on a different context.



Figure 12 – Phoenix3D components defining the stock (Warmuth et al., 2021)

Within the Phoenix3D tool reused stock can be defined with the component as shown in figure 12. The stock can be defined by materialization, cross-section, length, the number of elements, if it can be cut or not and a name to tag the elements. Where this calculation probably takes less computation time, it doesn't allow for other scenarios. This is different from what is explained in Brütting, Senatore, et al. (2020).

2.2.5 Conclusion

Within the reuse realm of the building industry five ways of reusing are identified by Brütting et al. (2019):

- At the existing site, reuse and renovation of the building structure;
- At a new site, reuse the whole system for the same purpose;
- At a new site, reuse the whole system for different purposes;
- At a new site, reuse of individual components for the same purpose;
- At a new site, reuse individual components for different purposes.

In this research the focus will be on reuse at a new site for the same (deconstruction) and for a different purpose (stockpile).

The bottleneck in the reuse of building components is the lack of supply and demand (Gorgolewski, 2019). When looking at existing databases such as [matchingmaterials.com](https://www.matchingmaterials.com), marktplaats.insert.nl and www.oogstkaart.nl, next to no stock could be identified (apart from the fact that the found stock doesn't necessarily apply to gridshell structures). The case study of the London Olympic Stadium shows that building component stock doesn't need to be harvested from actual buildings (Cleveland Steel & Tubes Ltd, 2022).

Another important aspect of reusing structural members is guaranteeing their structural integrity. Different testing protocols are defined by Girao Coelho et al. (2020). Also, a more theoretical method to make estimations of mechanical properties for reused steel is proposed by Fujita and Kuki (2016).

A calculation method to calculate the embodied greenhouse gas emissions for reused steel members is also needed. This defines if the reuse of steel members is actually beneficial. A calculation method is proposed by Brütting et al. (2020) based on Life Cycle Assessment. This same method is integrated into the stock-constrained optimization tool Phoenix3D (Warmuth et al., 2021).

2.3 Optimization in gridshells

This chapter will focus on the optimization part. First, it will describe some of the more general theory of optimization. Then it will focus more on optimization within gridshell structures.

2.3.1 Optimization in general

Structural systems can be divided into two classes based on their response to loading conditions. The classes can be described as form-active and form-passive. When the structure actively adjusts its shape in reaction to the performed loads it is called a form-active structural system. When this is not the case the structural system is called form-passive. Examples of form-active systems are: hanging-, tension- and pneumatic structures. The shell, or rigid gridshell as described by Dyvik et al. (2021), is an example of a form-passive structure (Li, 2018). In the context of this research the focus will be on form-passive structural systems.

For finding the most efficient structural form two approaches exist. The first approach is with the use of physical models. Physical models were mainly used at a time computers weren't commonly used in form-finding practice. Physical models can be divided into hanging models, tension models and pneumatic models (Li et al., 2017). The other approach to finding the most efficient structural form is by numerical analysis methods. Numerical analysis methods can be divided into the categories: stiffness matrix method, geometric stiffness method and dynamic equilibrium method (Adriaenssens et al., 2014). Within the scope of this research the focus is on numerical method approaches. In the upcoming chapter this method will be further elaborated on.

The general formulation of a basic optimization problem is written as follows:

$$\begin{aligned} & \text{minimize}_x && f(x) \\ & \text{subject to} && x \in X \end{aligned}$$

Where x is a variable that influences the design and the objective f within the feasible region of X . In this example $f(x)$ can be minimized or maximized depending on the formulated problem. Another important part of the formulation of an optimization problem is the set of constraints. The constraints define what solutions are possible and valid. The set of constraints defines the region of feasibility in X (Kochenderfer & Wheeler, 2019). Examples of constraints in structural design are mass, strength, stability and deformation (Gythiel & Schevenels, 2022).

Finite element methods are widely used in the engineering field to analyze static structures. With this general numerical approach partial differential equations can be solved (Lyu, 2022). The body of a structure first needs to be discretized into simple-shaped elements. In 2D problems triangle and quadrilateral shapes are mostly used. In 3D cases hexahedral or tetrahedral shapes are often used (Burczyński et al., 2020). The equilibrium equation used in finite element methods can be written as: $\{f\} = [K] * \{q\}$. Whereby the nodal forces are f , K is the stiffness matrix and where q the nodal displacement represents (Andriotis, 2022).

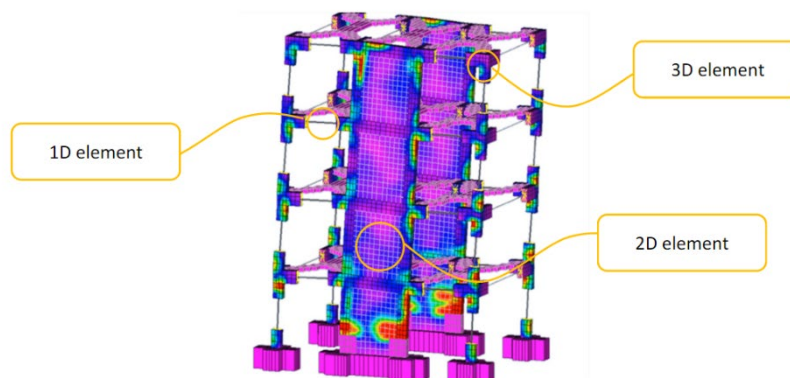


Figure 13 – examples of 1D, 2D and 3D elements in a structure (Andriotis, 2022)

Different finite element software exists. One of them is Karamba3D. This software is integrated into the visual programming environment of Grasshopper in Rhino3D. With this integration it is possible to combine parametric modelling and existing optimization algorithms with finite element analysis (Karamba3D, 2016).

Optimization of structures can be divided into the optimization of sizing, shape and topology (see fig. 13). Size optimization is about finding the optimal cross-section and dimensions. Shape optimization is about the overall shape of the structure and can be performed by setting boundary conditions for maximum or minimum overall sizes. In the context of gridshells this method is also described as form-finding (Schober, 2015). Topology optimization focuses on the spatial order and connectivity of members. Some of the topology optimization methods include shape optimization by restricting the structural modification to the existing boundaries defined within the design context (Huang & Xie, 2010). In the following sections those different levels of focus will be elaborated on. Shape and topology optimization are further investigated taking the context of this research into account. This means that here the application to (grid)shells is included. Size optimization is further investigated within the context of this research by emphasizing stock-constrained optimization.

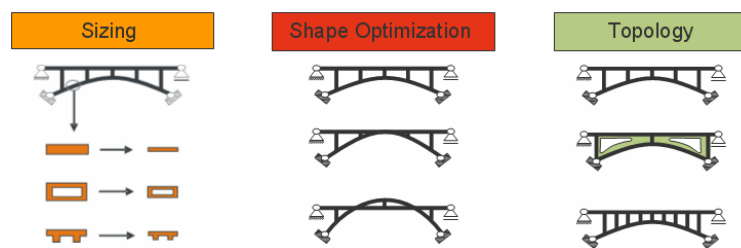


Figure 13 - examples of sizing, shape and topology optimization (Li, 2018)

2.3.2 Optimization related to gridshells

Shape optimization

Optimization of shape in the context of gridshells is also referred to as form-finding. Current form-finding methods can be subdivided into three main families according to Veenendaal and Block (2012):

- Stiffness matrix methods, this method is based on standard geometric stiffness and elasticity matrices;
- Geometric stiffness methods, this method is material independent and only uses geometric stiffness;
- Dynamic equilibrium methods, this method is solved through dynamic equilibrium arriving at an equivalent of static equilibrium.

Adriaenssens et al. (2014) describes the parts that are always present in a form-finding procedure. One of those parts is the discretization of the geometry of the structure. Another part is a data structure that stores information about the form, the connectivity of the discrete elements and the forces within the structure. Additionally, there needs to be an equilibrium equation to describe the relationship between internal and external forces. Lastly, the form-finding procedure needs a solver. This solver is needed to solve the equilibrium equation.

The decision to choose one form-finding method over another relies on the level of knowledge about the overall shape and materiality of the structure. When a lot about the structure is unknown it is better to apply a geometric stiffness method. When materiality and the general shape of the structure are known dynamic equilibrium methods are more applicable (Adriaenssens et al., 2014).

Although the above-mentioned form-finding methods are widely used it also needs to be mentioned that they have shortcomings when used for gridshells. First of all the methods mentioned do not include complex behaviour of material such as buckling. Secondly, form-finding methods do not include complex objective functions and constraints such as manufacturing constraints. Thirdly, the optimization is based

on a single load case. Lastly, the resultant optimized structure works in compression or tension only (Gythiel & Schevenels, 2022; Rombouts et al., 2019).

Topology optimization

Topology optimization in the context of gridshells is described as the connectivity between nodes and members (Gythiel & Schevenels, 2022). As mentioned earlier, topology optimization methods can also include the optimization of shape, also known as form-finding (Bendsøe et al., 2013 in Oval et al., 2019).

The distinguishment of different topological methods is less defined in the literature compared to the shape optimization methods. Within the context of gridshells two main focus areas were found. One of them is the structural-based topology optimization method. In this case the result is a structurally efficient gridshell. The other one is the more rationality-based topology optimization method. In this case the result is a gridshell pattern with optimized similarity/singularity and least geometrical distortions. In Appendix '8.3 Structural optimization' a diagram sorting the different sources is illustrated.

A method that is mentioned in structural-based topology optimization research is the “ground structure method” (Gythiel & Schevenels, 2022; Jiang et al., 2017; Richardson et al., 2013). With the ground structure method the entire design space is covered with potential nodes and bars. Optimization happens by excluding members with low utilization. This method can also be combined with node-shifting. Here the nodes can move to generate different structural topologies. With node-shifting a general problem is that nodes tend to move to the same locations. This results in irrational designs (He & Gilbert, 2015). This could be tackled by limiting the movement of the nodes, merging nodes when they tend to move too close to each other or in the case of gridshells specifically, by setting a deflection limit to the glass (Gythiel & Schevenels, 2022). From the resultant grid patterns presented in the research it can be concluded that different levels of complexity are possible (fig. 14).

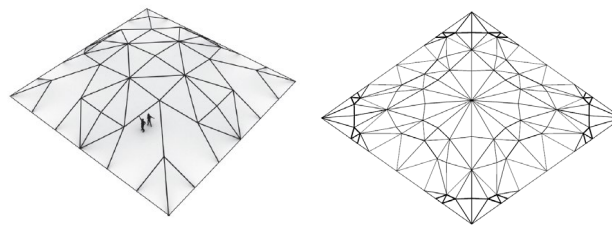


Figure 14 – difference in complexity, (L) Richardson et al., 2013 and (R) Gythiel & Schevenels, 2022

A method that is mentioned in rationality-based topology optimization research is the “bubble-packing method” (Li et al., 2022; Wang et al., 2019; Wang, Gao & Wu, 2019; Ye et al., 2021). The bubble-packing method works by creating “bubbles” on a set of randomly placed points. Overlap of bubbles creates an internal force within the bubbles. By moving the points resulting in a change of the internal forces within the bubble an equilibrium can be reached. Equilibrium will result in equally distributed points on a surface. With the points a Voronoi diagram can be projected on the surface and the surface mesh can be generated by using the Delaunay triangulation method (fig. 15). The Delaunay triangulation method is a robust way of creating a reasonable triangulation out of a set of random points. The method overcomes small triangle corner angles. With this method a point can never be in the circumcircle of any generated triangle (Wolfram Research, Inc., n.d.).

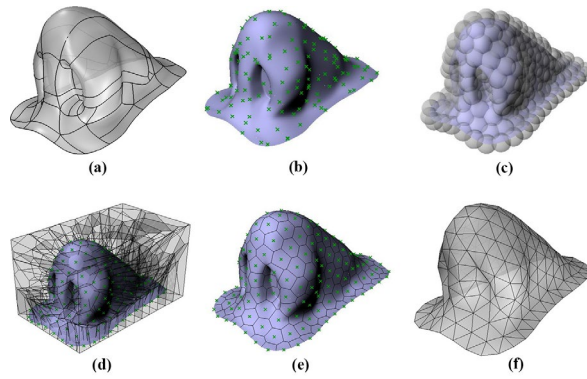


Figure 15 – (a) initial surface, (b) random points, (c) bubble-packing equilibrium, (d) 3D Voronoi, (e) 2D Voronoi projection, (f) Delaunay triangulation (Wang, Gao & Wu, 2019)

Size optimization

Within the context of this research size optimization is limited to stock-constrained design optimization. The definition of stock-constrained design optimization within a structural context is best described as an approach where: “structure topology and geometry must be designed to make best use of available stock elements” (Warmuth et al., 2021 pp. 1). On the one hand existing stock must be assigned at the right place in the structure and on the other hand the topology of the overall structure must allow the right assignment. This interaction happens within the boundaries of the set constraints.

Conducted research within stock-constrained design shows different approaches. The distinguishment of those different approaches is based on the configuration of the stock. In Kovacs et al. (2017) the stock exists of an infinite amount of standardized elements. The design space is efficiently filled with standardized elements (in this case bottles) which are limited in structural capacity. Another approach can be found in von Buelow et al. (2018), Clifford et al. (2018), Allner et al. (2019) and Brütting, Senatore, et al. (2021). In this research the stock is finite and the structure is based on this finite stock. A bigger stock size will result in more possibilities for the configuration of the structure. The third approach can be found in Brütting et al. (2021), Warmuth et al. (2021) and Marshall et al. (2020). Here the stock is finite and insufficient. By combining new and reused members a hybrid structure can be configured. The gap that is left is filled up with new members with a theoretical infinite length. This last-mentioned approach seems the most promising for a real-world application. Here the design is not completely dependent on the available stock. Insufficient reused stock can always be replaced by newly produced elements. When the stock size is sufficient designs can still be generated with a high reuse rate.

In the research conducted by Warmuth et al. (2021) a computational tool for stock-constrained design is developed. This tool operates in the visual programming environment Grasshopper within Rhino3D (see fig. 16). For the assignment problem two approaches are mentioned: “Mixed Integer Linear Programming” and “Best-Fit heuristic”. Using a MILP algorithm is beneficial because it can reach a global optimality (Wolsey & Nemhauser, 1999). The downside from this is that when a complex problem needs to be solved a lot of computation time may be needed (Warmuth et al., 2021). The opposite of this approach is the Best-Fit heuristic algorithm. The approach of a heuristic algorithm is different because instead of finding the global optimal solution it tries to approximate it (Pearl, 1984). This reduces the computation time at the expense of perfection. In the context of the computational tool designed by Warmuth et al. (2021), the Best-Fit heuristic approach doesn’t consider topology optimization, service limit states and deformation limits. The MILP approach does take those aspects into account. The Best-Fit approach only considers the capacity of the members.

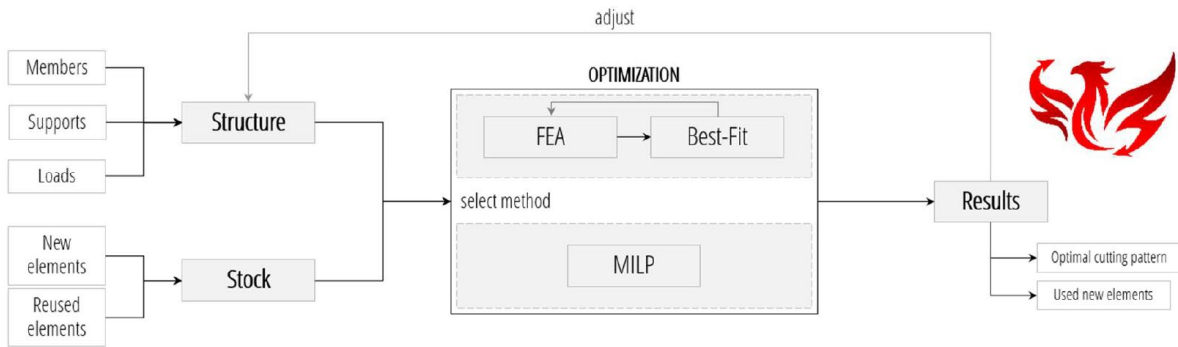


Figure 16 - workflow of the stock-constrained design optimization tool (Warmuth et al., 2021)

Although it is specifically mentioned that Phoenix3D is developed to optimize truss structures it is in this research still tested for use on gridshell topologies. During the integration of the Phoenix3D tool, some major flaws were found related to the gridshell topology. One of those flaws is the fact that this tool only takes steel (or wood) into account. Therefore it is not possible to also include limitations for glass. Another flaw is that only point loads can be used at member intersections. This makes it impossible to simulate a line load. A line load is most commonly used in the case of a gridshell topology. Although the mentioned flaws are of major impact the tool seems to be completely unworkable with gridshell topologies because of an unknown error message after running an optimization (see fig. 17). For this error message the developer of the tool was contacted (J. Warmuth, e-mail, 24 April 2023), unfortunately the developer as well the author weren't able to fix this error message.

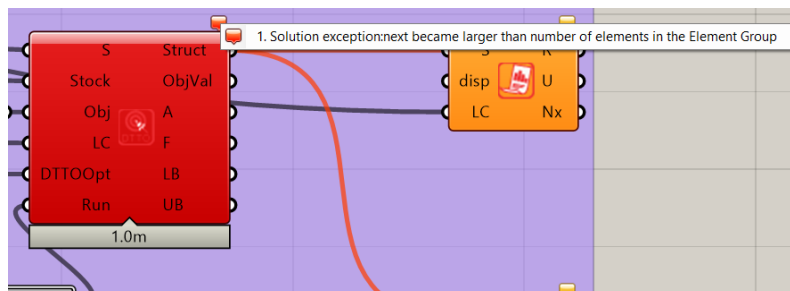


Figure 17 – error message when testing a gridshell topology

In the research conducted by Bukauskas et al. (2017) new computational strategies are tested for the assignment of a finite set of members with diverse geometries and properties. Within this research not only Best-Fit formulations are tested but also First-Fit formulations. The difference between those two strategies is that the First-Fit strategy places the member in the first “bin” that fits, whereby the Best-Fit strategy places the member into the “bin” that will result in the best objective. Apart from testing the difference in Best-Fit and First-Fit algorithms the researcher also proposes different methods of sorting the members and bins. The members in this context is the existing stock. The bins are the members that are used for the initial design of the truss. All strategies can be found in ‘8.3 Structural optimization’. According to the results the strategies BFDE(L), BF(L) and FFDE were performing best (see table 1). The objective of the tests was bins used, items remaining and the waste length.

Table 1 – best-performing strategies

Abbreviation	Type	Member strategy	Bin strategy
BFDE(L)	Best-Fit	Pre-sorting members on effect (decreasing resistance to tension/compression)	Minimizing remaining length
BF(L)	Best-Fit	No member strategy	Minimizing remaining length
FFDE	First-Fit	Pre-sorting members on effect (decreasing resistance to tension/compression)	No bin strategy

Combination of levels

Combining different levels is important for a good optimization process. When there is no combination of size (SO) and topology optimization (TO) Grande et al. (2018) suggests combining them with form-finding (FF). Within this research a mixed SO/TO approach is suggested (see fig. 18).

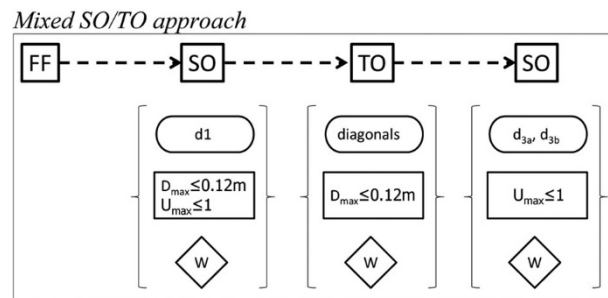


Figure 18 – approach that is suggested by Grande et al. (2018)

The objective of all the phases in this approach is minimizing the weight. The first phase of the approach is the FF-phase. Here dynamic relaxation is used followed by the first SO-phase. Within the SO-phase the full structure is optimized with a single-diameter cross-section. Utilization and deflection are used as constraints. Then there is the TO-phase which includes removing diagonals in the grid (ground structure method). Only deflection is used as a constraint. Finally, there is the second SO-phase. Here different cross-sections can be assigned. Here the constraint is the utilization of the members.

The research conducted by Grande et al. (2018) illustrates a promising approach regarding the combination of different levels. It needs to be mentioned that a predefined grid pattern is used. This means that the translation from the FF-phase to the first SO-phase is much easier. Additionally, the TO-phase is restricted by the first initiated grid pattern.

2.3.3 Grasshopper optimization algorithms

Because optimization in architectural design is getting more common more Grasshopper-integrated optimization algorithms are developed. In architectural design optimization the common optimization problem is the simulation-based problem. The relationship between variables and performance isn't defined by a mathematical function rather it is defined by evaluating a parametric model with simulation (Wortmann, 2018).

The optimization algorithms can be divided into three groups: direct search, metaheuristics and model-based methods. The direct search method evaluates in a deterministic sequence. The model-based method makes use of surrogate models to guide the search space. Metaheuristic algorithms rely on natural processes instead of mathematical proofs of convergence (Wortmann, 2018).

Different benchmarking studies are conducted for certain problems solved with optimization algorithms (Wortmann et al., 2017; Wortmann, 2018). It is concluded to use direct search when the set of variables is not too large. Additionally, it is suggested to use different approaches because of the dependency of the problem. This phenomenon is endorsed by the *no free lunch theorem*. This theorem states that if an algorithm performs well at solving a certain problem it will perform worse at another problem. Therefore, there isn't something as a best-performing optimization algorithm (Wolpert & Macready, 1997 in Kochenderfer & Wheeler, 2019).

Optimization algorithms in Grasshopper

Because further research will be conducted with the use of the software Grasshopper in Rhino3D the possible optimization algorithms are limited to the ones that are integrated into this software. In Ekici (2022) a mapping of different optimization solvers is made. This mapping includes the solvers: Galapagos, Goat, Silvereye, Opossum, Dodo, Nelder-Mead and their own developed Optimus. The table below summarizes the available optimization algorithms. This summary is made with the sources: Cichocka et al., (2017), Wortmann et al., (2017), Wortmann (2018), Waibel et al., (2019), Ekici (2022) and McNeel Europe, (n.d.).

Grasshopper plug-in	Library/Source code	Algorithm	Solver type
Galapagos	Galapagos	GA/SA	Metaheuristic
Goat	NLOpt	DIRECT	Direct search
SilEye	PSO	SilEye (PSO)	Metaheuristic
Opossum	RBFOpt library	RBFOpt	Model-based
Dodo	NLOpt	Various possibilities	N/A
Nelder-Mead	N/A	Nelder-Mead	Direct search
Optimus	N/A	jEDE	Metaheuristic

For the creation of data loops in Grasshopper plugins such as Anemone (2022) are needed. An often discussed topic within the Grasshopper community is triggering optimization algorithms in combination with looping data. One of the reasons why you want to do this is because you can feed output data back into the script. Coding an optimization algorithm with the so-called Framework for Optimization in Grasshopper (FrOG) it is possible to integrate a trigger (Wortmann, 2017). Experienced knowledge in coding is needed to develop such an algorithm. Unfortunately, most of the existing optimization algorithms lack the mentioned option to trigger an optimization sequence (Rutten, 2019).

2.3.4 Conclusion

With the optimization of structures different levels of focus exist. There is topology-, size- and shape optimization (Li, 2018). In the context of gridshells shape optimization is often called form-finding (Veenendaal and Block, 2012). In the context of gridshells topology optimization can be divided into rationalization-based and structural-based optimization. Size optimization in the context of this research is named stock-constrained optimization. An assignment optimization tool is developed by Warmuth et al., (2021). Within this tool a MILP formulation and a Best-Fit formulation are proposed.

It is advised to combine the different levels of focus in an optimization process. The advised approach introduced by Grande et al. (2018), uses the different levels of focus with different constraints. In their example they introduce the size optimization twice. Both with a different set of constraints. The downside of this method is that a predefined grid pattern is used which results in less freedom for the topology optimization phase.

In architectural design optimization algorithms are often used (Wortmann, 2018). Different types of algorithms are benchmarked. It is still advised to try different algorithms because they can function differently based on the proposed problem (Wortmann et al., 2017; Wortmann, 2018; Wolpert & Macready, 1997 in Kochenderfer & Wheeler, 2019).

2.4 Knowledge gaps

As it is described by Gorgolewski, (2019), a current bottleneck for reuse in the built environment is the uncertainty of material supply. Currently, some online material databases and marketplaces try to bring supply and demand together (matchingmaterials.com, marktplaats.insert.nl and www.oogstkaart.nl). Those databases/marketplaces aren't intensively used and the supply is relatively low. For example, during a search for structural steel profiles (executed on the 13th of December, 2022) the results were not more than 20 profiles. Thereby, the profiles that were found consisted of mostly HEA- and IPE-profiles. Within the context of gridshells those profiles are in most cases too bulky and therefore not suitable.

In Fivet and Brütting, (2020) it is described that the current LCA (Life Cycle Analysis) methods calculate the life-cycle impact of a product within certain boundaries. Products that are designed to be reused aren't integrated into this method. LCA methods calculate the impact during the manufacturing phase of a product. Reuse is about avoiding the manufacturing phase. Currently, there are no methods to predict the reuse potential of a certain product. Therefore it is hard to calculate the actual impact of a product designed for reuse.

The current tool for the optimization of structures made from a finite stock of members is Phoenix3D. This tool is developed by Warmuth et al. (2021) and uses the research conducted by Brütting et al. (2020) as the theoretical foundation. Within the tool it is possible to optimize structures by minimizing the greenhouse gas (GHG) emissions as an objective. The total GHG emissions are calculated with a relatively simple equation that includes some fixed values. The fixed values are calculated by adding all GHG emission coefficients relevant to the phase. Interestingly the transport distance is also taken as a fixed value instead of a variable, even though it is clearly stated in Brütting, Vandervaeren, et al. (2020) that the travel distance can highly impact the intention to reuse. Phoenix3D doesn't allow for other reuse scenarios than the one described in Brütting, Senatore, et al. (2020).

The case studies (Brütting, Ohlbrock, et al., 2021; Brütting, Senatore, et al., 2020; Brütting, Vandervaeren, et al., 2020; Warmuth et al., 2021) related to the developed methods in stock-constrained design optimization are mostly based on truss structures. For the implementation in gridshells this means a different approach. Different constraints need to be taken into account. An example of this is that none of the case studies accounted for cladding. Also, the constraints differ taking the characteristics of the site into account. The approach of topology optimization could also be different compared to the implementation of truss designs. Additionally, it is concluded that the developed tool Phoenix3D doesn't work in combination with gridshell topologies.

It is already mentioned that there is currently no relation between stock-constrained design optimization and gridshells. Therefore it is also unknown what type of gridshell could perform better in terms of GHG emissions. Two types of topology gridshell optimization approaches were identified being structural- and rationality-based. Were the structural topology optimization results in often complex designs (Gythiel & Schevenels, 2022), its freedom in design could possibly lead to better-performing structures in terms of GHG emissions. To confirm this, this should be tested.

In the literature it lacks a clear overview or extensive mapping of different topology optimization methods related to gridshells. Within this literature study, in a short amount of time, a relatively general literature search was conducted. This resulted in identifying different approaches for topology optimization. Because of the limited amount of time it is therefore uncertain if all methods were identified.

As stated in the literature (Wortmann et al., 2017; Wortmann, 2018; Wolpert & Macready, 1997 in Kochenderfer & Wheeler, 2019) certain algorithms are suitable for certain problems. Therefore it is currently not possible to tell what optimization algorithm should be used. Figure 19 illustrates the mentioned knowledge gaps.

2.4.1 Design focus

From this literature research a computational tool is developed that will focus on some of the mentioned knowledge gaps. First of all it will tackle the problem of small stock sizes from different locations by integrating the option to optimize with a versatile stock composition. Additionally, the in this research developed tool will be designed in such a way that it can comply with gridshell topologies, something that Phoenix3D is currently lagging. By making the script completely parametric it will be possible to compare different types of grid configurations. In the following chapters the computational tool and the produced results will be elaborated on.

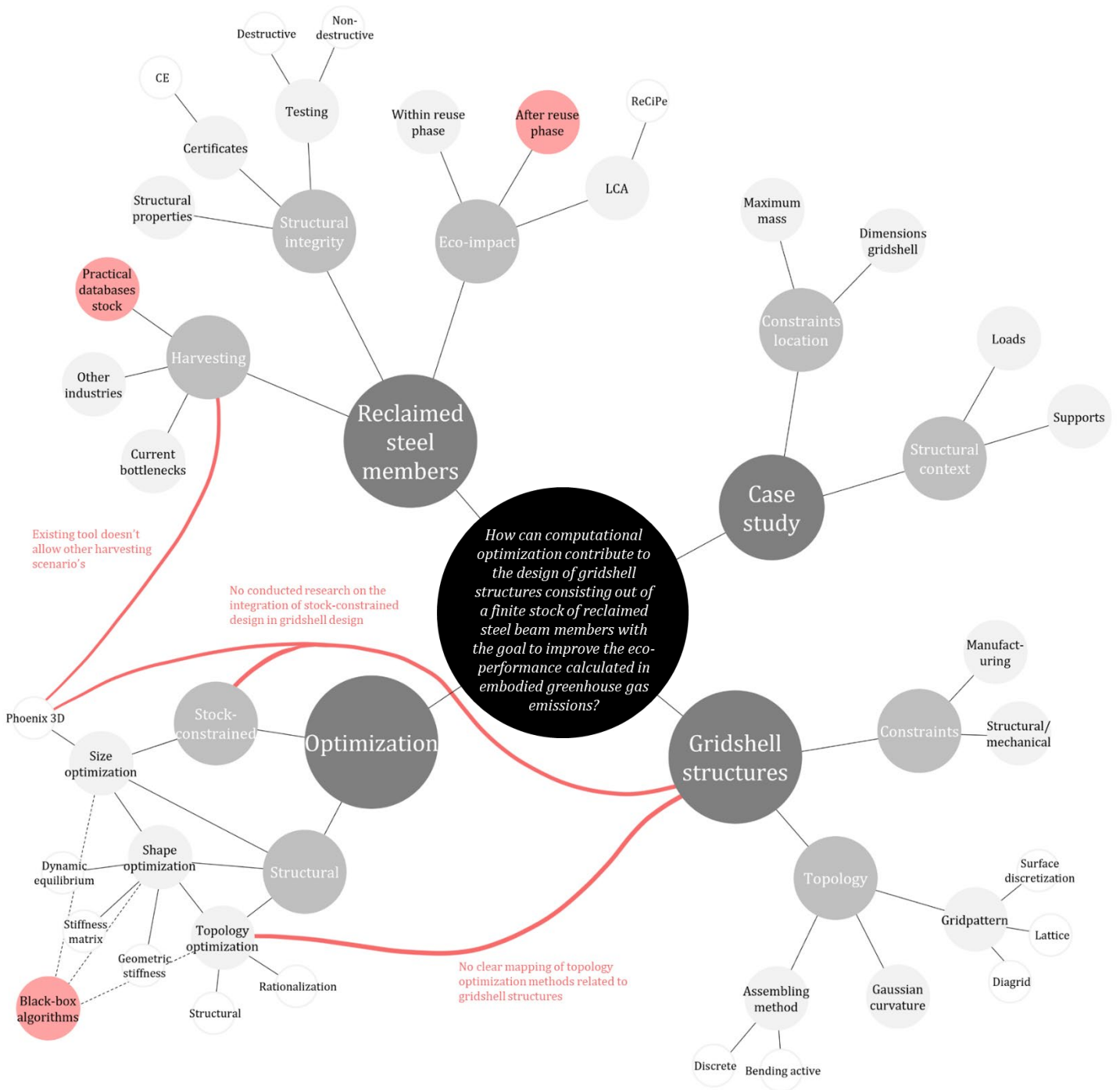


Figure 19 - the knowledge gaps that were found according the literature research

3. Computational optimization tool

This chapter is dedicated to the computational optimization tool that is designed according to the literature and current knowledge. Within this chapter an overview of the developed computational tool will be elaborated on. The build-up of the computational tool will be explained containing the constraints, load conditions and supports. Furthermore, the calculation of greenhouse gas emissions for beam members, nodes and glass will be elaborated on. After this the parametric definition and the optimization algorithms will be treated.

3.1 Overview of the computational tool

Based on the literature a computational tool is designed. This tool is used to optimize gridshell structures in terms of greenhouse gas emissions by assigning reused stock as efficiently as possible. The following scheme (diagram 2) gives an overview of the developed computational tool. The most important steps within the computational tool are highlighted in the scheme and contain the following processes:

1. In the first step a bubble packing method is used to evenly distribute the nodes over a triangular surface (1/8th of the full gridshell). The bubble packing method is mainly used to start the optimization within a reasonable boundary regarding the geometry for glass manufacturing.
2. The generated nodes in the first step are projected on a surface and the Delaunay triangulation method is used to create a triangular mesh. With the use of an optimization algorithm the nodes on the surface can be shifted. During the shifting of the nodes the sizes of the generated triangles are checked. When they comply the geometry goes through. When the triangles are too big the loop will add a node. This happens the other way around when the triangles are too small.
3. In the third step a finite element analysis will be executed by the Grasshopper-integrated software Karamba3D. According to the forces calculated in this process stock will be assigned by a Best-Fit algorithm. This algorithm uses the kgCO_{2eq} (greenhouse gas emissions) as the objective.
4. From the third step a stock-assigned structure will be the resultant. This structure will be checked on some additional constraints. Those constraints are displacement of beams and glass, utilization of beams and glass, uniformity of the structure and the minimum angle of the triangles. When the structure complies with those constraints the objective in terms of kgCO_{2eq} will be calculated. When the structure doesn't comply with the constraints it will receive a penalty value for the objective in terms of kgCO_{2eq}. In this way the optimization algorithm knows between which boundaries the most optimal objective will be resultant. All results that comply with the constraints will be recorded. In this way not only the most optimal result is saved, but also the steps leading towards it. This also makes it possible the use different randomized seeds for generating the structure.

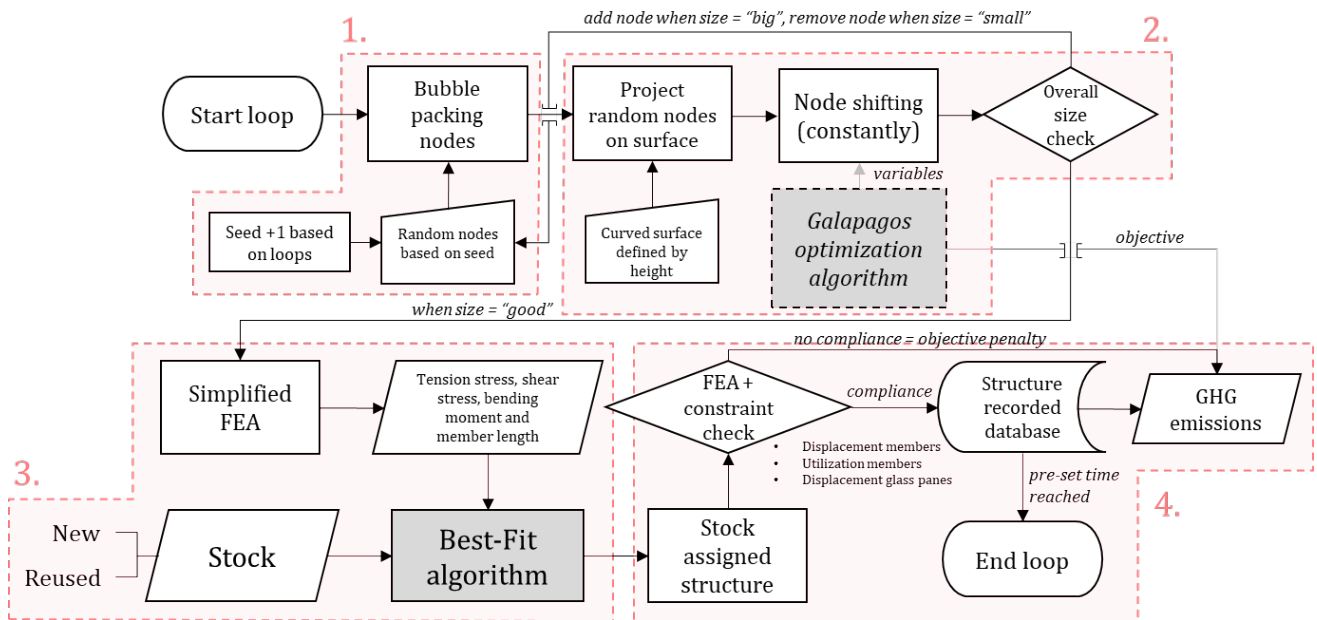


Diagram 2 – overview of the in this research developed tool

The members of the gridshell are the main focus of this research. To see how they perform within the bigger picture an estimation is made for the glass and the nodes. Within the computational tool the members are first assigned and based on this the emissions for nodes and glass are calculated. In the following chapters a more detailed description of constraints, context and definition of input will be covered. For the total insights of the Grasshopper script see Appendix '8.9 Grasshopper script'.

3.1.1 Overview of used plugins

Within the visual programming environment Grasshopper it is possible to use developed plugins. Within the design of the computational tool a couple of plugins are used (see fig. 21). The following plugins are used:

- OpenNest, this plugin is used for determining the cutting pattern of the glass. From this an estimation is made of how much gross glass is needed to cut out the triangulated panes;
- Python, this is used to code within the Grasshopper environment. The Best-Fit algorithm is coded with this language and also data is processed with Python;
- Karamba3D, this plugin is used to perform finite element analysis. In chapter '3.8 Finite element analysis Karamba3D' this is elaborated on;
- Kangaroo, this is a plugin that has a lot of different purposes. In this case Kangaroo is used to perform a bubble-packing sequence. See also chapter '3.6.2 Bubble-packing';
- Anemone, this is a plugin that is used for creating loops of data within Grasshopper. In this case it is used to loop the output data from the stock assignment of the Best-Fit algorithm back into the script.

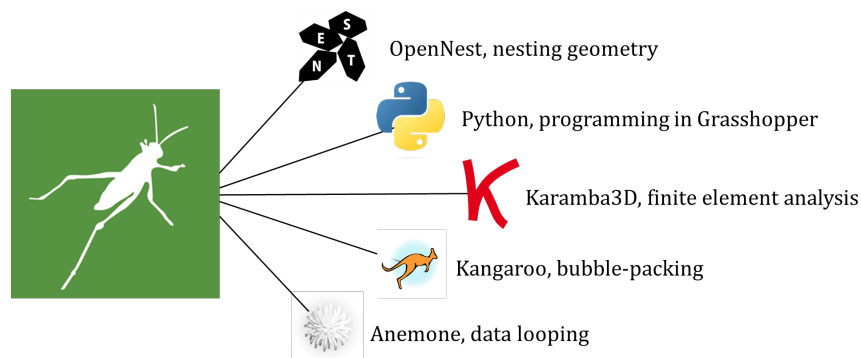


Figure 21 – plugins used in Grasshopper

3.2 Context and constraints

In this chapter the focus will be on the context and the constraints that are integrated into the developed tool. It is mostly related to the structural analysis of the tool.

3.2.1 Load conditions

Within the computational tool a total of four potential load cases are integrated. The load cases are based on Ultimate Limit State design. The load cases are formulated as follows:

- $LC1 = 1.2 * F_{weight} + 1.5 * F_{snow}$
- $LC2 = 1.2 * F_{weight} + 1.5 * F_{maintenance}$
- $LC3 = 1.2 * (F_{weight} + F_{maintenance} + F_{suction})$
- $LC4 = 1.2 * F_{weight} + 1.5 * F_{suction}$

Hereby is F_{weight} based on laminated glass that is built up from two 6-mm heat-strengthened panes and one 8-mm fully tempered pane. This makes the total thickness of the glass 20-mm. Glass has a density of 2500 kg/m^3 and this makes the weight of the glass $0,5 \text{ kN/m}^2$. The weight of the steel is excluded in the load cases because the finite element analysis software Karamba3D takes this into account. For the snow load F_{snow} a value of $0,56 \text{ kN/m}^2$ is used. This value is derived from a simplified calculation. In this case the equation of undrifted snow load is used. This equation is stated as $s = \mu_i * c_e * c_t * s_k$, for the shape coefficient μ_i a value of 0,8 is used, for both the exposure coefficient c_e and the thermal coefficient c_t a value of 1,0 is used and lastly, for the gross snow load a value of $0,7 \text{ kN/m}^2$ is used (NEN-EN 1991-1-3+C1+A1:2019 Nl, 2019). For $F_{maintenance}$ a distributed load of $0,4 \text{ kN/m}^2$ is used and for $F_{suction}$ a distributed load of $-0,4 \text{ kN/m}^2$ is used. Both of the mentioned values are based on the guidelines provided by Oikonomopoulou (2021).

For the glass the load conditions are in kN/m^2 as mentioned above. For the beams this value is converted to a uniformly increasing line load towards the center in kN/m (see fig. 23). The conversion from distributed load to line load is calculated by multiplying the distributed load times the distance between the midpoint of the concerned triangle and the midpoint at the edge of the triangle (see fig. 22).

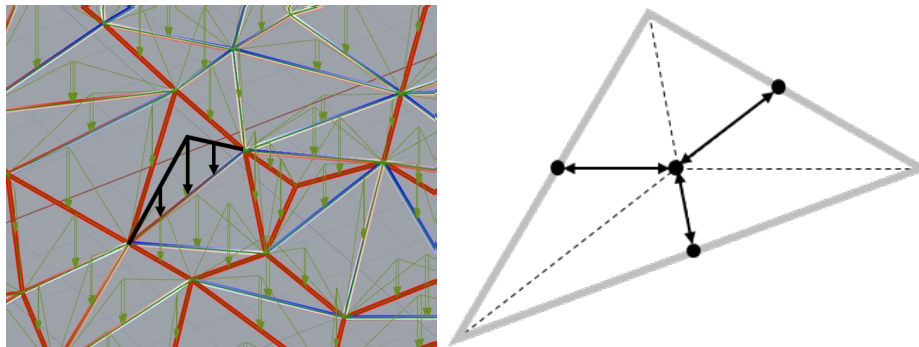


Figure 23 - in green the line load as illustrated by Karamba3D
 Figure 22 - calculation of the highest load in the line load

3.2.2 Support conditions

In figure 24 the free movement of the supports of the gridshell structure is illustrated. All supports are fixed in the Z-axis. When gridshells are placed on top of existing facades (for example the C30 shell by Octatube and the Glass Roof Dutch Maritime Museum by NEY + partners) no bearing forces perpendicular to the existing façade are allowed. For this reason forces in the axis perpendicular to the façade are not supported.

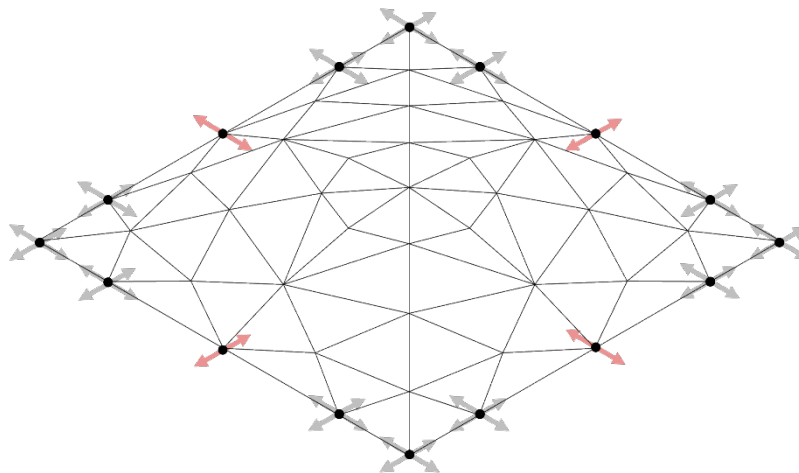


Figure 24 - free movement of the supports in the gridshell structure

3.2.3 Connections

The connection between members is designed as a fixed connection. Because the gridshell is triangulated it is not self-evident that all connections need to be fixed. In terms of reusability the author is aware that this is not beneficial within the context of a circular strategy. This decision is therefore mainly motivated by employing simplification and the reduction of computation time. Optimization of joint types is out of the scope of this research.

3.2.4 Constraints

To end up with valid designs some constraints for beams and glass are integrated. The utilization of both glass and beams are calculated in the finite element analysis software Karamba3D. Within Karamba3D the utilization of the beams is based on axial forces, shear forces and bending moments. To meet the criteria the utilization of beams and glass should be below 100%.

Beams and glass are also checked on the maximum allowed deflection. Within Karamba3D for each individual beam the maximum deflection is calculated. The deflection of the beams meet the criteria when $w_{max} < \frac{L}{250}$, where L is the span of each structural member. For the glass there are two deflection checks. With the use of Karamba3D the maximum deflection in the center of the glass and the maximum deflection at the longest length of the edge of the glass are calculated. The deflection of the glass meets the criteria when for the midpoint $u_{dia,max} \leq \frac{L_{dia}}{65} \leq 50$, where L_{dia} the largest diagonal of the glass represents. For the deflection at the longest edge of the glass the following equation applies $u_{max} \leq \frac{L_z}{100}$, where L_z the length of the longest edge represents.

Additionally, the constraints regarding the manufacturing of glass are taken into account. The sizes of the triangulated glass panes are checked on the maximum and minimum manufacturable glass sizes. For the maximum and minimum manufacturing sizes documentation from Octatube is used. The maximum size for x and y (see fig. 25) is based on 6-mm heat-strengthened glass and can be of a maximum of 5000-mm by 2700-mm. The minimum sizes are based on fully tempered 8-mm glass (*Min Max Size Guide | Oakland Glass, 2016*) and need to be a minimum of 250-mm by 100-mm.

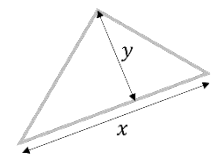


Figure 25 – x and y of the triangles

It needs to be noted that within the workflow of the computational tool the maximum sizes of the glass will not be reached since the glass is also checked for its maximum utilization and deflection. Sizes that do not comply with the manufacturing constraints in most cases also do not comply with the constraints in terms of utilization and deflection.

3.3 Definition of stock

The stock is based on the stocklist published by the company Cleveland Steel & Tubes Ltd. (2022). This stocklist contains circular hollow section (CHS) steel profiles. The stocklist contains both certified and uncertified stock. The certified stock includes the steel grade. For this research only the certified stock is taken into account. Additionally, the stock is further filtered by only using steel grades S235, S275 and S355. The diameter of the stock ranges from 34-mm up to 2300-mm. It is chosen to limit the diameter of the used stock to a maximum of 219-mm. It is stated that the stock is kept in random lengths ranging from 4,5-m up to 15-m. For an overview of the stock see '8.5 Comparison scenarios'. It is chosen that within this research the newly produced members are also based on the available stock presented in this stocklist.

In this research-developed computational tool the occurring forces are calculated and beam members from stock are assigned based on the capacity of this stock member. Therefore it would also be possible to integrate profiles differing from the CHS profiles used in this research.

3.4 Description of scenarios

Within this research three different scenarios are identified that go by the name deconstruction-, stockpile- and new production scenario. Both the deconstruction and the new production scenario are based on the scenarios presented by Brütting et al. (2020). The stockpile scenario is newly introduced and derives from the literature study. The three scenarios mentioned relate to the beam members only.

3.4.1 Deconstruction

The deconstruction scenario starts with an obsolete building. Beam members in the building need to be deconstructed first. Afterwards, those beam members are transported to a fabrication workshop. In the fabrication workshop beam members can be pre-assembled into bigger prefabricated parts of the gridshell. Then those prefabricated parts are transported to the site where they are assembled. From the workshop the cut-off steel waste is transported to a scrapyards.

3.4.2 New production

The new production scenario is based on production from recycled content. New produced beam members are transported to the fabrication workshop and pre-assembled into prefabricated parts. Then

those prefabricated parts are transported to the site where they are assembled. Because the new beam members are produced in the needed lengths no cut-off waste will be generated.

3.4.3 Stockpile

According to the literature there is another scenario that isn't mentioned in the research conducted by Brütting et al. (2020). This scenario is called the stockpile scenario. In this scenario there is a third party that harvests reused beam members or offers reused beam members through an existing online database. Within this scenario the beam members are cut at the location of the third party, where it is assumed that the cut-off waste can still be used for new customers. The needed steel will be transported to the fabrication workshop and pre-assembled into prefabricated parts. Similar to the other two scenarios the prefabricated parts are transported to the site where they are assembled.

In figure 26 a diagram illustrates all phases that are taken into account in the three different scenarios. This diagram also illustrates where the boundary of calculated emissions is drawn. The calculations do not take the lifecycle of the beam members before ending in a stockpile into account neither is the new production phase of beam members calculated before they ended up in the obsolete building. Calculation of the emissions is kept within those boundaries. Phases that fall out of those boundaries are not within the scope of this research.

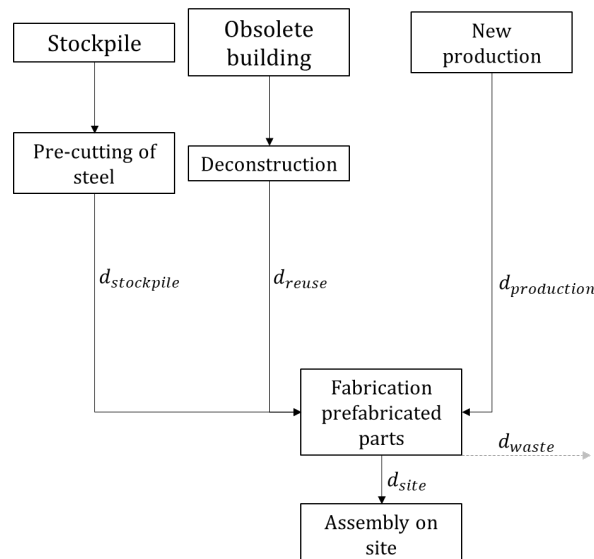


Figure 26 – illustration of the stockpile-, deconstruction- and new production scenario

3.5 GHG-calculations

Within this research the objective is calculated by the amount of $\text{kgCO}_{2\text{eq}}$ (in other words the greenhouse gas emissions) of the structure. This research is more focused on steel beam members. Therefore the calculation of the objective in $\text{kgCO}_{2\text{eq}}$ for the steel beam members is more detailed compared to the objective calculated for the glass and the nodes. Nevertheless, a substantiated assumption is presented for the calculation of nodes and glass. This will give a sense of the distribution of the objective for the gridshell. The nodes and the glass are based on new production.

For the calculation of the objective emission coefficients are used. The coefficient for the different phases is presented in Brütting et al. (2020). Whereby the coefficients for different operations with machinery (hoisting cranes, opening connections, loading preparations) are directly taken from this research. Coefficients for production and transport are in this case taken from the Granta Edupack database (2022). The main reason for using the Granta Edupack database is that data from this database is used in other parts of the research. It is assumed that the conditions that make up the values are more aligned when they are retrieved from one source instead of different sources. Another reason for using the Granta Edupack database is the available access. The reasoning behind still getting the machinery process data from the KBOB database in Brütting et al. (2020) is that it is assumed that the emissions for the

machinery processes are more generic. In table 2 the coefficients from Brütting et al. (2020) are illustrated. The coefficients are different in the phases of new production and transport, and an additional coefficient is added for cutting.

Table 2 – coefficient processes, sources: 1) KBOB, 2016 in Brütting et al. (2020), 2) Granta Edupack database (2022)

Phase	Abbreviation	Process name	Unit	Emission coefficient [kgCO _{2eq}]/unit	Source
Deconstruction	EC_{DC}	Total	[kg]	0,337	1)
		Opening connections	[kg]	0,188	1)
		Hoisting crane	[kg]	0,110	1)
		Preparing and loading	[kg]	0,039	1)
Demolition	EC_{DM}	Total	[kg]	0,050	1)
		Demolition	[kg]	0,031	1)
		Preparing and loading	[kg]	0,019	1)
Profile cutting	EC_C	Cutting of steel	[kg]	0,0012	2)
New production	EC_P	Production steel profiles	[kg]	2,030	2)
Assembly	EC_A	Hoisting crane	[kg]	0,110	1)
Transport	EC_T	Transport by truck	[kg * km]	5,9 * 10⁻⁵	2)
		Rail freight	[kg * km]	2,5 * 10⁻⁵	2)
		Air freight long haul	[kg * km]	26,1 * 10⁻⁵	2)
		Ocean freight	[kg * km]	1,3 * 10⁻⁵	2)
		Coastal freight	[kg * km]	1,9 * 10⁻⁵	2)

3.5.1 Steel beam members

For the steel beam members three different scenarios exist and are explained in chapter ‘3.4 Description of scenarios’. As mentioned previously for most data the Granta Edupack database is used. One of the bigger differences in emissions is the coefficient for newly produced steel. Where in Brütting et al. (2020) a new steel production coefficient is mentioned as being 0,7 kgCO_{2eq}/kg a different value can be found in the Granta Edupack database. Here the coefficient value is stated as 2,03 kgCO_{2eq}/kg. In Orr et al. (2020) an overview from different sources is presented for the emissions of structural steel profiles. Here the emissions range from 1,13 – 2,45 kgCO_{2eq}/kg. Therefore the value extracted from the Granta Edupack database seems to be reasonable. The following equations are used to calculate the total amount of emissions [kgCO_{2eq}]. The emissions of the different scenarios are calculated as follows:

$$GHG_{new} = Mass * (EC_P + EC_A + EC_T) \text{ [kgCO}_{2eq}\text{]} \quad (10)$$

$$GHG_{deconstruction} = Mass * (EC_{DC} + EC_A + EC_C + EC_T) + Mass_{waste} * EC_T \text{ [kgCO}_{2eq}\text{]} \quad (11)$$

$$GHG_{stockpile} = Mass * (EC_A + EC_C + EC_T) \text{ [kgCO}_{2eq}\text{]} \quad (12)$$

With:

$$EC_T = EC_{transporttype} * d_{phase} \text{ [kgCO}_{2eq}\text{/kg]}$$

d_{phase} = distance [km] related to the current phase

3.5.2 Nodes

In the nodes beam members with different cross-sections need to be connected. Because of the high level of customization the nodes are produced with the wire + arc additive manufacturing method (WAAM). The emissions [kgCO_{2eq}] for WAAM manufacturing are derived from the research conducted by Bekker (2018). In this research the emissions are calculated taking stainless steel 308L into account. It is mentioned that the emissions are derived from stainless steel 316L because none of their databases contained information for stainless steel 308L at the time of this research. The current Granta Edupack database (2022) does contain this type of information and is therefore used in this research. The emissions for stainless steel 308L changed from 7,46 kgCO_{2eq}/kg to 3,96 kgCO_{2eq}/kg, based on production in typical grade. All other coefficients are derived from the research conducted by Bekker (2018). Table 3 sums up the emission coefficients of WAAM manufacturing.

Table 3 – coefficients that make up the total for WAAM manufacturing of the nodes

Unit	Stainless steel 308L	Continuous casting	Hot rolling	Wire drawing	WAAM	Sand blasting	Total
kgCO _{2eq} /kg	3,96	0,873	0,206	0,37	3,69	0,00575	9,1

The emissions of the nodes are calculated with the following equation:

$$GHG_{node} = \frac{\pi}{4} * D^2 - (D - 2t)^2 * L * \rho * (EC_{WAAM} + EC_A + EC_T * d_{phase}) \text{ [kgCO}_{2eq}\text{]}$$

(13)

With:

D = diameter [cm]

L = length node “arm” [cm]

ρ = density of stainless steel 308L [kg/cm³]

EC_{WAAM} = the total emissions needed for WAAM manufacturing of steel [kgCO_{2eq}/kg]

$EC_T = EC_{transporttype} * d_{phase}$ [kgCO_{2eq}/kg]

d_{phase} = distance [km] related to the current phase

In this equation the diameter D is determined by the diameter of the assigned beam members. Also the thickness t is determined by the thickness of the assigned beam members. Figure 27 shows an example of

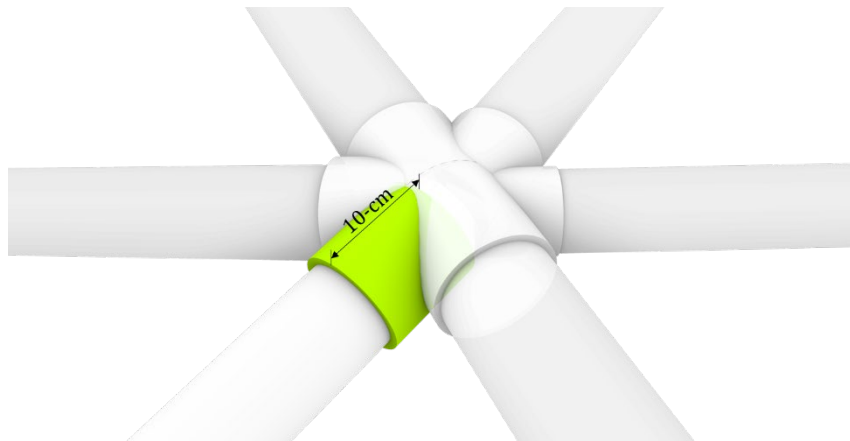


Figure 27 - illustration of the node and how the mass is calculated

how the node is calculated and what mass is used. It needs to be mentioned that the mass of the node is an assumption and isn't backed by structural calculations or analysis.

3.5.3 Glass

The emissions of the glass are calculated according to the calculation method presented in the proposed methodology by Ladipo (2022). The glass used in this case is based on the same glass used in the Glass Roof Dutch Maritime Museum project by NEY + partners. This glass is built up out of two panes of 6-mm heat-strengthened glass and one pane of 8-mm fully tempered glass. The equation for the emissions of laminated glass presented by Ladipo (2022) is as follows:

$$GHG_{glass} = A * (EC_M + EC_{LAM} + z * EC_{INT} + t * \rho_{glass} * EC_A + EC_T * d_{phase}) \text{ [kgCO}_{2eq}\text{]} \quad (14)$$

With:

$EC_M = EC_{FL,t} + EC_{P,v} * t$ = embodied carbon of monolithic glass sheet [kgCO_{2eq}/m²]

$EC_{FL,t} = 2,96$ = embodied carbon factor mid-iron float glass [kgCO_{2eq}/m²/mm]

$EC_{P,v} = 0,47$ = embodied carbon factor for toughening/heat strengthening [kgCO_{2eq}/m²/mm]

t = total thickness of the laminated glass (no IGU) [mm]

EC_{LAM} = embodied carbon factor of the lamination process [kgCO_{2eq}/m²]

z = the number of interlayers

EC_{INT} = embodied carbon factor each interlayer [kgCO_{2eq}/m²]

A = the total area of the glass [m²]

$EC_T = EC_{transporttype} * d_{phase}$ [kgCO_{2eq}/kg]

d_{phase} = distance [km] related to the current phase

In the Granta Edupack database the emissions for laminated glass (without any specific built-up) are stated as 1,67 up to 1,84 kgCO_{2eq}/kg. The glass built-up as mentioned is calculated as 74,58 kgCO_{2eq}/m². To compare this value to the value in the Granta Edupack database the volume in 1 m² needs to be multiplied by the density of laminated glass. This results in 2400 kg/m³ * 0.02 m³ = 48 kg of glass within 1 m². In addition 74,58 / 48 = 1,55 kgCO_{2eq}/kg. Compared to the values given in the Granta Edupack database the results are slightly lower. It is still chosen to go with the equation provided by Ladipo (2022) as it includes a more detailed definition of the glass built-up.

To determine what area of glass is needed the Grasshopper integrated plugin OpenNest (2022) is used. This plugin includes a nesting algorithm. The purpose of a nesting algorithm is to fit a set of geometries into a bigger geometry as efficiently as possible. Within Grasshopper the triangulated glass panes are first fitted in a geometry with a width of 3,2-meter and a theoretically unlimited length. The nesting algorithm fits the geometry of the glass panes on one side of the theoretically endless glass pane. After the nesting algorithm ran, a bounding rectangle is applied to exactly determine the area of the glass that is needed (see fig. 28). Within the nesting component some settings were defined. The spacing between geometries is set to zero. The placement of nested geometries is set to the left side. A tolerance of 0,1 is used with the possibility of rotating the nested geometries 360-degrees. The nesting algorithm runs for 10 iterations. It was tested with more iterations, but no better results were achieved.



Figure 28 – the geometries of the glass panes nested in a rectangle

3.5.4 Remaining output

Some additional output is calculated to give more insight into the generated designs. This output relates to the steel beam members only. Examples of this output are the reuse rate, the waste in length and the percentage of reused stock that is assigned. The reuse rate is based on the mass of the steel beam members (equation 15). The remaining waste is only based on the length of the stock (equation 16). The waste is calculated by the total initial length of the assigned stock from reuse minus the total length of the beam members in the structure that got a reused beam member assigned divided by the same value (equation 17).

$$RR\% = (Mass_{reuse}/Mass_{total}) * 100\% \quad (15)$$

$$W\% = (L_{stock;assigned} - L_{member;reuse}) / L_{member;reuse} * 100\% \quad (16)$$

$$Assigned\% = (L_{stock;assigned} - L_{stock;reuse}) * 100\% \quad (17)$$

3.6 Parametric definition gridshell

In this chapter the parametric definition of the gridshell is elaborated on. This definition includes the basic measurements that are used, how the general shape of the gridshell is defined and what methods are used to generate the mesh.

3.6.1 Basic measurements and shape

For the length and width of the gridshell 8-meter is used (see fig. 29). At first a length and width of 27-meters was taken into account because this would be comparable with the dimensions of the C30 gridshell by Octatube. Unfortunately, this would take too much computation time for quick testing. Therefore it was chosen to downsize the overall problem by using a smaller size. Nevertheless, because of the parametric nature of the designed computational tool it is still possible to change this size based on the needs of the design.

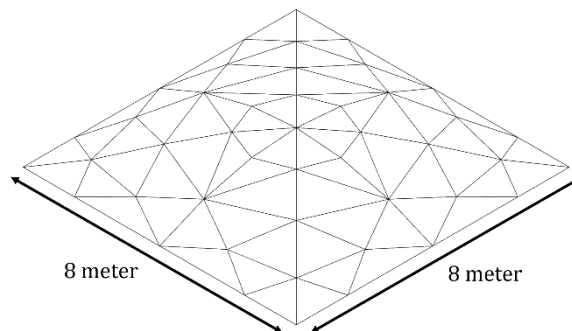


Figure 29 – the overall dimensions of the gridshell

Apart from the length and the width of the gridshell structure, the height is also fixed. The height of the structure is taken as 1-meter. This value also determines the overall shape of the structure. The formulation of the overall shape of the gridshell is taken from the research conducted by Gythiel (2022). With this equation 1/4th of the gridshell shape is generated as can be seen in figure 30. In this research equation 18 is used as seen below.

$$z(x, y) = \frac{H}{\left(\frac{L}{2}\right)^4} \left(x^2 - \left(\frac{L}{2}\right)^2 \right) \left(y^2 - \left(\frac{L}{2}\right)^2 \right) \quad (18)$$

With:

z = z-coordinate of the point

x = x-coordinate of the point

y = y-coordinate of the point

H = height of the structure

L = length/width of the structure

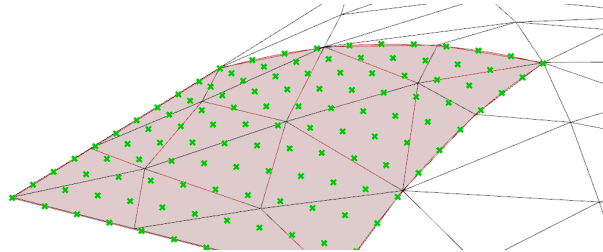


Figure 30 – 1/4th of the gridshell overall shape generated by the points

3.6.2 Bubble-packing

Before the points can be projected onto the generated shape in chapter '3.6.1 Basic measurements and shape' a bubble-packing algorithm is applied. For this method the Grasshopper integrated plugin Kangaroo 2 is used. The bubble-packing method makes it possible to distribute the points on a shape in a structured way. This means that the distance from the point to a closest point is for every point almost the same. Still, this method is able to integrate some randomness to it by changing the seed number. Therefore different kinds of structures can be generated. The method and the plugin Kangaroo 2 are developed by Piker (2021). The working of this method is described by the developer as the circles having repulsion between the centers at the areas where the circles overlap and are solved by creating an equilibrium with minimized energy. Additionally, the circles are constrained by the boundary of the surface and can never move past it (see fig. 31).

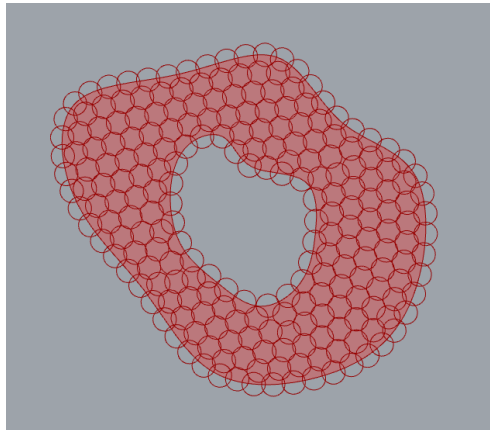


Figure 31 – principle of the bubble-packing method with the use of Kangaroo 2, Piker (2021)

3.6.3 Delaunay triangulation

After the overall shape is generated and the bubble-packed points are projected on the surface a triangulated mesh is generated according to the Delaunay principle (see chapter '2.3.2 Optimization related to gridshells' for the theory behind the Delaunay triangulation). For the triangulation of the mesh the Grasshopper integrated 'Delaunay Mesh' component is used.

3.6.4 Variables optimization algorithm

Optimization of the structure happens by shifting the nodes in combination with a Grasshopper-integrated optimization algorithm. Shifting of nodes happens for $1/4^{\text{th}}$ of the structure and for only the internal (clothed) points. In the z-axis points can move 0,2-m and -0,2-m (see fig. 32), which makes a total movement of 0,4-m. Over the x- and y-axis points can move 0,5-m and -0,5-m, which makes a total movement of 1,0-m. Every shift of the nodes will result in remeshing with the Delaunay method.

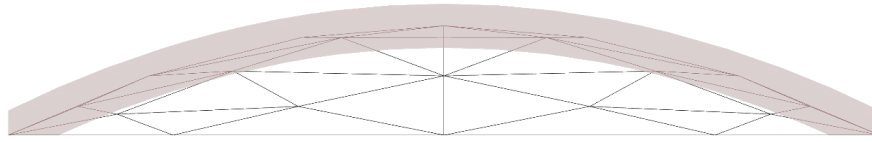


Figure 32 – illustration of the boundary (pink) of the movement of points over the z-axis

3.7 Stock assignment and optimization algorithm

The stock assignment algorithm is coded in the programming language Python and integrated into the Grasshopper workflow. The algorithm is in the form of a Best-Fit algorithm. For the overall design of this algorithm the pseudocode published by Brütting et al. (2021) is used as guidance. The Best-Fit algorithm is designed to efficiently assign beam members only.

3.7.1 Basic principle Best-Fit

In this chapter the steps of the Best-Fit algorithm are described. For the full breakdown of the algorithm see '8.10 Pseudocode'. An overview of the algorithm is also illustrated in the diagram below. For clarification, gridshell-members in this case are the beam members that are part of the gridshell structure, stock-members are the beam members that are available in the stock and therefore optionally assigned. Before the stock assignment algorithm can run a finite element analysis need to be executed. This finite element analysis will output the forces and stresses that act in the structure. The algorithm that assigns the stock consists of the following major steps:

1. For every gridshell-member in the initial structure the code runs through all available stock-members;
2. All stock-members are checked if they meet the sufficient length and capacity. Whereby the capacity consists of compression-, tension-, bending moment- and shear force capacity;
3. If the stock-members meet the criteria of length and capacity the objective is calculated in terms of greenhouse gas emissions [$\text{kgCO}_{2\text{eq}}$];
4. From all of the calculated objectives the stock-member that has the lowest objective will be assigned to the gridshell-member after the loop is finished;
5. When the stock-member is assigned the length of this member will be extracted from the total length;
6. Data from every stock-assigned member will be outputted for a finite element analysis in Grasshopper with Karamba3D. Outputted data based on the geometry of the stock is thickness and diameter. Outputted data based on the steel grade is young's modulus, density, tensile strength and compressive strength. Additional outputted data is the type of the stock (reuse/new) and assignment information;
7. If all gridshell-members are assigned the waste of the reused members is calculated and added to the total amount of $\text{kgCO}_{2\text{eq}}$ of the steel beam members.

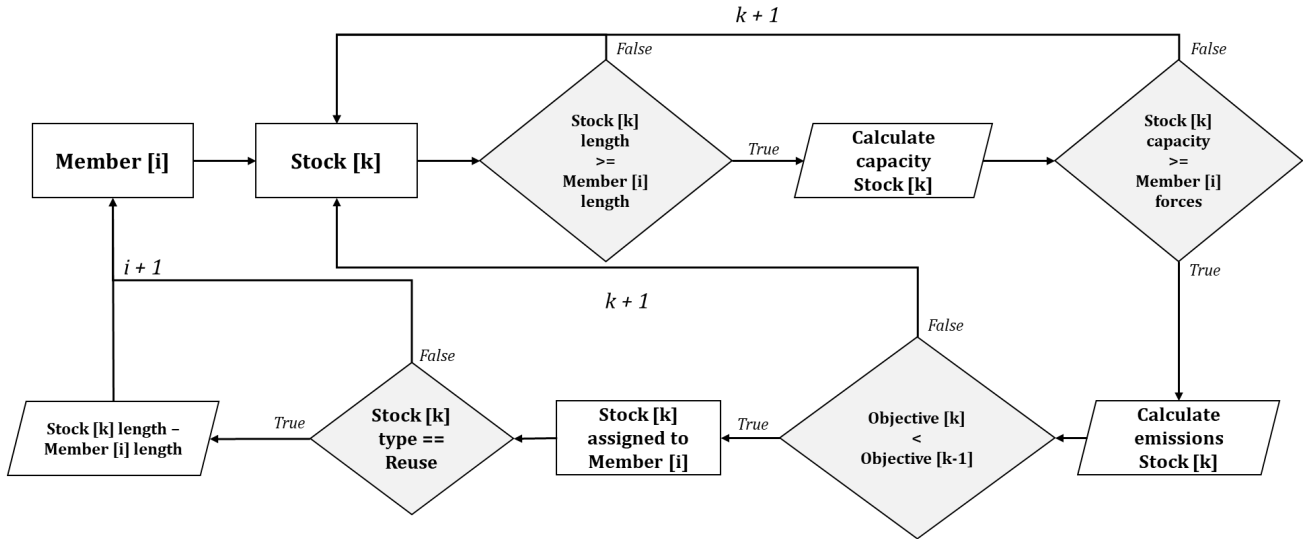


Diagram 3 – workflow of the Best-Fit algorithm in Python

3.7.2 Capacity check Best-Fit

As mentioned in the previous chapter the stock-members are checked if they meet the capacity in compression (equation 19), tension (equation 20), bending moment (equation 22) and shear force (equation 21). This is calculated according to the guidelines provided by Overend (2023). Compression capacity is calculated according to the buckling resistance with the following equation:

$$N_{b,Rd} = \frac{\chi A f_y}{\gamma_{m1}} \quad (19)$$

$$N_{t,Rd} = \frac{A f_y}{\gamma_{m0}} \quad (20)$$

$$V_{c,Rd} = \frac{(0,6 * A) f_y}{\gamma_{m0} \sqrt{3}} \quad (21)$$

$$M_{p,Rd} = \frac{W_p f_y}{\gamma_{m0}} \quad (22)$$

With:

A = cross-section area

f_y = yield strength

χ = buckling reduction factor = $\frac{1}{\phi + \sqrt{\phi^2 - \bar{\lambda}^2}}$

$\phi = (0,5[1 + a(\bar{\lambda} - 0,2) + \bar{\lambda}^2])$

$\bar{\lambda}$ = relative slenderness = $\frac{L_{cr}}{i} \frac{1}{\lambda_1}$

$\lambda_1 = \pi \sqrt{\frac{E}{f_y}}$

γ_{m0} = resistance of cross-section = 1.0

γ_{m1} = safety factor related to the resistance of elements tested for stability = 1.0

W_p = plastic section modulus of steel member

3.7.3 Optimization algorithm: Galapagos

When the computational tool was developed up to the point when optimization could be conducted different optimization algorithms were tested. From the resultant list that was found during the literature study (see chapter '2.3.3 Grasshopper optimization algorithms') the testing of algorithms was brought down to Galapagos, GOAT and Opossum. Where GOAT contains a total of five different integrated algorithms (COBYLA, BOBYQA, Sbplx, DIRECT and CRS2). From the tested algorithms only the evolutionary algorithms worked (Galapagos and CRS2). It is not entirely clear why this is the case. It is assumed that this is related to the looping of data within Grasshopper. For this test the settings described below are used. The difference here is that no stagnant is used and the optimization algorithms ran for 1-hour with an initial boost of two times the normal population. The results of the two tested algorithms are illustrated in figure 33. For both of the algorithms a similar best-objective value was reached (Galapagos: 12205 kgCO_{2eq} and CRS2: 12211 kgCO_{2eq}).

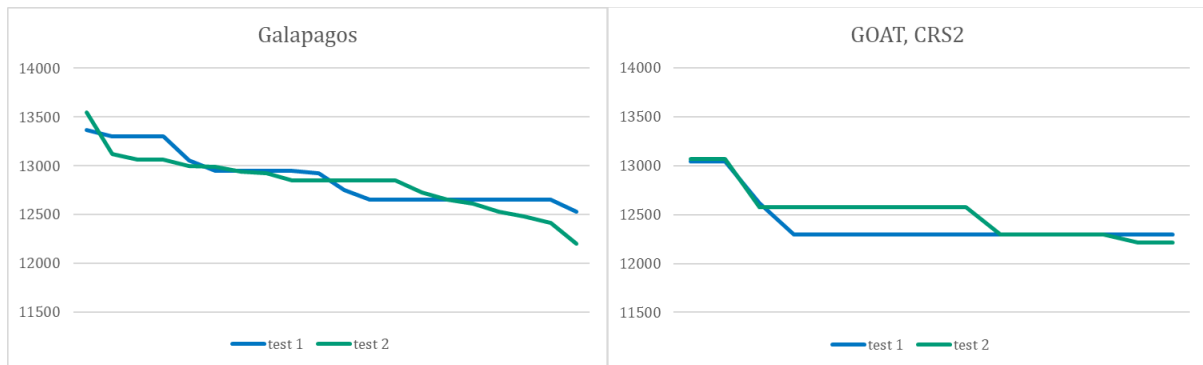


Figure 33 - results of testing Galapagos (left) and results of testing GOAT, CRS2 (right)

For further optimization it was chosen to work with Galapagos as it includes a better interface where resulting data is constantly displayed during the optimization.

Within Galapagos a number of settings can be set. Within the generic settings there is the option to optimize towards a maximum or minimum value. Here you can also find the option to work towards a threshold. A threshold value defines at what value the optimization needs to stop. When no threshold is defined, Galapagos will optimize endlessly until stopped. There is also a time limit that can be set. Unfortunately, according to a response on an online topic the time limit function is bugged and won't be fixed before Grasshopper 2 is announced (Rutten, 2016). Within the evolutionary solver settings there is the option to set a maximum stagnant. The maximum stagnant is the number of generations produced that do not result in a better objective at which Galapagos needs to stop running the optimization. The population is the number of genomes (design versions resulting in an objective) it should contain before moving to the next population (group of genomes). The initial boost option is introduced to overcome the algorithm getting stuck at a local optimum directly in the beginning. Because the optimization needs to start from scratch the first produced population is important. With the initial boost the population size of the first generated population can be increased. When the optimization is complicated and it includes a lot of local optimum it is interesting to have a higher initial boost. The maintain setting is there to set the percentage of the population that should remain and be used for the next population. Lastly, the inbreeding setting determines the number of similar genes that can be generated (*Galapagos Optimization - TOI-Pedia*, n.d., *On Getting Lucky in Higher Dimensions*, 2012).

For the upcoming tests presented in the next chapters a set of values for the settings is defined. Those settings in Galapagos are set as follows. Within the generic settings the objective is minimized without a threshold or a time limit. The maximum stagnant and the population size are both kept at 50. Because this is a relatively complex optimization with a lot of freedom the initial boost is set to five times. During the optimization 5% of the generations is maintained and the inbreeding rate is kept at a positive 75%. At first the maximum stagnant was filled in with the highest possible value. This results in an almost infinite run. This method was tried twice, where the optimization ran for approximately 48-hours. Unfortunately in both of the cases Galapagos froze when stopped manually. Therefore, it was chosen (also taking time constraints into account) to apply a maximum stagnant of 50. For all tests the mentioned settings are used unless stated otherwise. Optimization runs ran on a laptop with the following processor specs: Processor Intel(R) Core(TM) i7-8750H CPU @ 2.20GHz, 2208 Mhz, 6 Core(s), 12 Logical Processor(s).

The gene pools (the group of sliders where the variables are grouped) always start at 0 before running a

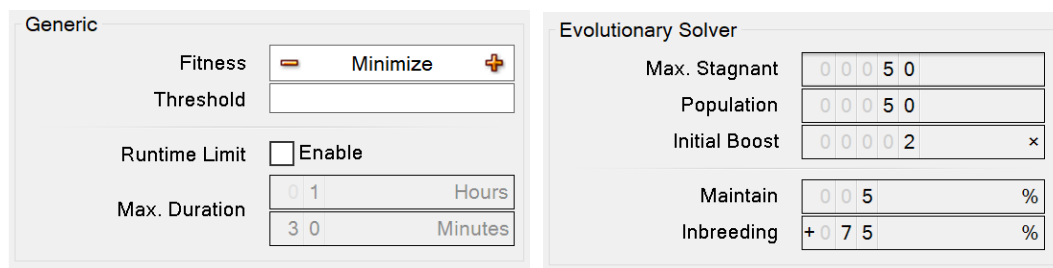


Figure 34 – different parameters available in Galapagos

new optimization. Within the designed tool all data from every generated design is saved. This results in having data of not only the best-performing design, but also the designs generated in between. Due to a delay in calculation time within the script it was not possible to save only the slider setup. The stored data brought in the case of long runs (48-hours) some difficulties as Galapagos would not exit the optimization interface after finishing an optimization. Using a stagnant value did in some cases work. When also using a stagnant didn't work it was possible to note the latest best objective for those runs. In some cases the optimization was run again with the threshold set at the last known best objective.

3.8 Finite element analysis Karamba3D

As mentioned earlier in this report the software used to conduct finite element analysis is Karamba3D. The software has its integration into Grasshopper, which makes it easier to combine finite element analysis with parametric modelling and optimization. Within the computational tool the finite element analysis is performed twice. The first analysis is mostly focused on the occurring stresses and forces in the structure. The stresses and forces are used as input for the Best-Fit algorithm. The second finite element analysis is more focused on checking if the utilization and deflection of beams and glass are within limits after stock members are assigned. In figure 35 it is illustrated how the two finite element analyses are integrated into the computational tool.

3.8.1 First finite element analysis

Before the beam members are inputted in the analysis, the beam members are sorted descending the value of the z-coordinate of the midpoint determined by the total length. Within Karamba3D a model needs to be assembled consisting of elements (in this case beam-elements), supports, cross-sections, materials and joints. In this case no special joint type is indicated so Karamba3D automatically recognizes this joint as fixed. With the line-to-beams component the structural elements are generated. In the first

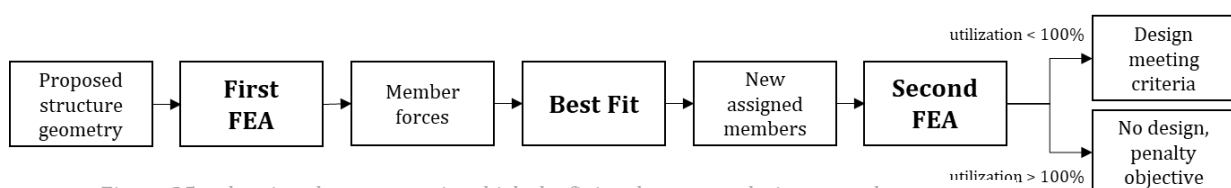


Figure 35 – showing the sequence in which the finite element analysis are used

run all cross-sections and materialization is defined with the following properties. Properties are based on stainless steel with steel grade S235 The thickness of the cross-section is defined as 0,25-cm and the diameter is defined as 3,4-cm (based on the smallest cross-section from the stocklist by Cleveland Steel & Tubes Ltd.). Both the in-plane and transverse shear modulus are defined as 7890 kN/cm². The specific weight is set to 78,3 kN/m³. Both the compressive and tensile strength are kept at 23,5 kN/cm². After the first run new properties calculated by the Best-Fit algorithm are fed back into the calculation with the use of a data loop. As mentioned previously a representative area load is translated to a line load. By multiplying this line load with the length of the beam the highest value of the center concentrated line load is calculated. In Karamba3D this highest value is fed in the trapezoidal line load component. Here the highest calculated value is placed in the middle of the beam member (see also fig. 23). Also the weight of the members in the structure is taken into account. The weight of the glass is already integrated into the calculation of the line load. Because the design is based on Ultimate Limit State the weight is multiplied by 1,2. When the model is assembled it is ready to be analyzed. The model is analyzed according to the first-order theory. By adding the beam force component all forces in the members are analyzed. The output of this finite element analysis is the shear force [kN], the tension and compression forces [kN] and the maximum bending moment [kNm]. This output is then used by the Best-Fit algorithm to assign suiting stock members.

3.8.2 Second finite element analysis

The second finite element analysis by Karamba3D is a final check of the design. Here the build-up of the assembled model is practically the same. The main difference is that now the properties of the assigned members are used that are outputted by the Best-Fit algorithm. The calculation of the glass is independent of the members that are assigned by the Best-Fit algorithm and therefore can be calculated with just the basic geometry. By using the utilization of shells and the nodal displacement component the displacement and utilization of the glass is checked. Displacement and utilization in the beam members are calculated by the utilization of beams and beam displacement components. When the analysis of the structure by Karamba3D is finished the results are processed by a Python code that checks for overall compliance including manufacturing constraints (see '8.10 Pseudocode').

3.9 Multiple loops with seed addition

Most of the tests performed within this research are based on a single seed. The reason for this is the time efficiency and ease of comparison. Nevertheless, the computational tool is designed to generate multiple design alternatives based on different seeds. This was initially added to the designed tool for the reason to give the user more freedom to choose between designs based on aesthetics. This chapter is mainly included to give a sense of the added value of outputting designs based on more than one seed value.

3.9.1 Adding seeds

Within the computational tool it is possible to change the seed value every X amount of iterations. The variable of X could be based on the iterations it takes before getting an optimal value. Because a size check is integrated the computational tool will always keep the size within the boundaries of manufacturing. The bubble packing method is related to the seed value. The bubble packing sequence in combination with the Delaunay triangulation can in some cases result in unfeasible designs (missing beams). Therefore also a uniformity check is introduced. This uniformity check solves the intersection

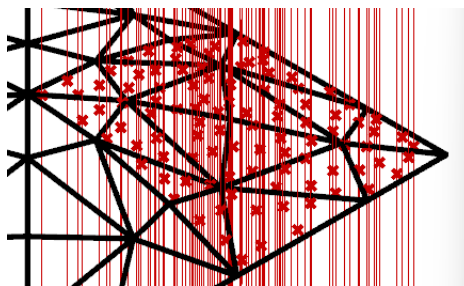


Figure 36 - checking the intersection of curves and mesh

between the mesh and a group of curves (fig. 36). When there is no intersection detected this means that the structure is missing a beam member and is therefore invalid. This results in the structure not being recorded.

3.9.2 Design explorer

To get an overview of the different outputted designs the web-integrated visualization tool Design Explorer is used (*Design Explorer | Thornton Tomasetti, n.d.*). The interface of Design Explorer is shown in figure 37. In the box marked with number one an overview of all the extracted data for every design is illustrated. Here there is also the option to filter out designs. In this way the designer can filter out designs that fall between a set of relevant constraints (for example a maximum weight). In box the marked with number two the design data of different designs are plotted in a graph. Lastly, the box marked with the number three shows an overview of all generated and/or filtered designs. When clicking on one of the images Design Explorer shows the design with some additional attributes related to that specific design.

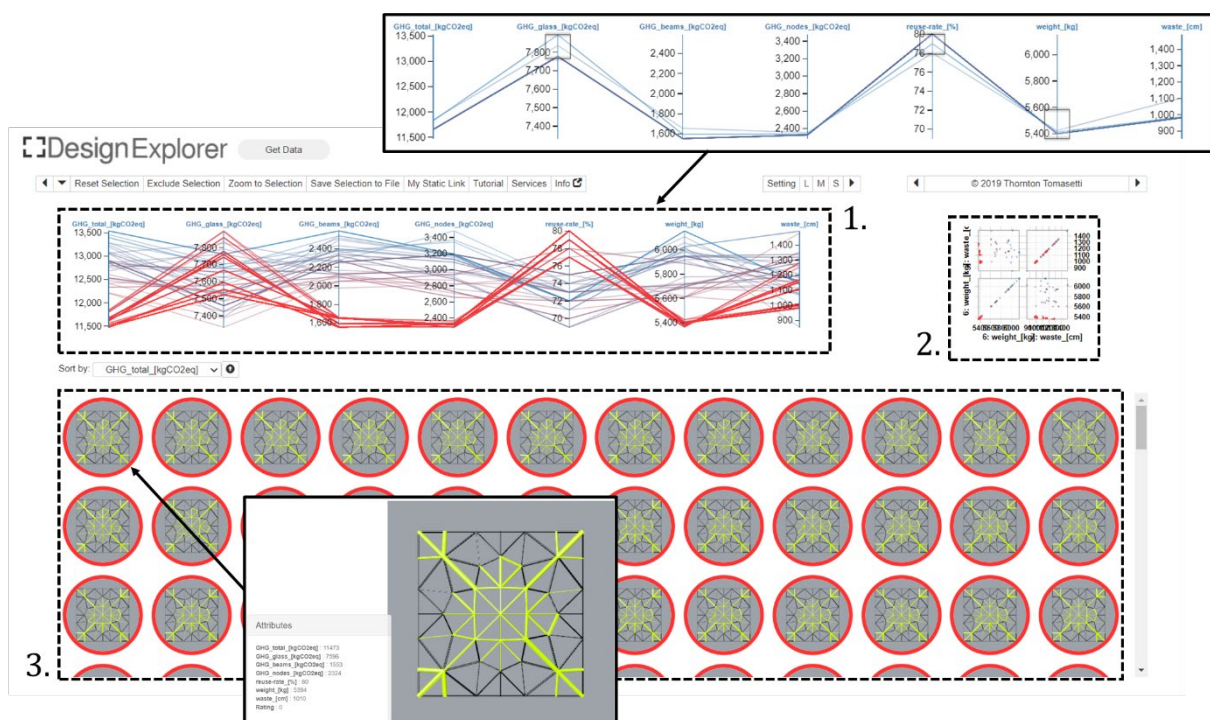


Figure 37 – interface of Design Explorer

4. Optimization results

In this chapter the results are presented for the different tests using the in this research developed computational tool. The first test is dedicated to testing the different scenarios that are introduced within this research. Secondly, different stock-sizes are tested ranging from a small to a large stock. Because in the previous tests the emissions for transport were almost negligible, also a test is performed by increasing the distance and changing the transport type to see how this influences the overall emissions. After this a case-study is tested where a stock is used consisting of all three scenarios. This chapter closes of with an extensive benchmark of Phoenix3D using a truss topology.

4.1 Testing different input

This chapter will test the developed computational tool by changing the input of the stock. Examples here are testing different scenarios and testing different stock sizes. Also, the impact of transportation is tested.

4.1.1 Comparison scenarios

This section is dedicated to comparing the different scenarios (see also chapter '3.4 Description of scenarios'). Firstly, a gridshell is optimized with the objective to minimize total emissions with only new members. For this optimization the cross-sections are limited to the ones provided by Cleveland Steel & Tubes Ltd. (2022). A list of the different cross-sections can be found in Appendix '8.4 Comparison scenarios'. An optimization run of around 10-hours was carried out twice (fig. 51 in '8.5 Comparison scenarios'), and in both cases the same best objective was achieved. Out of a total of 2419 generated designs a best objective with a value of 12146 kgCO_{2eq} is reached. The topology of this structure is then translated to a gridshell made out of beam members with a single cross-section, the optimized version with only the deconstruction scenario and an optimized version with only the stockpile scenario. For the version with a single cross-section the first cross-section with the least area was chosen that complied with the maximum utilization of 100% for each member. This resulted in a cross-section with a diameter of 10,2-cm and a thickness of 0,36-cm. In the reuse scenarios an ideal stock size is taken into account. This means that all lengths are sufficient and there is no waste generated. The distances that are taken into account for $d_{production}$, d_{reuse} , $d_{stockpile}$, d_{nodes} and d_{glass} are 70-km. In all scenarios the distance for d_{site} is taken as 15-km.

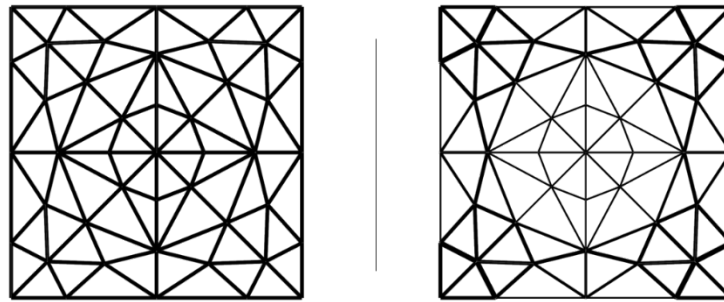


Figure 38 – optimization from singular cross-sections to optimized cross-sections

An overview of the distribution of emissions for beam members resulting from the different tests can be found in figure 39. The weight of the total structure comparing the single cross-section and the optimized cross section version reduces from 1704,8-kg to 1073,5-kg. This is a reduction of 37% (see fig. 38). In terms of emissions the stockpile scenario performs best. It needs to be mentioned that in this case cutting is excluded as the length of the stock is equal to the length of the structure. This therefore also results in no transport emissions for the transportation of waste. When comparing the single cross-section gridshell with the gridshell from stockpile beam members a decrease of 96,5% in the emissions can be noted. The share of the beam members on the total emissions, including glass and nodes, reduce from 27% in the single cross-section gridshell to just 1% in the gridshell from stockpile beam members. In the versions where new beam members are used the production phase is the predominant factor of the emissions. In the scenarios related to reuse this is either the deconstruction phase or the assembly phase. When comparing the best single cross-section gridshell with the optimized gridshell from the stockpile and also taking the emissions of nodes and glass into account a reduction of 26,3% of the total emissions can be noted. For an overview of the distribution of the total emissions see figure 52 in Appendix '8.5 Comparison scenarios'. Visualizations of the different generated gridshells can be found in Appendix '8.11 Visualisations gridshell'.

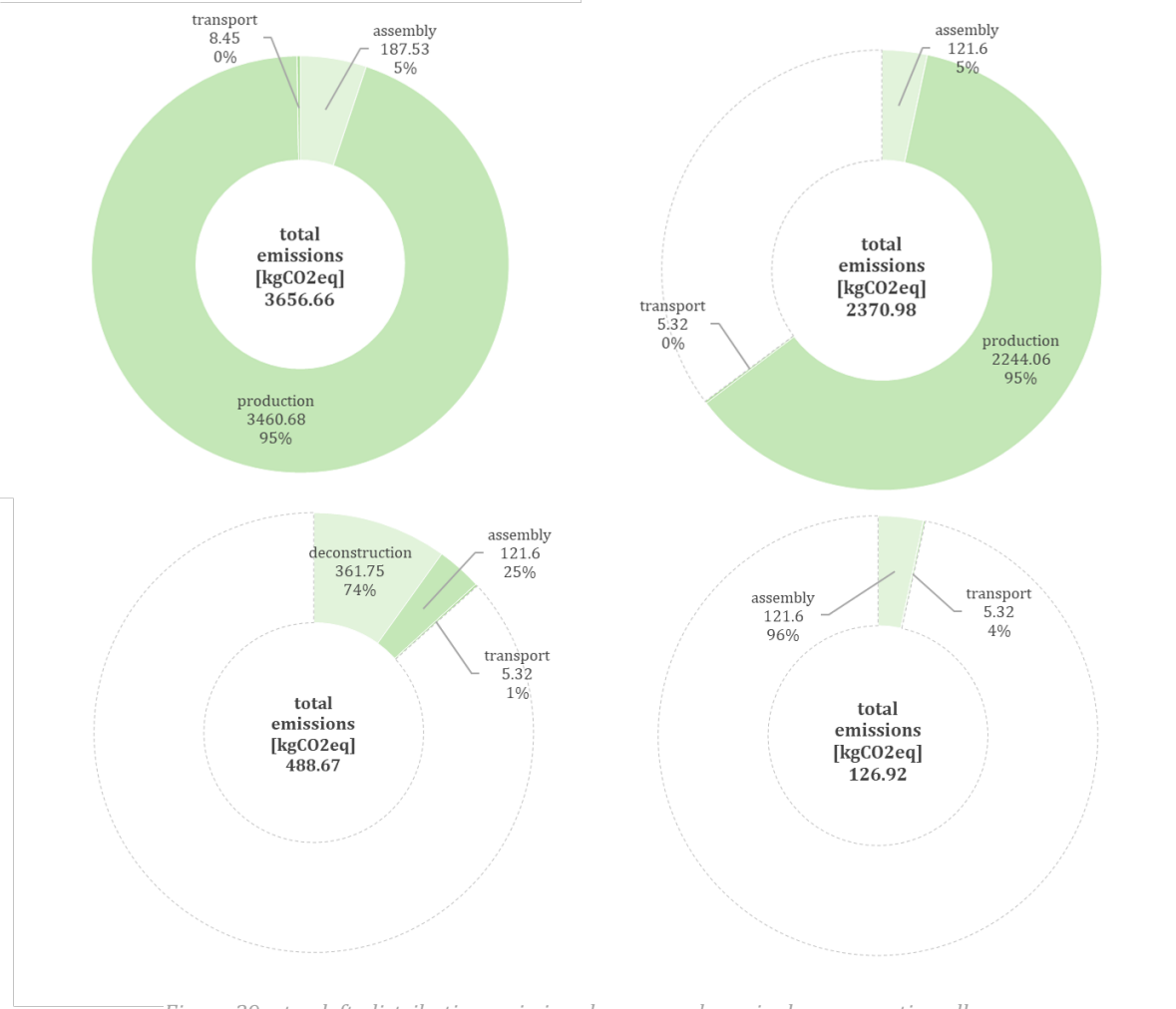


Figure 39 – top left: distribution emissions beam members single cross-section all new scenario, top right: distribution emissions beam members optimized cross-section all new scenario, bottom left: distribution emissions beam members optimized cross-section deconstruction scenario, bottom right: distribution emissions beam members optimized cross-section stockpile scenario

4.1.2 Comparison stock-sizes

This chapter is dedicated to testing different stock sizes. Firstly, the total length of the members was measured in a neutral state (where the nodes are not shifted yet). The total length of the tested seed in a neutral state accounted for 183-meter. Based on this length the stock sizes were determined. The initial length of individual stock is kept at 4,5-meter. This is the minimum length as described in the stock database from Cleveland Steel & Tubes Ltd. (2022). For this chapter the stock is limited to only the deconstruction scenario. All used cross-sections can be found in Appendix ‘8.5 Comparison scenarios’. The first test is with a stock size of 56% of the total length of the structure. Here one unit of 4,5-meter is used for every unique cross-section. Then the stock size is tested with double the amount of stock. This

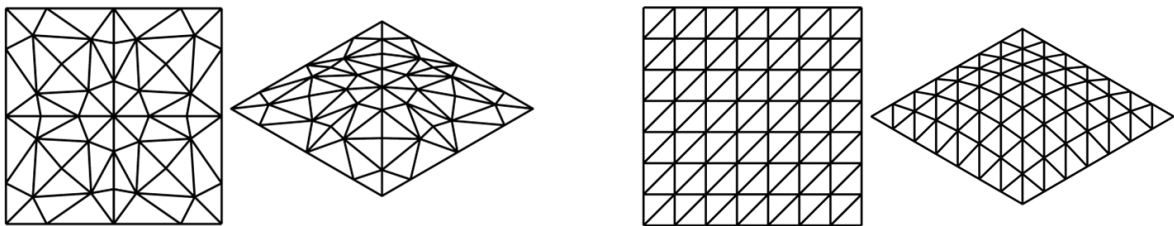


Figure 40 – left: the starting point of the optimized gridshell, right: the regular gridshell

accounts for 112% of the total length of the structure. Here two times a unit of 4,5-meter is used for every unique cross-section. Lastly, the stock size is tested with triple the amount compared to the first test. This accounts for 168% of the total length of the structure. Here three times a unit of 4,5-meter is used for every unique cross-section. To equally compare the scenarios the same travel distances are used. The distance that is taken into account for $d_{production}$, d_{reuse} , $d_{stockpile}$, d_{nodes} and d_{glass} is 70-km. For both scenarios the distance for d_{site} is taken as 15-km. To get more insight into the influence of the stock on the generated gridshells the non-regular gridshell is compared to a gridshell with a regular right-cornered triangulated grid (fig. 40). The size of the grid is determined by adding UV-values (distribution of grid over x- and y-axis) until the utilization for each beam in the structure reaches below 100%. The triangles in the grid ended up being on average 1,62-meter over the long side and 1,14-meter over the short side. The finite element analysis are conducted from a starting cross-section with a diameter of 10,2-cm and a thickness of 0,36-cm. Also this cross-section is based on the maximum utilization. In contradiction to the non-regular optimized gridshell the regular gridshell only uses the Best-Fit assignment from the neutral state. This means that the nodes are not shifted and therefore only the cross-section is optimized and the topology isn't.

The setup of the optimization is according to '3.7.3 Optimization algorithm: Galapagos'. It needs to be mentioned that the optimization algorithm is a metaheuristic. Although using the same setup in every optimization it is hard to predict how close the results are to a global optimum. Therefore it needs to be taken into account that when comparing the different optimization runs one can be closer to the global optimum compared to another. The results of the different tests are summarised in the table below.

Table 4 – results of the optimization runs taking different stock sizes into account

Test case	GHG emissions [kgCO _{2eq}]	Reuse-rate [%]	Structure mass [kg]	Waste [cm]	Waste [%]	Stock used from total [%]
Small stock – regular gridshell	2492,64	33,47	5115,88	872,64	16,08	52,44
Small stock – optimized gridshell	1404,79	52,09	4599,25	541,32	9,40	55,64
Medium stock – regular gridshell	2008,63	59,85	5317,30	1675,07	15,33	52,78
Medium stock – optimized gridshell	1197,88	78,71	4907,09	1124,36	9,09	59,79
Large stock – regular gridshell	1452,15	84,88	5547,70	2267,85	13,64	53,57
Large stock – optimized gridshell	707,82	97,34	4820,40	2210,96	12,90	55,20

When looking at the total emissions of the beam members it can be noticed that when the stock size is increased the emissions reduce. First focussing on the reduction from a small stock size to a large stock size the total reduction of the beam members in the regular gridshell. A reduction from 2492,64 kgCO_{2eq} towards 1452,15 kgCO_{2eq} can be noticed. This is a reduction of 41,7%. Comparing this to the reduction from a small stock size to a large stock size in the optimized gridshell. A reduction from 1404,79 kgCO_{2eq} towards 707,82 kgCO_{2eq} can be noticed. This is a reduction of 49,6%. The difference in emissions can be explained by looking at the reuse rate and for a smaller part at the amount of waste that is generated. The reuse-rate difference between the regular gridshell and the optimized gridshell seems relatively low, but this difference is noticeable when looking at the embodied emissions. For the optimized gridshell this difference in reuse-rate results in lower emissions within the new production phase and higher emissions within the deconstruction phase. This leads to an overall greater reduction in emissions. Also, a difference in the generated waste can be noticed when comparing the two types of gridshells. For the generation of waste only the emissions for transportation are taken into account. As can be concluded from different tests the transportation emissions are in most cases relatively small. In figure 41 the distribution of the emissions of the beam members is illustrated.

To give an impression how the emissions of the beam members relate to the emissions of the nodes and glass an assumption is made for those elements (see chapter '3.5.2 Nodes' and '3.5.3 Glass'). First looking at the total reduction from a small stock size towards a large stock size for the regular gridshell. A total reduction from 13528,41 kgCO_{2eq} towards 12934,90 kgCO_{2eq} can be noticed. This is a reduction of 4,4%. This small reduction can be explained by the increase in the emissions for the nodes. Looking at the total reduction from a small stock size towards a large stock size for the optimized gridshell. A total reduction from 11049,10 kgCO_{2eq} towards 10443,13 kgCO_{2eq} can be noticed. This is a reduction of 5,5%. It is important to conclude that, in this case mostly with the medium-sized stock, the emissions of the nodes overtake the emissions of the beam members. This is mainly due to the Best-Fit algorithm preferring to assign a bigger cross-section because of their better individual emissions without taking the higher emissions of the nodes into account. The assignment of stock in the gridshells is illustrated and can be found in Appendix '8.6 Comparison stock sizes'. Visualizations of the different generated gridshells can be found in Appendix '8.11 Visualisations gridshell'. In figure 57 in Appendix '8.6 Comparison stock sizes' the distribution of the emissions for the total structure is illustrated including beam members, glass and nodes. In Appendix '8.12 Overview stock assignment' all assigned stock is summarized.



Figure 41 - distribution of the emissions for the beam members with different stock-sizes

4.1.3 Different transport context

Within the stock definition of the computational tool it is also possible to fill in different modes of transport. Taking into account the distribution of emissions resulting from the different scenarios and stock sizes the share of transportation emissions is almost negligible. The distances that were taken into account for $d_{production}$ and d_{reuse} were 70-km. For both scenarios the distance for d_{site} is taken as 15-km. The mode of transportation that was used was a 36-axle truck. It is interesting to see what the impact is of different distances and modes of transportation on the embodied emissions. For this comparison only the beams from a small stock size are taken into account. The worst performing mode of transport in terms of emissions which is integrated into the tool is air freight for long haul. Compared to transportation by truck the coefficient of this mode of transport is 4,4 times higher. First, only the difference in the mode of transport is calculated with the same travel distances. Then distances $d_{production}$ and d_{reuse} are increased to 7000-km. The difference is illustrated in figure 42.

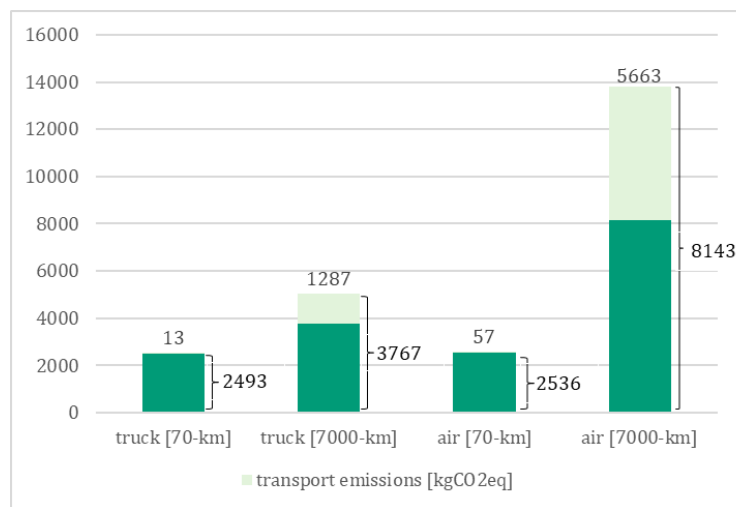


Figure 42 – distribution emissions focused on stock from, light green is the emissions cause by transportation and dark green are all other emissions, left to right: truck (70-km), truck (7000-km), air (70-km) and air (7000-km)

At first, the emissions from transportation seemed to be negligible. This test illustrates that depending on the context transportation can end up being the dominant factor in terms of embodied emissions. Therefore it is an added value that within the definition of the stock different modes of transport are integrated. This same conclusion is also drawn in Colabella et al. (2017) and Brütting et al. (2020).

4.1.4 Conclusion

When looking at the comparison of the different scenarios it can be concluded that there is already a relatively high reduction in weight (for the beam members from 1704,8 kg to 1073,5 kg) as well the emissions (from 14026,94 kgCO_{2eq} to 12145,97 kgCO_{2eq}) of the structure when comparing the single cross-section gridshell with the gridshell with optimized cross-sections. It can also be concluded that within the same context the stockpile scenario performs best. Comparing the cross-section optimized gridshell with newly produced stock with the one from stockpile stock a reduction of almost 95% for the emissions of the beam members can be seen.

Comparing the different stock sizes it can be concluded for the emissions of the beam members that when the stock size is bigger the reuse rate is higher resulting in lower emissions. When also looking at the emissions of the nodes it can be seen that in some cases the emissions of the nodes tend to nullify the reduction of the emissions of the beam members. This is because of the assignment of bigger cross-sections. It can also be concluded that the optimized stock pattern compared to the standardized pattern performs better in terms of emissions and resulting waste. The tests are performed with the Grasshopper

integrated metaheuristic optimization algorithm Galapagos. With this type of algorithm it is possible that it gets stuck at local optimum.

The results of the tests of scenarios and stock sizes show an almost negligible share of the transportation emissions on the total. This is the reason why the impact was tested for beam members with increased emission coefficients and transportation distance. It can be seen that with increased distance and a different mode of transportation, transport emissions can be the dominant factor. Therefore it can be concluded that defining the mode of transport with the transport distance is an added value to the developed computational tool.

4.2 Case-study

To translate the developed computational tool into a more real-world scenario a case study is tested. In this case study, the focus is on using different scenarios from different locations. The different locations are based on existing manufacturers, building sites and transportation hubs.

4.2.1 Description of context

The following context will be used for this case study. The building site will be in this case at the same location as the C30 gridshell from Octatube and is located in The Hague. It is assumed that the new produced steel is produced at Tata steel, located in IJmuiden. The fabrication workshop, where members will be prefabricated, is located in Delft at the company Octatube. The reused members are harvested from the gas fields in Groningen. Waste steel is brought to a scrapyard located in The Hague. The newly produced glass comes from the manufacturer AGC glass Europe. This manufacturer has a production facility in Moustier in Belgium. The nodes are manufactured by the company MX3D specialized in WAAM manufacturing. Their production facility is located in Amsterdam. Finally, the stockpile that is used is from the company Cleveland Steel & Tubes and is located in Thirsk, England. For the stockpile scenario it is assumed that the tubes first need to be transported to the nearest harbour, in this case the Immingham Docks. From here the stock will be transported overseas to the harbour of Rotterdam and then transported to the steel workshop of Octatube. The distances of this context are summarized in table 5 and illustrated in figure 58 in Appendix '8.7 Case study'.

The initial length of individual stock is kept at 4,5-meter. This is the minimum length as described in the stock database from Cleveland Steel & Tubes Ltd. (2022). Scenarios that are taken into account are the deconstruction, stockpile and new production scenarios. For the two reuse scenarios one unit of 4,5-meter for every unique cross-section is taken as the size of the stock.

Table 5 – summary of the travel distances used within the case study

Abbreviation	Description	Distance [km]
d_{reuse}	Distance from the obsolete building to the fabrication workshop	256
$d_{production}$	Distance from the production facility to the fabrication workshop	69
d_{site}	Distance from the fabrication workshop to the building site	15
d_{waste}	Distance from the fabrication workshop to the scrapyard	10
d_{glass}	Distance from glass production to site	262
d_{nodes}	Distance from node production to site	67
$d_{stockpile}$	Distance from the stockpile to harbor England to harbor in the Netherlands to fabrication workshop	153 – 345 – 42

With the resultant design a reuse rate of almost 96% is achieved. This reuse rate is relatively high because the reuse rate is based on mass rather than length. The total weight of the structure is 6404,38-kg. This also results in high assembly emissions. With the higher amount of reused stock available also the length of waste steel is automatically higher. The generated waste in this case study is 1805,35-cm. It can also be concluded that in this case-study the emissions for transportation have a more significant share in the total emissions of the beam members. Comparing the distribution of the greenhouse gas emissions it

can be noted that, comparing this case study to the previous tests, the emissions of the nodes are way higher. In figure 43 the distribution of emissions for the beam members is illustrated. The assignment of stock and the distribution of emissions including the nodes can be found in figure 60 in Appendix '8.7 Case-study'.

Table 6 – generated design from the case-study

GHG emissions [kgCO ₂ eq]	Reuse-rate [%]	Structure mass [kg]	Waste [cm]	Waste [%]	Deconstruction stock used from total [%]	Stockpile stock used from total [%]
826,51	95,97	6404,38	1805,35	11,8	57,84	88,34

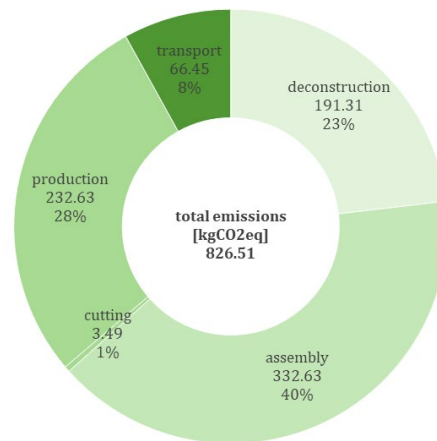


Figure 43 - distribution of emissions for beam members within the case-study

4.2.2 Conclusion

Within the context of this case-study stock from the stockpile scenario is preferred over other scenarios. This results in low emissions for the beam members. Bigger cross-sections from the stockpile scenario are preferred over smaller cross-sections from the deconstruction scenario based on their individual emissions. This results in a structure with increased mass. The increase of the average assigned cross-section results in higher assembly emissions. Also the calculated emissions of the nodes tend to increase. When looking at the emissions of the nodes it can be concluded that the emissions in this case study are clearly higher than the emissions of the nodes in previous tests.

4.3 Benchmarking against Phoenix3D

The tool developed in this research will be compared to the existing plugin Phoenix3D (n.d.). On the platform Food4Rhino, where plugins for the software Rhino and Grasshopper can be downloaded, Phoenix3D is described as an open-source tool to optimize truss structures from a stock of reused and new members.

4.3.1 Testing truss structure

As mentioned in chapter ‘2.3.2 Optimization related to gridshells’ Phoenix3D is not compatible with gridshell topologies. Therefore, this tool is compared to the in this research developed computational tool by testing a truss topology.

Phoenix3D has two integrated optimization formulations that are compared to the tool developed in this research. The two formulations are Mixed-Integer Linear Programming (MILP) and the Best-Fit. The difference between the two formulations is that the MILP formulation reaches a global optimal objective whereas the Best-Fit formulation is the best objective calculated for every member. The Best-Fit approach therefore also doesn’t consider topology optimization. Within Phoenix3D the assignment is constrained by its length and the capacity of the member. The capacity is determined by tension and compression taking buckling into account (Warmuth, 2021). The tool designed in this research is best comparable to the Best-Fit approach, although a topology optimization is integrated externally in the form of shifting nodes. In this chapter the MILP and Best-Fit formulations are compared to the designed tool in neutral state and after optimization.

According to Warmuth (2021) the travel conditions are based on the research conducted by Brütting, Senatore, et al. (2020). In table 7 the travel distances are summarized.

Table 7 – travel distances as taken from the case study in Brütting, Senatore, et al. (2020)

Abbreviation	Discription	Distance [km]
d_{reuse}	Distance from the obsolete building to the fabrication workshop	150
$d_{recycling}$	Distance from the obsolete building to the production facility of new steel	10
$d_{production}$	Distance from the production facility to the fabrication workshop	10
d_{site}	Distance from the fabrication workshop to the building site	10
d_{waste}	Distance from the fabrication workshop to the scrapyard	10

A truss with a span of 16-meters supported at the ends is taken as a test case. The structure is built up out of a total of 17 members. At the nodes at the top of the structure point loads are applied with a value of 420-kN. For all of the optimization tests circular hollow section profiles are used with a starting value with a diameter of 3,4-cm and a thickness of 0,25-cm. The connection member to member is for this case fixed. In figure 44 the starting condition of the truss is illustrated.

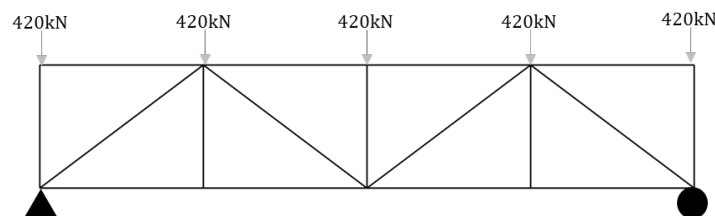


Figure 44 – illustration of the starting position of the analysed truss

For this test case different settings in Galapagos are used then mentioned in chapter ‘3.7.3 Optimization algorithm: Galapagos’. The differences are that no maximum stagnant was used. The optimization was manually stopped at 50 populations.

In this case the node-shift version is allowed to shift all nodes except the nodes at the supports. The nodes are allowed to move -1 and +1-m over the Z- and X-axis. In this case the nodes and members are not able

to clash. Timewise the methods are not comparable. The formulations used in Phoenix3D takes less than 5-seconds to produce a result were the tool designed in this research can take more than an hour. This can be explained by the difference in freedom and therefore complexity. The tool designed in this research shifts the nodes, which results in a lot of freedom that needs to be solved by the optimization algorithm. Time could be decreased by decreasing the freedom in node movement although it will never come close to the time reached by Phoenix3D. For this test the optimization algorithm produced 50 populations which took around 8-hours to complete.

When looking at the results of the optimizations and in particular to the ones with stock compiled from new- and deconstruction scenario. It can be noticed that the reuse rate is similar for all formulations. The weight therefore differs. Where the weight and embodied emissions of the MILP, Best-Fit and the Best-Fit formulation from this research are similar. The emissions of the node-shifted truss is way lower. A reduction of around 36% can be achieved. In table 10 in Appendix '8.8 Benchmark Phoenix3D' the different results are illustrated. Here the reused members are marked in lime green and the new members in black. Within the hybrid versions of the truss, the cutting waste is marked in grey.

4.3.2 Conclusion

Because Phoenix3D couldn't handle a gridshell topology the in this research designed computational tool is benchmarked against Phoenix3D with the use of a truss topology. When looking at only the objective it can be concluded that the designed tool can outperform Phoenix3D. The best-performing hybrid structure with the formulation from this research has an objective that is 35% lower. Thereby, it also needs to be mentioned that the truss designs produced by the Phoenix3D MILP formulation are not really feasible due to the inability to take stability into account. The method in this research-designed tool can be given a lot more freedom compared to Phoenix3D. Therefore timewise, Phoenix3D outperforms the in this research designed tool.

5. Conclusion

5.1 Discussion

Within the calculation of the embodied greenhouse gas emissions different emission coefficients [$\text{kgCO}_{2\text{eq}}/\text{kg}$] are used. It was noted that different sources state different coefficient values. For most of the coefficients in this research the Granta Edupack database is used. The values that are presented in this database are based on a certain industry with its own conditions. Therefore, a different context could result in the need for different coefficients.

For the optimization runs conducted in this research the optimization algorithm Galapagos is used. This optimization algorithm is a metaheuristic algorithm. This means that it reaches an objective relatively time efficient at the cost of perfection. A metaheuristic algorithm has the possibility to reach a local optimum instead of a global optimum. Although the same setup is used this can still be an issue when comparing different optimization runs and their values.

Although the calculation methods of embodied emissions for the nodes and the glass are not as developed as the calculation method for the steel beam members it can be said with high certainty that the steel is not the predominant factor of greenhouse gas emissions. The full integration of glass and nodes in the optimization sequence was out of the scope of this research.

Apart from the emissions of the nodes also an assumption is made for the thickness of the used material. For the nodes no structural analysis is conducted. The full verification of the structural integrity of the nodes is out of the scope of this research.

5.2 Conclusion & recommendations

This research was conducted based on the following research question:

“How can computational optimization contribute to the design of gridshell structures consisting out of a finite stock of reclaimed steel beam members with the goal to improve the eco-performance calculated in embodied greenhouse gas emissions?”

To answer this research question it is important to first understand the current situation when talking about the reuse of steel profiles. One of the bottlenecks in the reuse of steel profiles and building materials in general is the lack of supply and demand (Gorgolewski, 2019). During the literature two different reuse scenarios were identified. One of those scenarios is getting material from a so-called second-hand building material platform. The problem here is the small quantities scattered around in different locations. A scenario related to this is within this research called a stockpile scenario. Here there is a third party that gathers and stores second-hand material. This results in bigger quantities of the materials. Another scenario that was identified was the deconstruction scenario. The research conducted by Brütting et al. (2020) focuses mainly on this scenario. A computational optimization tool must allow for this diversity of scenarios.

Optimization of structures based on a finite stock is called stock-constrained optimization. This form of optimization can be conducted with the objective of minimizing embodied greenhouse gas emissions. Based on the research from Brütting et al. (2020), Warmuth (2021) developed a Grasshopper integrated plugin for the optimization of truss structures from a finite stock called Phoenix3D. This plugin is limited to only the reuse scenario of deconstruction within a fixed context as presented in Brütting et al. (2020). Additionally, this plugin was tested on a gridshell structure. It can be concluded that for a gridshell topology this plugin is not suitable.

Within this research a computational tool is developed that optimizes gridshell structures with the objective of reducing the embodied greenhouse gas emissions. The topology of the gridshell is designed parametrically and the variables are used by an optimization algorithm. This tool has an integrated Best-Fit algorithm comparable to the algorithm presented by Brütting et al. (2021). Additionally, this tool also

estimates the greenhouse gas emissions of nodes and glass. The computational tool doesn't only take mechanical constraints into account but also manufacturing constraints.

Looking at the resulting designs produced with the computational tool and taking the optimal reuse stock conditions into account a reduction of 96,5% is possible for the emissions of the beam members. This is by comparing a gridshell designed from a single cross-section with newly produced members and an optimized gridshell from stockpile members. Results are highly dependent on the context, but in general it can be concluded that the emissions of the beam members decrease when the reuse-rate increases. This reuse rate can be increased by increasing the stock size. Comparing the in this research tested grid types it can be concluded that the optimized non-regular grid performs better than the non-optimized regular grid. It can also be concluded that within the context of the tests conducted for different stock-sizes, the optimization tool will not always use 100% of the available stock from a reuse scenario. This also shows the complexity as well as the added value of the tool. Full use of stock from a reuse scenario doesn't necessarily mean lower embodied greenhouse gas emissions. Within the tests of stock sizes a bigger decrease in emissions can be spotted with a large stock size. This can be concluded as one of the vulnerabilities of the used metaheuristic optimization algorithm Galapagos. For further elaboration on this see the discussion.

In terms of aesthetics it is hard to conclude anything as it is assumed to be subjective. It can be concluded that visually the gridshells that are resultant are impacted by the size and composition of the stock. It can be noticed that when the stock size of reuse is bigger the larger cross-sections shift to the edge of the gridshell. This also has to do with the order of members. Stock assignment sometimes leads to asymmetric gridshells. In practice this could be overcome by fine-tuning the symmetry by assigning newly produced members with sufficient structural capacity. Of course, this will be at the cost of the embodied carbon of the structure.

Comparing the formulation made in this research with the formulation by Warmuth (2021) in Phoenix3D it can be concluded that in terms of the objective the formulation in this research can outperform the formulation in Phoenix3D. This is based on a truss topology. As concluded earlier Phoenix3D couldn't be used for a gridshell topology. The formulation in this research has more freedom and therefore a more complex problem to solve. This results in an increased computation time that is not comparable with the formulation in Phoenix3D. It can also be concluded that in the case of the tests performed in this research the MILP formulation of Phoenix3D doesn't always result in feasible designs as it doesn't take stability into account.

As mentioned the developed computational tool also includes an estimation of the greenhouse gas emissions for glass and nodes. From the calculation of those emissions it can be concluded that the steel beam members are not the dominant factor of the total greenhouse gas emissions. It can also be concluded that in some cases when bigger cross-sections from a reuse scenario are chosen over smaller cross-sections from a new production scenario the emissions for the nodes end up being higher. In some cases the increase of the emissions for the nodes even tend to nullify the reduction of the emissions of the beam members. This therefore leads to the following recommendations.

It is recommended to develop the calculation methods for greenhouse gas emissions for nodes and glass further and also integrate this into the optimization sequence. Additionally, it is interesting to apply the in this research-developed tool to a more steel-dominant structural topology. Because the optimization is dependent on the stock and therefore on the context it is interesting to try out more case studies. This will give more body to the validation of the designed computational tool in different circumstances. Lastly, it could be interesting to perform a multi-objective optimization instead of a single-objective optimization. In this way more knowledge is gained about the relationship between different design parameters. In terms of computation it is recommended to develop the proposed method further in terms of data storage. Currently, data regarding the generated designs is stored within Grasshopper. Long optimization runs can lead to the software crashing when trying to exit the optimization algorithm. When data is stored externally it is assumed that this issue is solved. Because it was decided to focus more on the visualization of output an additional recommendation is to further develop the interface of the in this research designed tool.

5.3 Reflection

In this part there will be reflected on the bigger meaning of this research, the influence of the research on the design, the approach that was taken during this research, the value of this research within academic and societal aspects, the reproducibility of this research, the possibilities of application of the designed computational tool in practice and the collaboration with Octatube.

This research combines knowledge in design informatics and structural engineering. Therefore it is related to the chair's structural design and design informatics. This also makes it related to the master track Building Technology. By including the circular economy strategy of reuse, this topic also aligns with the long-term vision of sustainability of the TU Delft.

When looking at the relation between research and design it can be stated that the research formed the fundamental basis of the design. A lot of approaches found during the literature research were implemented in the design of the tool. Examples are the way of calculating the objectives, the design of the algorithms and the overall approach taken for the computational tool. On the other hand within the design also a lot of "finding by doing" was involved. This resulted in finding out what kind of approach did and didn't work for the scope of this research. For this type of research the mentioned approach worked because the design is based on factual knowledge. This makes the design more objective rather than based on emotions.

The approach of first doing research into the topics of reuse, optimization and gridshells worked to get a good understanding of the current knowledge in those fields. Within the field of optimization the search for practical examples helped finding the right methods that could be applied within the design of the tool resulting from this research. Using example projects and the relevant documentation provided by Octatube professionalized and made the designed tool more applicable to real user cases. Focussing on the chosen methods for the optimization part a different approach could be an option. Here the optimization time could be reduced at the expense of the quality of the results. This would make the tool more applicable at the early stages of the design. Another approach that could have been taken was the order of research. Quite early in the research the focus was on steel beam members because of their reuse potential. The structure of the research was designed from this knowledge. Later on in the research it was concluded that also the glass has a significant impact on the emissions. If this was the focus point from the start, the research would have been way different. This could have been another interesting approach, but maybe less related to reuse.

The academic value of this project lies in that it gives new insights and directions for further research. Additionally, the computational tool presented in this research could find other applications. This research also stimulates the focus on sustainability and reuse. This could be seen also as beneficial for societal value.

Within this research all data that is used is communicated in a transparent way. Stated knowledge is always backed by literature. When data differs between sources it is clearly explained why one value is chosen over another. The internal working of used algorithms and the process of testing is explained step by step to give full insight into the process that preceded the results. Therefore this research could be reproduced.

When looking at the applicability of this research to real building practice it needs to be admitted that this still needs some work. For now the designed tool is most useful in the early design phase. It can give the designer an overview and insight into what members could be interesting to harvest and are beneficial for the total emissions of the structure. The computational tool could for example handle large databases of possible reuse members and pick the ones that make a difference. Extensive structural analysis of nodes and members still need to be applied in later design phases. In terms of accessibility of the computational tool itself it could be said that with some Grasshopper knowledge it can be operated by someone other than the author of this research. In the script all variables and results are clearly indicated and therefore no knowledge about the working of the script itself is necessary.

Overall the collaboration with Octatube was an added value to this research. Mostly for practical questions such as glass sizes or determining load cases the company could always be contacted. They also granted full access to needed documentation. Reflecting on the overall process Octatube could have been involved more by keeping them updated on the current status of the research.

Lastly, reflecting on the computational aspect of this research. The combination of computational complexity and time pressure ended up being somewhat tricky. Because this research included some time-consuming optimization runs it was key to have some certainty that everything is set correctly before running. A small mistake in the computational workflow can already lead to incorrect results and this is something that is noticed after taking an in-depth look into the data.

6. Figures

Figure 1 - Schwedler dome on the Gasometer in Vienna circa. 1896 (Schober, 2015).....	9
Figure 2 - a. Cone, b. Ellipsoid, c. Hyperbolic (Gokul Santosh et al., 2022).....	14
Figure 3 - diagrid, lattice and geodesic setup (Bouleau et al., 2019).....	14
Figure 4 - example of a Kagome grid pattern.....	15
Figure 5 - influence of gridshell topology on node design (Stephan et al., 2004).....	16
Figure 6 - different node options (Stephan, 2022).....	16
Figure 7 - steel printed node combined with the VISS profiles (Study Jansen VISS3, n.d.).....	17
Figure 8 - examples of gridshells following the gridpattern, sources: Octatube, n.d., NEY+partners, n.d., AURA Foto Film Verlag, 2022.....	17
Figure 9 - the roof trusses of the stadium made out of reused steel (International Olympic Committee, 2013).....	19
Figure 10 - the process of estimation of mechanical properties (Fujita & Kuki, 2016).....	20
Figure 11 - phases taken into account for the calculation of GHG (Brütting, Senatore, et al., 2020).....	22
Figure 12 - Phoenix3D components defining the stock (Warmuth et al., 2021).....	23
Figure 13 - examples of 1D, 2D and 3D elements in a structure (Andriotis, 2022).....	25
Figure 14 - difference in complexity, (L) Richardson et al., 2013 and (R) Gythiel & Schevenels, 2022.....	27
Figure 15 - (a) initial surface, (b) random points, (c) bubble-packing equilibrium, (d) 3D Voronoi, (e) 2D Voronoi projection, (f) Delaunay triangulation (Wang, Gao & Wu, 2019).....	28
Figure 16 - workflow of the stock-constrained design optimization tool (Warmuth et al., 2021).....	29
Figure 17 - error message when testing a gridshell topology.....	29
Figure 18 - approach that is suggested by Grande et al. (2018).....	30
Figure 19 - the knowledge gaps that were found according the literature research.....	33
Figure 20 - overview of the in this research developed computational tool.....	35
Figure 21 - plugins used in Grasshopper.....	36
Figure 22 - calculation of the highest load in the line load.....	37
Figure 23 - in green the line load as illustrated by Karamba3D.....	37
Figure 24 - free movement of the supports in the gridshell structure.....	37
Figure 25 - x and y of the triangles.....	38
Figure 26 - illustration of the stockpile-, deconstruction- and new production scenario.....	39
Figure 27 - illustration of the node and how the mass is calculated.....	41
Figure 28 - the geometries of the glass panes nested in a rectangle.....	42
Figure 29 - the overall dimensions of the gridshell.....	43
Figure 30 - 1/4 th of the gridshell overall shape generated by the points.....	44
Figure 31 - principle of the bubble-packing method with the use of Kangaroo 2, Piker (2021).....	44
Figure 32 - illustration of the boundary (pink) of the movement of points over the z-axis.....	45
Figure 33 - results of testing Galapagos (left) and results of testing GOAT, CRS2 (right).....	47
Figure 34 - different parameters available in Galapagos.....	48
Figure 35 - showing the sequence in which the finite element analysis are used.....	48
Figure 36 - checking the intersection of curves and mesh.....	49
Figure 37 - interface of Design Explorer.....	50
Figure 38 - optimization from singular cross-sections to optimized cross-sections.....	52
Figure 39 - top left: distribution emissions beam members single cross-section all new scenario, top right: distribution emissions beam members optimized cross-section all new scenario, bottom left: distribution emissions beam members optimized cross-section deconstruction scenario, bottom right: distribution emissions beam members optimized cross-section stockpile scenario.....	53
Figure 40 - left: the starting point of the optimized gridshell, right: the regular gridshell.....	53
Figure 41 - distribution of the emissions for the beam members with different stock-sizes.....	56
Figure 42 - distribution emissions focused on stock from left to right: truck (70-km), truck (7000-km), air (70-km) and air (7000-km).....	57
Figure 43 - distribution of emissions for beam members within the case-study.....	59
Figure 44 - illustration of the starting position of the analysed truss.....	60

Figure 45 – flowchart indicating the steps of reuse in steel.....	74
Figure 46 - testing techniques presented in Girao Coelho et al. (2020).....	75
Figure 47 - a comprehensive mapping of all phases that are included in the recycling and the reuse of steel (Yeung et al., 2016).....	76
Figure 48 - assignment formulations (Brütting, Senatore, et al., 2020).....	77
Figure 49 - mapping of gridshell topology optimization research.....	78
Figure 50 - definition of stock, used as input in the computational tool.....	80
Figure 51 – illustration of the objective of all generated designs for the comparison of scenarios.....	101
Figure 52 - top left: distribution of emissions for the single cross-section gridshell, top right: distribution of emissions for the cross-section optimized gridshell all new scenario, bottom left: distribution of emissions for the cross-section optimized gridshell all deconstruction scenario, bottom right: distribution of emissions for the cross-section optimized gridshell all stockpile scenario.....	101
Figure 53 - illustration of a medium sized stock assigned to the regular gridshell structure where black indicates new beam members and lime green indicates reused beam members.....	102
Figure 54 - illustration of the objective of all generated designs for a small stock-size and illustration of stock assigned to the structure where black indicates new beam members and lime green indicates reused beam members.....	103
Figure 55 - illustration of the objective of all generated designs for a large stock-size and illustration of stock assigned to the structure where black indicates new beam members and lime green indicates reused beam members.....	104
Figure 56 - illustration of the objective of all generated designs for a medium stock-size and illustration of stock assigned to the structure where black indicates new beam members and lime green indicates reused beam members.....	104
Figure 57 - total distribution of greenhouse gas emissions over the different stock sizes and gridshell structures, from top to bottom: small-, medium- and large stock-size.....	105
Figure 58 – illustration of the context used within the case-study.....	106
Figure 59 - illustration of the objective of all generated designs for a hybrid stock and illustration of stock assigned to the structure where black indicates new beam members, lime green indicates reused beam members and light blue indicates beam members from stockpile.....	107
Figure 60 - distribution of the emissions within the gridshell of the case-study.....	107
Figure 61 - example of how Phoenix3D is built up in Grasshopper (Phoenix3D, n.d.).....	108
Figure 62 – illustration of the Grasshopper script making the computational tool of this research.....	113
Figure 63 - zoom in on part 1 of the Grasshopper script.....	114
Figure 64 - zoom in on part 2 of the Grasshopper script.....	115
Figure 65 - zoom in on part 3 of the Grasshopper script.....	116
Figure 66 - zoom in on part 4 of the Grasshopper script.....	116
Figure 67 - zoom in on part 5 of the Grasshopper script.....	117
Figure 68 - zoom in on part 6 of the Grasshopper script.....	117
Figure 69 - zoom in on part 7 of the Grasshopper script.....	118
Figure 70 - zoom in on part 8 of the Grasshopper script.....	119
Figure 71 - zoom in on part 9 of the Grasshopper script.....	120
Figure 72 - all new production scenario single cross-section.....	123
Figure 73 - all new production scenario optimized cross-sections.....	123
Figure 74 – standardized gridshell pattern single cross-section.....	124
Figure 75 – standardized gridshell pattern assignment small stock.....	124
Figure 76 - standardized gridshell pattern assignment medium stock.....	125
Figure 77 - standardized gridshell pattern assignment large stock.....	125
Figure 78 - optimized gridshell pattern assignment small stock.....	126
Figure 79 - optimized gridshell pattern assignment medium stock.....	126
Figure 80 - optimized gridshell pattern assignment large stock.....	127
Figure 81 – case-study assignment hybrid stock (all scenarios).....	127

7. Bibliography

- Addis, W., & Addis, W. (2006). *Building with Reclaimed Components and Materials: A Design Handbook for Reuse and Recycling*. Earthscan.
- Adriaenssens, S., Block, P., Veenendaal, D., & Williams, C. J. K. (2014). *Shell Structures for Architecture: Form Finding and Optimization*. Routledge.
- Allner, L., Kroehnert, D., & Rossi, A. (2019). Mediating Irregularity: Towards a Design Method for Spatial Structures Utilizing Naturally Grown Forked Branches. *O* 433–445(1).
https://doi.org/10.1007/978-3-030-29829-6_34
- Andriotis, C. P. (n.d.). Fundamentals of Finite Elements - 1 [Slide show]. brightspace.tudelft.nl.
<https://brightspace.tudelft.nl/d2l/le/content/536745/viewContent/3008588/View>
- Anemone. (2022, May 17). *Food4Rhino*. <https://www.food4rhino.com/en/app/anemone>
- AURA Foto Film Verlag. (2022, February 4). Atrium roof in Basel. structurae.net.
<https://structurae.net/en/media/372390-atrium-roof-in-basel>
- Bekker, A. C., & Verlinden, J. C. (2018). Life cycle assessment of wire + arc additive manufacturing compared to green sand casting and CNC milling in stainless steel. *Journal of Cleaner Production*, 177(1), 438–447. <https://doi.org/10.1016/j.jclepro.2017.12.148>
- Bertin, I., Saadé, M., Le Roy, R., Jaeger, J. M., & Feraille, A. (2022). Environmental impacts of Design for Reuse practices in the building sector. *Journal of Cleaner Production*, 349(1), 131228.
<https://doi.org/10.1016/j.jclepro.2022.131228>
- Bouleau, E., Isvoranu, F., Panetta, J., & Pauly, M. (2019). *X-Shell, a new spatial deployable lattice compared to traditional reticulated shells*. Proceedings of the IASS Annual Symposium 2019 — Structural Membranes.
- Brütting, J., De Wolf, C., & Fivet, C. (2019). The reuse of load-bearing components. *IOP Conference Series: Earth and Environmental Science*, 225(1), 012025. <https://doi.org/10.1088/1755-1315/225/1/012025>
- Brütting, J., Ohlbrock, P. O., Hofer, J., & D'Acunto, P. (2021). Stock-constrained truss design exploration through combinatorial equilibrium modeling. *International Journal of Space Structures*, 36(4), 253–269. <https://doi.org/10.1177/09560599211064100>
- Brütting, J., Senatore, G., & Fivet, C. (2021). Design and fabrication of a reusable kit of parts for diverse structures. *Automation in Construction*, 125(1), 103614.
<https://doi.org/10.1016/j.autcon.2021.103614>
- Brütting, J., Senatore, G., Schevenels, M., & Fivet, C. (2020). Optimum Design of Frame Structures From a Stock of Reclaimed Elements. *Frontiers in Built Environment*, 6(1).
<https://doi.org/10.3389/fbuil.2020.00057>
- Brütting, J., Vandervaeren, C., Senatore, G., De Temmerman, N., & Fivet, C. (2020). Environmental impact minimization of reticular structures made of reused and new elements through Life Cycle Assessment and Mixed-Integer Linear Programming. *Energy and Buildings*, 215(1), 109827.
<https://doi.org/10.1016/j.enbuild.2020.109827>
- Buelow P., Oliyan Torghabehi O., Mankouche S., & Vliet K. (2018). In Combining parametric form generation and design exploration to produce a wooden reticulated shell using natural tree crotches. (Eds.), Proceedings of the IASS Symposium 2018.

- Bukauskas A., Shepherd P., Walker P., Sharma B., & Bregula J. (2017). *In Form-Fitting Strategies for Diversity-Tolerant Design*. (Eds.), Proceedings of the IASS Annual Symposium 2017. International Association for Shell and Spatial Structures (IASS). https://www.researchgate.net/publication/320011783_Form-Fitting_Strategies_for_Diversity-Tolerant_Design
- Burczyński, T., Kuś, W., Beluch, W., Długosz, A., Poteralski, A., & Szczepanik, M. (2020). *Intelligent Computing in Optimal Design*. Springer Publishing.
- Chilton, J., & Chuang, C. C. (2017). Rooted in Nature: Aesthetics, Geometry and Structure in the Shells of Heinz Isler. *Nexus Network Journal*, 19(3), 763–785. <https://doi.org/10.1007/s00004-017-0357-5>
- Cichocka, J. M., Migalska, A., Browne, W. N., & Rodriguez, E. (2017). SILVEREYE – The Implementation of Particle Swarm Optimization Algorithm in a Design Optimization Tool. *Communications in Computer and Information Science*, 151–169. https://doi.org/10.1007/978-981-10-5197-5_9
- Cleveland Steel & Tubes Ltd. (2022). *Greener Steel*. In cleveland-steel.com. Retrieved January 12, 2023, from <https://cleveland-steel.com/sustainability>
- Cleveland Steel & Tubes Ltd. (2022). *Stocklist Q4 2022*. In cleveland-steel.com. Retrieved January 14, 2023, from <https://cleveland-steel.com/our-range-steel-tube-stock>
- Clifford, B., McGee, W., & Muhonen, M. (2018). Recovering Cannibalism in Architecture with a Return to Cyclopean Masonry. *Nexus Network Journal*, 20(3), 583–604. <https://doi.org/10.1007/s00004-018-0392-x>
- Colabella, S., Bernardino, D., Fivet, C., & Hoxha, E. (2017). Structural Design with Reclaimed Materials: an Elastic Gridshell out of Skis. &U>Interfaces: Architecture, Engineering, Science, Annual Meeting of the International Association of Shell & Spatial Structures (IASS), Hamburg, 25-27 September 2017, 1. &span><https://findanexpert.unimelb.edu.au/scholarlywork/1387869-structural-design-with-reclaimed-materials--an-elastic-gridshell-out-of-skis>
- Den Hollander, J. P. (2018). CE-markering en hergebruik van staal. In duurzamemetaalbouw.nl (No. 401007). Keten Beleids Groep. Retrieved December 4, 2022, from <https://duurzamemetaalbouw.nl/project/ce-markering-en-hergebruik-van-staal/>
- Design Explorer | Thornton Tomasetti. (n.d.). <https://www.thorntontomasetti.com/capability/design-explorer>
- Dyvik, S. H., Manum, B., & Rønnquist, A. (2021). Gridshells in Recent Research—A Systematic Mapping Study. *Applied Sciences*, 11(24), 11731. <https://doi.org/10.3390/app112411731>
- Ekici, B. (2022). *A+BE Architecture and the Built Environment - Towards -Self--Sufficient High-Rises: Performance Optimisation using Artificial Intelligence* (22nd ed.). TU Delft. <https://doi.org/10.7480/abe.2022.10>
- Feng, R. Q., Yao, B., & Ye, J. H. (2011). The Stability of Elliptic Paraboloid Grid Shell Lighting Roofs with Semi-Rigid Joints. *Advanced Materials Research*, 374–377, 2148–2151. <https://doi.org/10.4028/www.scientific.net/amr.374-377.2148>
- Fivet, C., & Brütting, J. (2020). Nothing is lost, nothing is created, everything is reused: structural design for a circular economy. *The Structural Engineer: Journal of the Institution of Structural Engineer*, 98(1), 74–81.

- Franco, J. T. (2022, December 22). How to Choose the Right Glass for Your Projects. ArchDaily. <https://www.archdaily.com/918008/how-to-choose-the-right-glass-for-your-projects>
- Fujita, M., & Kuki, K. (2016). An Evaluation of Mechanical Properties with the Hardness of Building Steel Structural Members for Reuse by NDT. *Metals*, 6(10), 247. <https://doi.org/10.3390/met6100247>
- Galapagos Optimization - TOI-Pedia. (n.d.). http://wiki.bk.tudelft.nl/toi-pedia/Galapagos_Optimization
- Girao Coelho, A. M., Pimentel, R., Ungureanu, V., Hradil, P., & Kesti, J. (2020). European Recommendations for Reuse of Steel Products in Single-Storey Buildings. In steelconstruct.com (No. 978-92-9147-170-6). ECCS – European Convention for Constructional Steelwork. Retrieved December 4, 2022, from https://www.steelconstruct.com/wp-content/uploads/PROGRESS_Design_guide_final-version.pdf
- Gokul Santosh, S., Singh, A. P., & Abdul Akbar, M. (2022). Parametric Studies and Optimization of Grid Shell Structures Using Genetic Algorithm. In Lecture Notes in Civil Engineering (Vol. 274). Springer. https://doi.org/10.1007/978-981-19-4055-2_10
- Gorgolewski, M. (2008). Designing with reused building components: some challenges. *Building Research & Information*, 36(2), 175–188. <https://doi.org/10.1080/09613210701559499>
- Gorgolewski, M. (2019). The architecture of reuse. IOP Conference Series: *Earth and Environmental Science*, 225(1), 012030. <https://doi.org/10.1088/1755-1315/225/1/012030>
- Grande, E., Imbimbo, M., & Tomei, V. (2018). Structural Optimization of Grid Shells: Design Parameters and Combined Strategies. *Journal of Architectural Engineering*, 24(1). [https://doi.org/10.1061/\(asce\)ae.1943-5568.0000286](https://doi.org/10.1061/(asce)ae.1943-5568.0000286)
- Granta Edupack (2022 R1). (2022). [Software]. Ansys. <https://www.ansys.com/products/materials/granta-edupack>
- Gythiel, W., & Schevenels, M. (2022). Gradient-based size, shape, and topology optimization of single-layer reticulated shells subject to distributed loads. *Structural and Multidisciplinary Optimization*, 65(5). <https://doi.org/10.1007/s00158-022-03225-w>
- He, L., & Gilbert, M. T. P. (2015). Rationalization of trusses generated via layout optimization. *Structural and Multidisciplinary Optimization*, 52(4), 677–694. <https://doi.org/10.1007/s00158-015-1260-x>
- Hopkinson, P., Chen, H. M., Zhou, K., Wang, Y., & Lam, D. (2019). Recovery and reuse of structural products from end-of-life buildings. *Proceedings of the Institution of Civil Engineers - Engineering Sustainability*, 172(3), 119–128. <https://doi.org/10.1680/jensu.18.00007>
- Huang, X., & Xie, M. (2010). *Evolutionary Topology Optimization of Continuum Structures: Methods and Applications*. Wiley.
- Jiang, Y., Zegard, T., Baker, W. F., & Paulino, G. H. (2017). Form-finding of grid-shells using the ground structure and potential energy methods: a comparative study and assessment. *Structural and Multidisciplinary Optimization*, 57(3), 1187–1211. <https://doi.org/10.1007/s00158-017-1804-3>
- Karamba3D. (2016, March 7). Retrieved January 17, 2023, from <https://www.karamba3d.com/>
- Kochenderfer, M. J., & Wheeler, T. A. (2019). *Algorithms for Optimization*. Amsterdam University Press.
- Kovacs, R., Seufert, A., Wall, L., Chen, H. T., Meinel, F., Müller, W., You, S., Brehm, M., Striebel, J., Kommana, Y., Popiak, A., Bläsius, T., & Baudisch, P. (2017). TrussFab. Proceedings of the 2017 CHI Conference on Human Factors in Computing Systems. <https://doi.org/10.1145/3025453.3026016>

- Ladipo, T., & Wild, W. (2022). How to calculate the embodied carbon of facades: A methodology. In www.cwct.co.uk (Issue 1). Centre of window and cladding technology. <https://www.cwct.co.uk/pages/embodied-carbon-methodology-for-facades>
- Li, Q. (2018). A+BE Architecture and the Built Environment #02-2018 - Form Follows Force: A theoretical framework for Structural Morphology, and Form-Finding research on shell structures (1st ed.). TU Delft.
- Li, Q., Su, Y., Wu, Y., Borgart, A., & Rots, J. G. (2017). Form-finding of shell structures generated from physical models. *International Journal of Space Structures*, 32(1), 11–33. <https://doi.org/10.1177/0266351117696577>
- Li, Z., Hu, B., Quan, G., Gao, B., & Wang, Q. (2022). A structured grid generation framework based on parameterization for the design of free-form gridshells. *Journal of Building Engineering*, 62(1), 105400. <https://doi.org/10.1016/j.jobee.2022.105400>
- Lyu, Y. (2022). *Finite Element Method: Element Solutions*. Springer Publishing.
- Madaster platform | Register materials and products. (2022, September 5). Madaster Global. Retrieved December 12, 2022, from <https://madaster.com/platform/>
- Marshall, D., Meuller, C., Clifford, B., & Kennedy, S. (2020). COMPUTATIONAL ARRANGEMENT OF DEMOLITION DEBRIS. *Detritus*, 11, 3–18. <https://doi.org/10.31025/2611-4135/2020.13967>
- McNeel Europe. (n.d.). Food4Rhino. www.food4rhino.com. Retrieved January 22, 2023, from <https://www.food4rhino.com/en>
- Mesnil, R., Douthe, C., & Baverel, O. (2017). Non-Standard Patterns for Gridshell Structures: Fabrication and Structural Optimization. *Journal of the International Association for Shell and Spatial Structures*, 58(4), 277–286. <https://doi.org/10.20898/j.iass.2017.194.893>
- Mesnil, R., Douthe, C., Baverel, O., & Léger, B. (2017). Linear buckling of quadrangular and kagome gridshells: A comparative assessment. *Engineering Structures*, 132(1), 337–348. <https://doi.org/10.1016/j.engstruct.2016.11.039>
- Min Max Size Guide | Oakland Glass. (2016, September 26). Oakland Glass. <https://oaklandglass.co.uk/min-max-size-guide/>
- Mixed-Integer Linear Programming (MILP) Algorithms. (n.d.). mathworks.com. Retrieved January 19, 2023, from <https://www.mathworks.com/help/optim/ug/mixed-integer-linear-programming-algorithms.html>
- NEN-EN 1991-1-3+C1+A1:2019 nl. (2019). In Eurocode 1: Belastingen Op Constructies (EN 1991-1-3). NEN. <https://www.nen.nl/nen-en-1991-1-3-c1-a1-2019-nl-263280>
- NEY+partners. (n.d.). Glass Roof Dutch Maritime Museum. Ney.Partners. <https://ney.partners/project/glass-roof-dutch-maritime-museum/>
- Octatube. (n.d.). C30 Shell. octatube.nl. https://www.octatube.nl/nl_NL/project-item/projectitem/216-c30-shell.html
- Octatube. (2021, July 8). C30. Retrieved December 28, 2022, from https://www.octatube.nl/nl_NL/project-item/projectitem/216-c30-shell.html
- On getting lucky in higher dimensions. (2012, June 12). I Eat Bugs for Breakfast. <https://ieatbugsforbreakfast.wordpress.com/2011/07/31/on-getting-lucky-in-higher-dimensions/>
- OpenNest. (2022, June 5). *Food4Rhino*. <https://www.food4rhino.com/en/app/opennest>

- Orr, J., Gibbons, O., & Arnold, W. (2020). A brief guide to calculating embodied carbon. *The Structural Engineer*, 24. <https://www.istructe.org/IStructE/media/Public/TSE-Archive/2020/A-brief-guide-to-calculating-embodied-carbon.pdf>
- Oval, R., Rippmann, M., Mesnil, R., Van Mele, T., Baverel, O., & Block, P. (2019). Feature-based topology finding of patterns for shell structures. *Automation in Construction*, 103(1), 185–201. <https://doi.org/10.1016/j.autcon.2019.02.008>
- Pearl, J. (1984). *Heuristics: Intelligent Search Strategies for Computer Problem Solving (First Printing)*. Addison-Wesley.
- Phoenix3D. (n.d.). epfl.ch. <https://www.epfl.ch/labs/sxl/index-html/tools/phoenix3d/>
- Piker, D. (2021, May). Compact circle packing on complex surface [Online forum post]. discourse.mcneel.com. <https://discourse.mcneel.com/t/compact-circle-packing-on-complex-surface/123707/3>
- Richardson, J. N., Adriaenssens, S., Filomeno Coelho, R., & Bouillard, P. (2013). Coupled form-finding and grid optimization approach for single layer grid shells. *Engineering Structures*, 52(1), 230–239. <https://doi.org/10.1016/j.engstruct.2013.02.017>
- Rombouts, J., Lombaert, G., De Laet, L., & Schevenels, M. (2019). A novel shape optimization approach for strained gridshells: Design and construction of a simply supported gridshell. *Engineering Structures*, 192(1), 166–180. <https://doi.org/10.1016/j.engstruct.2019.04.101>
- Rutten, D. (2016, February). Galapagos Run Time Limit Problem / Feature Request [Online forum post]. discourse.mcneel.com. <https://discourse.mcneel.com/t/galapagos-run-time-limit-problem-feature-request/29415>
- Rutten, D. (2019, November 27). Galapagos Future Plans [Online forum post]. McNeel Forum. <https://discourse.mcneel.com/t/galapagos-future-plans/92846>
- Schober, H. (2015). *Transparent Shells: Form, Topology, Structure*. Wiley.
- Stephan, S. (2022, September 12). Node Connectors and Their Influence on Free Form Structures. Novum Structures. https://novumstructures.com/eu/news_and_insights/node-connectors-and-their-influence-on-free-form-structures/
- Stephan, S., Sanchez-Alvarez, J., & Knebel, K. (Eds.). (2004). Reticulated Structures on Free-Form Surfaces. ResearchGate. https://www.researchgate.net/publication/228563882_Reticulated_Structures_on_Free-Form_Surfaces
- Study Jansen VISS<sup>3</sup>. (n.d.). Jansen. <https://www.jansen.com/en/building-systems-profile-systems-steel/topics/jansen-viss3.html>
- Summum Engineering. (n.d.). Circular algorithms. <https://www.summum.engineering/portfolio/circular-algorithms/>
- Van Der Linden, L. P. L. (2015). *Innovative joints for gridshells* [Masterscriptie]. TU Delft.
- Veenendaal, D., & Block, P. (2012). An overview and comparison of structural form finding methods for general networks. *International Journal of Solids and Structures*, 49(26), 3741–3753. <https://doi.org/10.1016/j.ijsolstr.2012.08.008>
- Waibel, C., Wortmann, T., Evins, R., & Carmeliet, J. (2019). Building energy optimization: An extensive benchmark of global search algorithms. *Energy and Buildings*, 187(1), 218–240. <https://doi.org/10.1016/j.enbuild.2019.01.048>

- Wang, Q., Gao, B., & Wu, H. (2019). Triangular mesh generation on free-form surfaces based on bubble dynamics simulation. *Engineering Computations*, 36(2), 646–663. <https://doi.org/10.1108/ec-09-2017-0352>
- Wang, Q. S., Ye, J., Wu, H., Gao, B. Q., & Shepherd, P. (2019). A triangular grid generation and optimization framework for the design of free-form gridshells. *Computer-Aided Design*, 113(1), 96–113. <https://doi.org/10.1016/j.cad.2019.04.005>
- Warmuth J., Brütting J., & Fivet C. (2021). In Computational tool for stock-constrained design of structures. (Eds.), Proceedings of the IASS Annual Symposium 2020/21 and the 7th International Conference on Spatial Structures. <https://www.researchgate.net/publication/354270307>
- Wolfram Research, Inc. (n.d.). Delaunay Triangulation -- from Wolfram MathWorld. <https://mathworld.wolfram.com/DelaunayTriangulation.html#:~:text=The%20Delaunay%20triangulation%20is%20a,94>.
- Wolsey, L. A., & Nemhauser, G. L. (1999). *Integer and Combinatorial Optimization*. Wiley.
- Wortmann, T. (2017, November 30). Scripting N stages optimizations with Galapagos / Other? [Online forum post]. McNeel Forum. <https://discourse.mcneel.com/t/scripting-n-stages-optimizations-with-galapagos-other/50498/3>
- Wortmann, T. (2018). Genetic evolution vs. function approximation: Benchmarking algorithms for architectural design optimization. *Journal of Computational Design and Engineering*, 6(3), 414–428. <https://doi.org/10.1016/j.jcde.2018.09.001>
- Wortmann T., Waibel C., Nannicini G., Evins R., Schroepfer T., & Carmeliet J. (2017). In *Are Genetic Algorithms Really the Best Choice for Building Energy Optimization?* (Eds.), SimAUD 2017 May 22-24 Toronto, Canada. <https://dl-acm-org.tudelft.idm.oclc.org/doi/10.5555/3289787.3289793>
- Ye, B., Wang, F., & Duan, Y. (2021). Considering Grid Division Optimization of Free-Form Surface Roof Structure. *IOP Conference Series: Earth and Environmental Science*, 719(2), 022037. <https://doi.org/10.1088/1755-1315/719/2/022037>
- Yeung, J., Walbridge, S., Haas, C., & Saari, R. (2016). Understanding the total life cycle cost implications of reusing structural steel. *Environment Systems and Decisions*, 37(1), 101–120. <https://doi.org/10.1007/s10669-016-9621-6>

8. Appendix

8.1 Reclaimed steel testing

The following flowchart was presented by Girao Coelho et al. (2020). Here all the steps are presented indicating when to reuse steel and what tests and checks need to be performed.

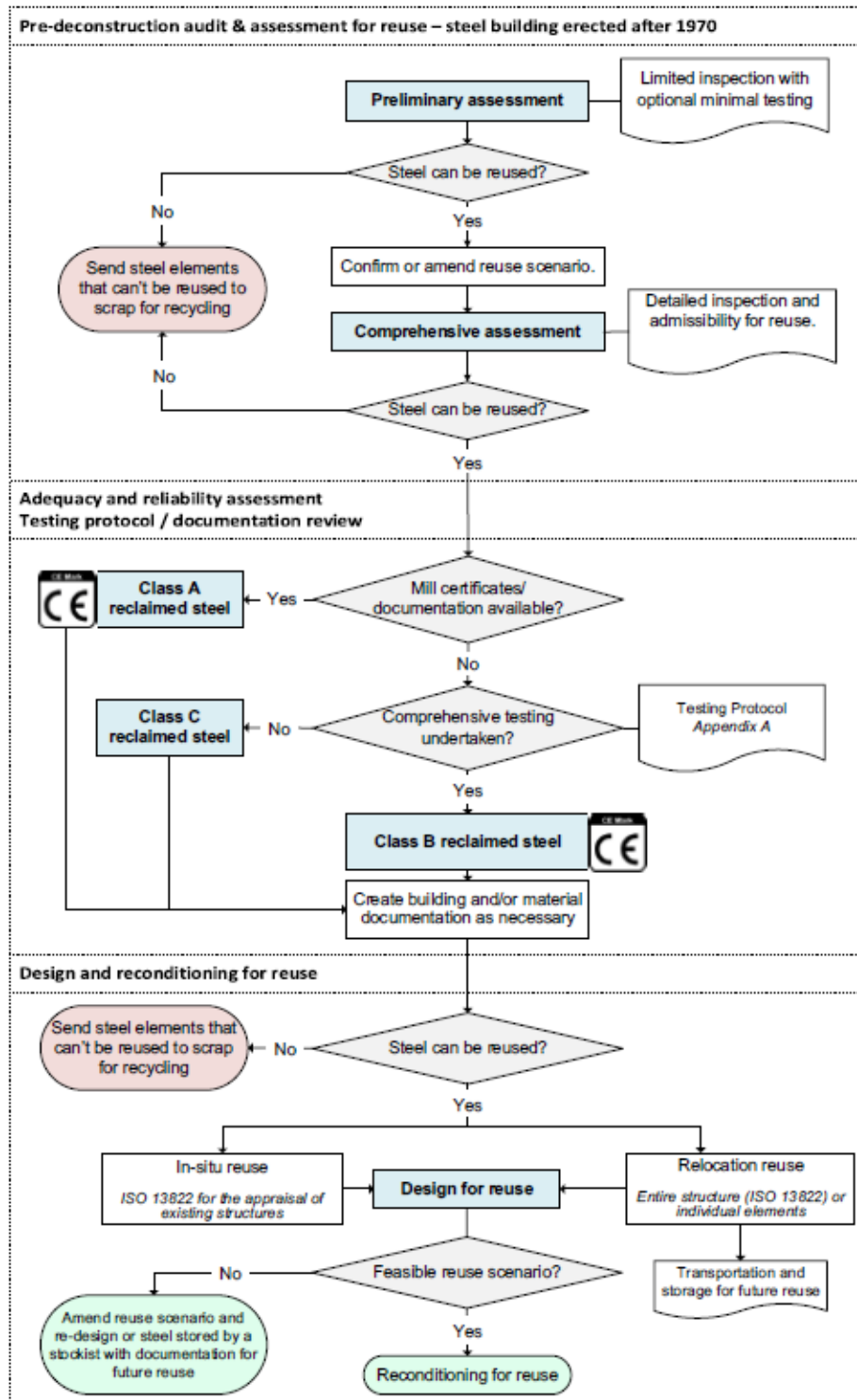


Figure 45 – flowchart indicating the steps of reuse in steel

In this report also a detailed description of all the testing techniques was provided. Here they also describe what mechanical properties are known after testing.

Technique	Description	Comments/Value
Hardness testing	Diameter of imprint measured when hardened steel ball is pressed against a smooth surface with known force.	Provides hardness number, e.g. Vickers according to ISO 6507 [158] hardness, which is a guide to yield and ultimate strength of the material. Vickers test method is stated on EN 1090-2. Other alternatives are Rockwell ISO 6508 [159] and Brinell ISO 6505 [160] test methods. See also ASTM 1038:2017 [161].
Positive metal identification	Uses X-ray Fluorescence and optical emission spectrometry to establish the metallic alloy composition, and grade identification by reading the quantities by percentage of its elements.	Essential for characterisation of weldability of steel structural members, as a function of the carbon equivalent. Provides additional information on the type and associated physical properties of steel and about its alloying materials. ISO 19272 [162]. See ASTM E572 [163] and ASTM 1476 [164].
Instrumented indentation testing	Instrumented indentation apparatus uses similar technique as hardness test with measured load and penetration in repeated loading and unloading cycles.	Output of the indentation test includes stress-strain relationship, elastic modulus, hardness and stiffness. See ISO 145775 [165].
Small punch testing	Small punch test uses ceramic ball pressed against the face of small circular specimen (diameter 8 mm, thickness 0.5 mm). The stress-strain relationship is then derived from the measured load versus ball displacement.	Calculation according to prEN 15627 [166] [167] can be used to predict yield and tensile strength of the steel. The equivalent stress-strain relationship of the tensile coupon may be obtained by more advanced Finite Element Modelling.

Technique	Description	Comments/Value
Tensile testing	Tensile tests on meaningful samples providing yield and ultimate tensile strength, modulus of elasticity, uniform elongation, and elongation at failure.	In the absence of material certificates. For test details see EN ISO 6892-1 [168].
Chemical composition analysis	Testing for carbon, silicon, manganese, sulphur, and phosphorus.	Essential for material identification and to check the weldability of the steel as a function of the carbon equivalent, as well as the impurity levels. Tests are carried out on drilling swarf or scrapings. It provides further information on the type and associated physical properties of steel. See EN ISO 14284 [169].
Charpy impact test	Brittleness and notch ductility at a range of temperatures determined by measuring the energy required to fracture a standard U- or V-notched sample with a blow from a pendulum.	Allows characterisation of the steel sub-grade when material certificates are not available. For test details see EN ISO 148-1 [170]. Impact toughness can be also tested on sub-sized specimen and the results recalculated to match the behaviour of the full-sized tests.
Metallography	Determination of the average grain size	Determination of internal structure of the material by microscopic examination of a sample with one flat surface. See ASTM E 112 [171].

Figure 46 - testing techniques presented in Girao Coelho et al. (2020)

8.2 Eco-impact calculation

A comprehensive mapping of all phases that are included in the recycling and the reuse of steel (Yeung et al., 2016).

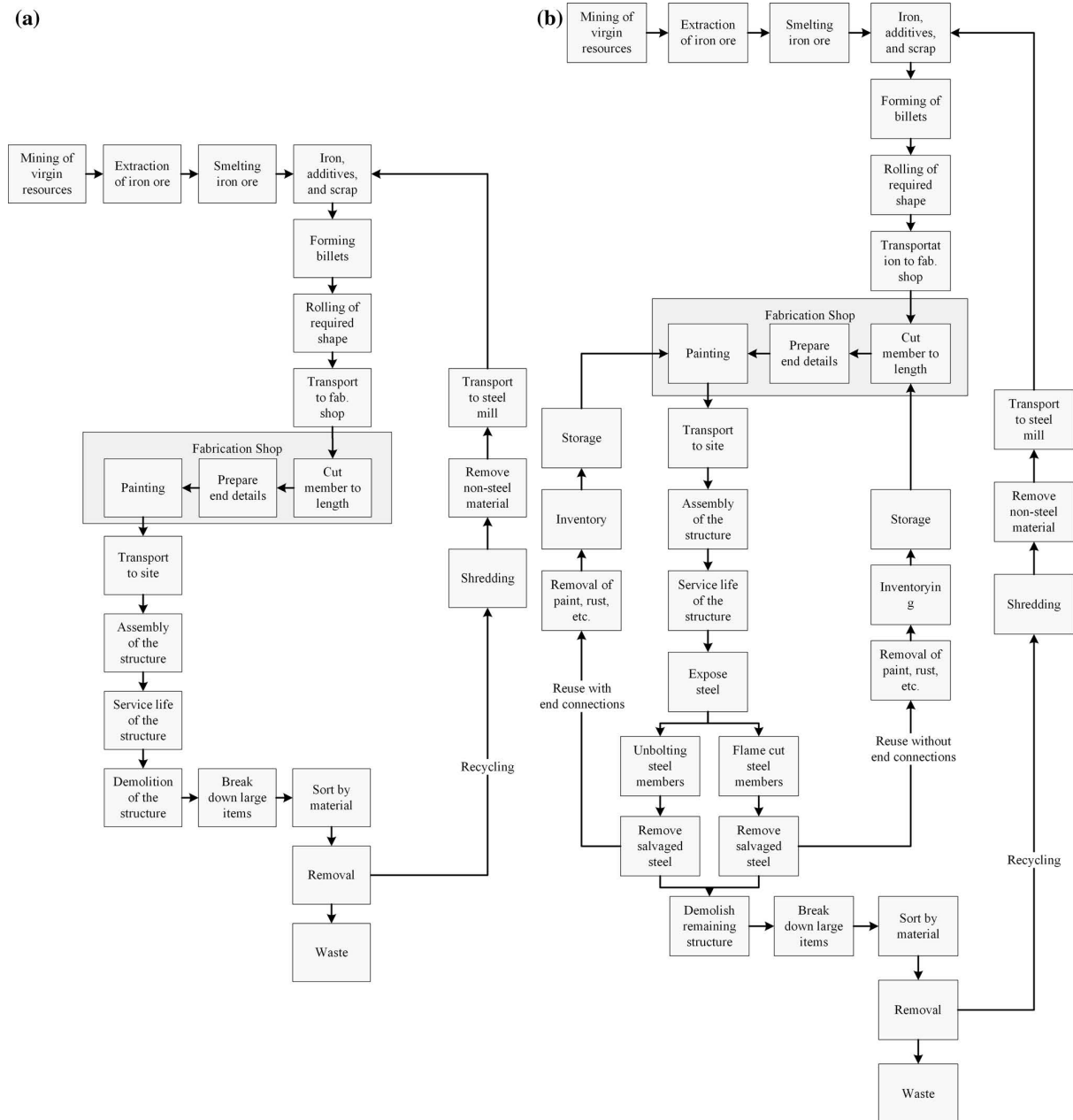


Figure 47 - a comprehensive mapping of all phases that are included in the recycling and the reuse of steel (Yeung et al., 2016)

In Brütting, Senatore, et al., (2020) two different assignment formulations are used (fig. 48). In formulation A the stock is grouped and the most suitable member will be assigned to the structure. Formulation B is an extension of formulation A. Here stock is efficiently cut. Every member is treated individually.

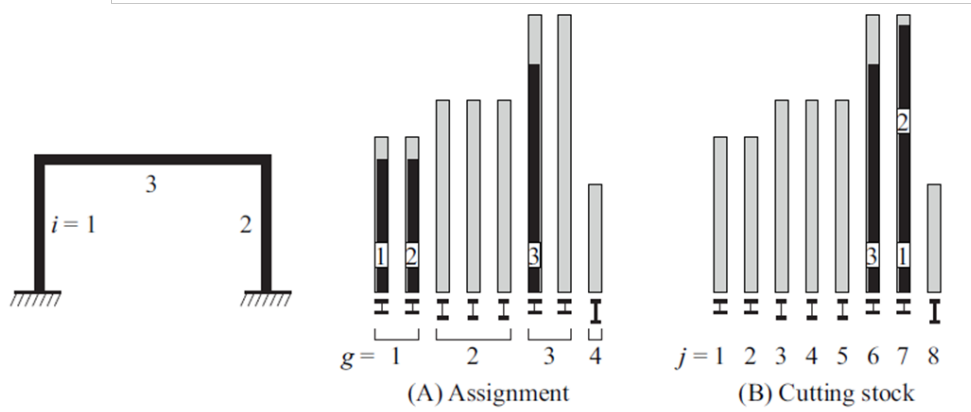


Figure 48 - assignment formulations (Brütting, Senatore, et al., 2020)

The GHG emissions [kgCO_{2eq}] with formulation A are calculated as follows:

$$GHG_{Reuse}^A = \sum_{i=1}^m \sum_{g \in S} t_{ig} c_{ig}^A$$

Whereby c_{ig}^A sums up all the emissions for deconstruction and transport and is formulated as:

$$c_{ig}^A = l_g a_g \rho_g * (EC^{DC} + EC^T d_{Reu}) + \bar{l}_i a_g \rho_g * (EC^A + EC^T d_S) + (l_g - \bar{l}_i) a_g \rho_g EC^T d_W$$

Whereby t_{ig} indicates if there is a member from the group assigned to a certain location.

The GHG emissions [kgCO_{2eq}] with formulation B are calculated as follows:

$$GHG_{Reuse}^B = \sum_{j \in S} y_j c_j^B + \sum_{i=1}^m \sum_{j \in S} t_{ij} c_{ij}^B$$

Whereby c_j^B sums up all the emissions for deconstruction and is formulated as:

$$c_j^B = l_j a_j \rho_j * (EC^{DC} + EC^T d_{Reu} + EC^T d_W)$$

Whereby c_{ij}^B sums up all the emissions for the transport and assembly of the frame and is formulated as:

$$c_{ij}^B = \bar{l}_i a_j \rho_j * (EC^T d_S + EC^A - EC^T d_W)$$

Whereby y_j indicates if the member is at least partly used ($y_j = 1$) or not ($y_j = 0$).

The sum of the total GHG emissions of new stock is formulated as follows:

$$GHG_{New} = Mass * (EC^{DM} + EC^P + EC^A + EC^T (d_{Rec} + d_P + d_S))$$

The following values are used for the GHG coefficients (EC).

Table 8 - all GHG coefficients

	Coefficient	Process name	Unit	GHG emission [kgCO _{2eq}]/unit
Deconstruction	EC ^{DC}	Total	[kg]	0.337
		Opening connections	[kg]	0.188
		Hoisting crane	[kg]	0.110
		Preparation and loading	[kg]	0.039

Demolition	EC ^{DM}	Total	[kg]	0.050
		Demolition	[kg]	0.031
		Preparation and loading	[kg]	0.019
New Production	EC ^P	Production of steel profiles	[kg]	0.734
Assembly	EC ^A	Hoisting crane	[kg]	0.110
Transport	EC ^T	Transport by truck	[kg*km]	1.1*10 ⁻⁴

8.3 Structural optimization

The diagram below summarizes the literature study conducted to gain knowledge of the different methods of topology optimization within gridshell structures. The second row indicates whether it is rationalization-based or structural-based optimization. The third row indicates all the sources. And the last row indicates all the objectives. In the text top left the search query is described with the additional constraints. Additionally, the database of sources from the systematic mapping research conducted by Dyvik (2021) was used.

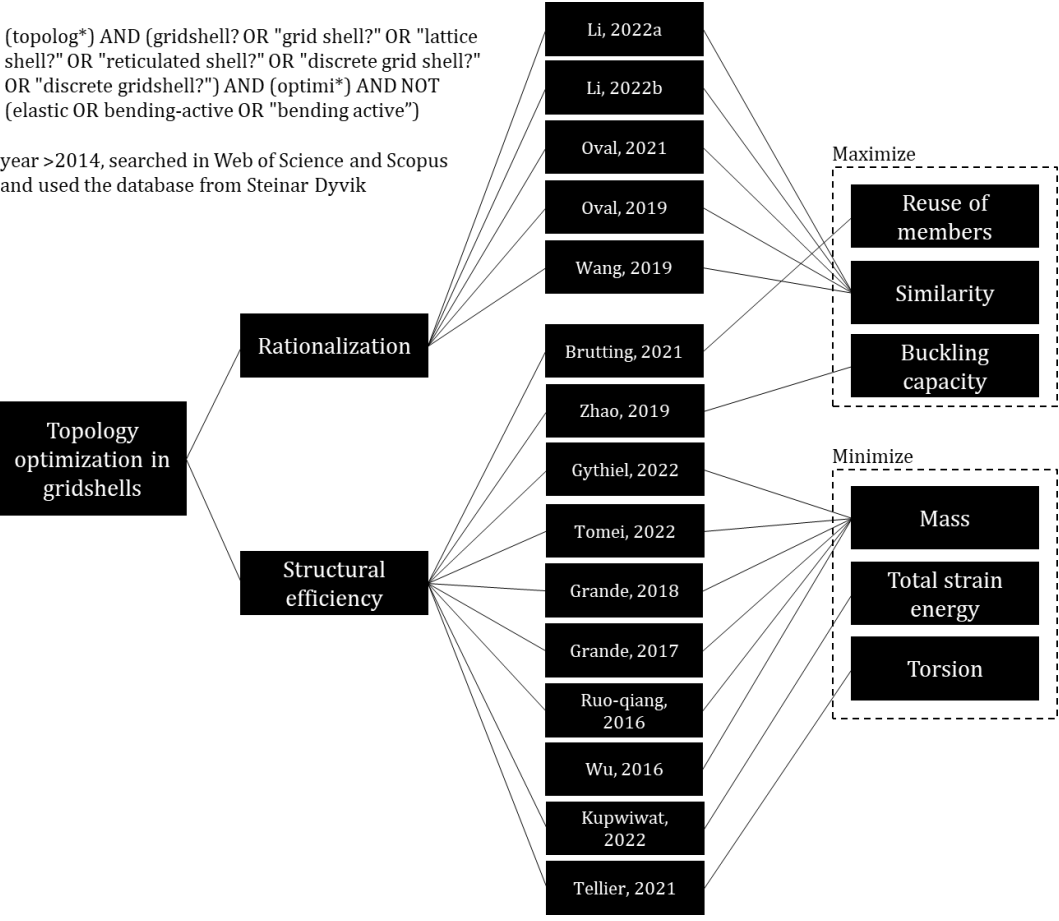


Figure 49 - mapping of gridshell topology optimization research

All methods that were tested by Bukauskas et al. (2017):

- FF: First-Fit, no pre-sorting;
- FFDL: First-Fit, pre-sorting members by length, no pre-sorting of bins;

- FFDE: First-Fit, pre-sorting members on effect (decreasing, resistance to tension/compression), no pre-sorting of bins;
- FFDL/L: First-Fit, pre-sorting members by length, pre-sorting of bins by length;
- FFDL/E: First-Fit, pre-sorting members by length, pre-sorting of bins by resistance;
- FFDE/L: First-Fit, pre-sorting members on effect (decreasing, resistance to tension/compression), pre-sorting of bins by length;
- FFDE/E: First-Fit, pre-sorting members on effect (decreasing, resistance to tension/compression), pre-sorting of bins by resistance;
- BF(L): Best-Fit, objective defined by minimizing remaining length;
- BF(E): Best-Fit, objective defined by maximizing utilization;
- BFDL(L): Best-Fit, pre-sorting members by length, minimizing remaining length;
- BFDL(E): Best-Fit, pre-sorting members by length, maximizing utilization;
- BFDE(L): Best-Fit, pre-sorting members on effect (decreasing, resistance to tension/compression), minimizing remaining length;
- BFDE(E): Best-Fit, pre-sorting members on effect (decreasing, resistance to tension/compression), maximizing utilization.

8.4 Definition of stock in Excel

Here an example is shown of the information that can be filled in Excel that defines the stock. Within the dashed boxes all values are filled in related to the properties of the stock. Everything marked with yellow is calculated automatically, the rest needs to be filled in by the user. All values that are not in the dashed boxes are related to the transport within the different phases. The reason why the transportation options are so extensive is because it includes a lot of variables. First, the total distance can be filled in followed by the main mode of transportation and the secondary mode of transportation. This needs to be filled in for every phase of the scenarios.

group [g]	member [j]	length initial [cm]	thickness [cm]	radius [cm]	area [cm ²]	steelgrade	density [kg/cm ³]
1	1	450	0.25	1.7	2.7	S235	0.00781
2	2	450	0.25	2.4	3.8	S275	0.00783
3	3	#####	0.32	2.4	4.8	S355	0.00783
yieldstrengt h [kN/cm ²]	type	scenario	#1 [km]	#1 main [type]	GHG co	#1 main [%*10 ⁻²]	#1 secon. [type]
23.5	reuse	reconstruction	70	ty_tonne_tru	0	1	nothing
27.5	reuse	stockpile	70	ty_tonne_tru	0	1	nothing
35.5	new	new_production	70	ty_tonne_tru	0	1	nothing
GHG co	#1 secon. [%*10 ⁻²]	#2 [km]	#2 main [type]	GHG co	#2 main [%*10 ⁻²]	#2 secon. [type]	GHG co
0	0	70	ty_tonne_tru	0	1	nothing	0
0	0	70	ty_tonne_tru	0	1	nothing	0
0	0	70	ty_tonne_tru	0	1	nothing	0
#2 secon. [%*10 ⁻²]	#3 [km]	#3 main [type]	GHG co	#3 main [%*10 ⁻²]	#3 secon. [type]	GHG co	#3 secon. [%*10 ⁻²]
0	70	ty_tonne_tru	0	1	nothing	0	0
0	70	ty_tonne_tru	0	1	nothing	0	0
0	70	ty_tonne_tru	0	1	nothing	0	0
#4 [km]	#4 main [type]	GHG co	#4 main [%*10 ⁻²]	#4 secon. [type]	GHG co	#4 secon. [%*10 ⁻²]	#5 [km]
15	ty_tonne_tru	0	1	nothing	0	0	70
15	ty_tonne_tru	0	1	nothing	0	0	70
15	ty_tonne_tru	0	1	nothing	0	0	70
#5 main [type]	GHG co	#5 main [%*10 ⁻²]	#5 secon. [type]	GHG co	#5 secon. [%*10 ⁻²]	#6 [km]	#6 main [type]
ty_tonne_tru	0	0.64	ocean_freigh	0	0.36	10	ty_tonne_tru
ty_tonne_tru	0	0.64	ocean_freigh	0	0.36		
ty_tonne_tru	0	0.64	ocean_freigh	0	0.36		
GHG co	#6 main [%*10 ⁻²]	#6 secon. [type]	GHG co	#6 secon. [%*10 ⁻²]			
0	1	nothing	0	0			

Figure 50 - definition of stock, used as input in the computational tool

8.5 Comparison scenarios

Table 9 illustrates all unique certified cross-sections available in the stock database from Cleveland Steel & Tubes (2022) followed by the material properties taken into account for the different steel grades. The properties for grades S235, S275 and S355 steel are used for the beam members and the 308L grade is used for WAAM manufacturing and thus calculation of the nodes emissions.

Table 9 – overview of all stock cross-sections available from Cleveland Steel & Tubes (2022)

Steel grade	Thickness [cm]	Radius [cm]	Area [cm ²]
S235	0,25	1,7	3
S235	0,25	2,4	4
S355	0,32	2,4	5
S355	0,9	2,4	14
S235	0,29	3	5
S235	0,3	3	6
S235	0,32	3	6
S235	0,25	3,8	6
S355	0,6	4,45	17
S355	0,76	4,45	21
S355	1,75	4,45	49
S235	0,36	5,1	12
S235	0,4	5,1	13
S355	0,6	5,1	19
S355	2,22	5,7	80
S355	1,9	5,9	70
S235	0,3	7	13
S355	1,27	8,4	67
S355	1,27	8,9	71
S355	0,95	10,95	65
S235	1	10,95	69
S355	1	10,95	69
S355	1,43	10,95	98

General information

Designation

Structural steel, S235J, wrought	
Condition	Hot rolled
EN name	S235JR, S235J0, S235J2
EN number	1.0038, 1.0114, 1.0117

Typical uses

Welded non-critical structures, general mechanical engineering, automotive components, construction, automotive, tools, axles, gears, springs, ships, rolling stocks, petroleum storage tanks, containers, open die forgings, frames for presses, heating plates for presses	
Included in Materials Data for Simulation	✓
Materials Data for Simulation name	Structural steel, S235J

Composition overview

Compositional summary

Fe98-100 (impurities: Mn<1.4, Cu<0.55, C<0.2, P<0.035, S<0.035, N<0.012)	
Material family	Metal (ferrous)
Base material	Fe (Iron)

Composition detail (metals, ceramics and glasses)

C (carbon)	0	-	0,2	%
Cu (copper)	0	-	0,55	%
Fe (iron)	* 97,8	-	100	%
Mn (manganese)	0	-	1,4	%
N (nitrogen)	0	-	0,012	%
P (phosphorus)	0	-	0,035	%
S (sulfur)	0	-	0,035	%

Price

Price	* 0,649	-	0,852	EUR/kg
Price per unit volume	* 5,06e3	-	6,72e3	EUR/m ³

Physical properties

Density	7,81e3	-	7,89e3	kg/m ³
---------	--------	---	--------	-------------------

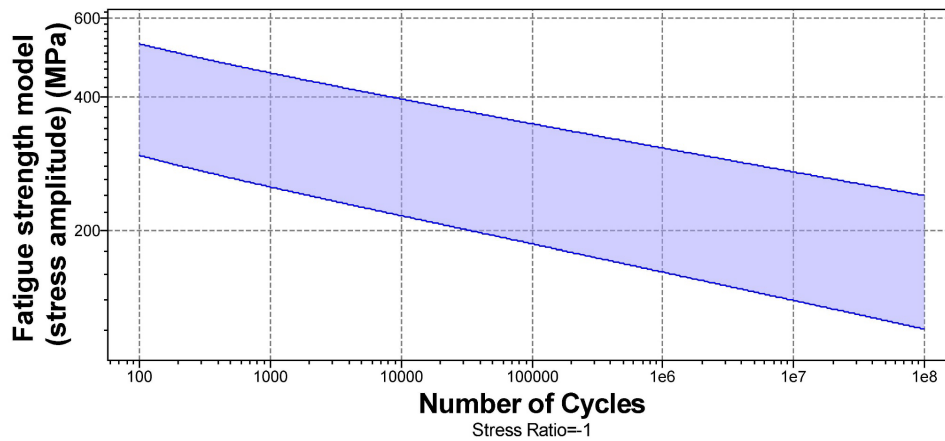
Mechanical properties

Young's modulus	205	-	215	GPa
Specific stiffness	* 26,1	-	27,4	MN.m/kg
Yield strength (elastic limit)	235	-	274	MPa
Notes	These values are applicable for minimum thickness for this grade.			
Tensile strength	360	-	510	MPa
Notes	These values are applicable for minimum thickness for this grade.			
Specific strength	* 29,9	-	34,9	kN.m/kg
Elongation	17	-	26	% strain
Tangent modulus	1,18e3			MPa
Compressive modulus	* 205	-	215	GPa

Values marked * are estimates.
ANSYS, Inc. provides no warranty for this data.

Compressive strength	* 235	-	274	MPa
Flexural modulus	* 205	-	215	GPa
Flexural strength (modulus of rupture)	* 225	-	319	MPa
Shear modulus	* 78,9	-	82,7	GPa
Shear strength	* 136	-	158	MPa
Bulk modulus	* 171	-	179	GPa
Poisson's ratio	0,3			
Shape factor	63			
Hardness - Vickers	* 107	-	152	HV
Hardness - Brinell	100	-	154	HB
Elastic stored energy (springs)	* 132	-	178	kJ/m ³
Fatigue strength at 10 ⁷ cycles	* 180	-	210	MPa
Fatigue strength model (stress amplitude)	* 140	-	271	MPa

Parameters: Stress Ratio = -1, Number of Cycles = 1e7cycles



Impact & fracture properties

Fracture toughness	* 45,5	-	55	MPa.m ^{0.5}
Toughness (G)	* 9,93	-	14,3	kJ/m ²

Thermal properties

Melting point	1,48e3	-	1,53e3	°C
Maximum service temperature	* 473	-	519	°C
Minimum service temperature	* -56,8	-	-46,8	°C
Thermal conductivity	40	-	57,4	W/m.°C
Specific heat capacity	460	-	480	J/kg.°C
Thermal expansion coefficient	11,5	-	12,5	µstrain/°C
Thermal shock resistance	* 92,2	-	110	°C
Thermal distortion resistance	* 3,32	-	4,81	MW/m
Latent heat of fusion	* 343	-	364	kJ/kg

Electrical properties

Electrical resistivity	18,3	-	18,5	µohm.cm
------------------------	------	---	------	---------

Values marked * are estimates.
ANSYS, Inc. provides no warranty for this data.

Electrical conductivity	9,32	-	9,42	%IACS
Galvanic potential	* -0,52	-	-0,44	V

Magnetic properties

Magnetic type	Magnetic
---------------	----------

Optical, aesthetic and acoustic properties

Transparency	Opaque
Acoustic velocity	* 5,11e3 - 5,24e3 m/s
Mechanical loss coefficient (tan delta)	* 2,2e-4 - 9,3e-4

Restricted substances risk indicators

SIN List indicator (0-1, 1 = high risk)	0
---	---

Critical materials risk

Contains >5wt% critical elements?	No
-----------------------------------	----

Processing properties

Metal casting	Unsuitable
Metal cold forming	Acceptable
Metal hot forming	Excellent
Metal press forming	Acceptable
Metal deep drawing	Limited use
Machining speed	41,5 m/min
Weldability	Good
Notes	Preheating and post weld heat treatments may be required
Carbon equivalency	* 0 - 0,298

Durability

Water (fresh)	Acceptable
Water (salt)	Limited use
Weak acids	Limited use
Strong acids	Unacceptable
Weak alkalis	Acceptable
Strong alkalis	Limited use
Organic solvents	Excellent
Oxidation at 500C	Acceptable
UV radiation (sunlight)	Excellent
Galling resistance (adhesive wear)	Acceptable
Notes	Aluminum bronze is the most suitable mating material to minimize galling.
Flammability	Non-flammable

Corrosion resistance of metals

Stress corrosion cracking	Slightly susceptible
Notes	Rated in chloride; Other susceptible environments: Nitrate, hydroxide, carbonate, ammonia

Primary production energy, CO2 and water

Embodied energy, primary production (virgin grade)	* 26,3 - 29 MJ/kg
Sources	

Values marked * are estimates.
ANSYS, Inc. provides no warranty for this data.

Estimated from sources including Hammond and Jones, 2008; Ecoinvent v3.7.1

Embodied energy, primary production (typical grade)	* 16,3	-	19,2	MJ/kg
CO2 footprint, primary production (virgin grade)	* 2,85	-	3,14	kg/kg

Sources

Estimated from sources including Voet, van der and Oers, van, 2003; Hammond and Jones, 2008; Ecoinvent v3.7.1

CO2 footprint, primary production (typical grade)	* 1,64	-	1,94	kg/kg
---	--------	---	------	-------

Processing energy, CO2 footprint & water

Roll forming, forging energy	* 2,34	-	2,58	MJ/kg
Roll forming, forging CO2	* 0,176	-	0,193	kg/kg
Extrusion, foil rolling energy	* 4,39	-	4,84	MJ/kg
Extrusion, foil rolling CO2	* 0,329	-	0,363	kg/kg
Wire drawing energy	* 15,7	-	17,3	MJ/kg
Wire drawing CO2	* 1,18	-	1,3	kg/kg
Metal powder forming energy	* 38,4	-	42,4	MJ/kg
Metal powder forming CO2	* 2,88	-	3,18	kg/kg
Metal powder forming water	* 43,5	-	62,7	l/kg
Vaporization energy	* 1,41e4	-	1,56e4	MJ/kg
Vaporization CO2	* 1,06e3	-	1,17e3	kg/kg
Vaporization water	* 6,12e3	-	8,81e3	l/kg
Coarse machining energy (per unit wt removed)	* 0,784	-	0,864	MJ/kg
Coarse machining CO2 (per unit wt removed)	* 0,0588	-	0,0648	kg/kg
Fine machining energy (per unit wt removed)	* 3,55	-	3,92	MJ/kg
Fine machining CO2 (per unit wt removed)	* 0,266	-	0,294	kg/kg
Grinding energy (per unit wt removed)	* 6,63	-	7,31	MJ/kg
Grinding CO2 (per unit wt removed)	* 0,497	-	0,548	kg/kg
Non-conventional machining energy (per unit wt removed)	* 141	-	156	MJ/kg
Non-conventional machining CO2 (per unit wt removed)	* 10,6	-	11,7	kg/kg

Recycling and end of life

Recycle	✓			
Embodied energy, recycling	7,2	-	8	MJ/kg
CO2 footprint, recycling	0,566	-	0,626	kg/kg
Recycle fraction in current supply	49,4	-	54,6	%
Downcycle	✓			
Combust for energy recovery	✗			
Landfill	✓			
Biodegrade	✗			

Notes

Other notes

The values shown in the datasheet are valid for the minimum thickness for this grade. S235J is a readily weldable low carbon manganese steel with excellent formability and good impact resistance including at sub-zero temperatures. The sub-grades JR, J0 and J2 define the structural steel's ability to behave in a ductile manner and thus avoid brittle fracture: the J corresponds to a minimum impact energy of 27J that the specimen must withstand at the test temperatures. The test temperatures are room temperature (+20°C) [JR], 0°C [J0] and -20°C [J2].

Keywords

Values marked * are estimates.
ANSYS, Inc. provides no warranty for this data.

General information

Designation

Structural steel, S275J, wrought	
Condition	Hot rolled
EN name	S275JR, S275J0, S275J2
EN number	1.0045, 1.0143, 1.0145

Typical uses

General engineering and structural applications, bridges, buildings, automotive, construction, yellow goods, tanks, rail, oil and gas industries, frames for presses, heating plates for presses.

Included in Materials Data for Simulation	✓
Materials Data for Simulation name	Structural steel, S275J

Composition overview

Compositional summary

Fe98-100 (impurities: Mn<1.5, Cu<0.55, C<0.22, P<0.035, S<0.035, N<0.012)	
Material family	Metal (ferrous)
Base material	Fe (Iron)

Composition detail (metals, ceramics and glasses)

C (carbon)	0	-	0,22	%
Cu (copper)	0	-	0,55	%
Fe (iron)	* 97,6	-	100	%
Mn (manganese)	0	-	1,5	%
N (nitrogen)	0	-	0,012	%
P (phosphorus)	0	-	0,035	%
S (sulfur)	0	-	0,035	%

Price

Price	* 0,649	-	0,852	EUR/kg
Price per unit volume	* 5,09e3	-	6,69e3	EUR/m ³

Physical properties

Density	7,85e3		kg/m ³
---------	--------	--	-------------------

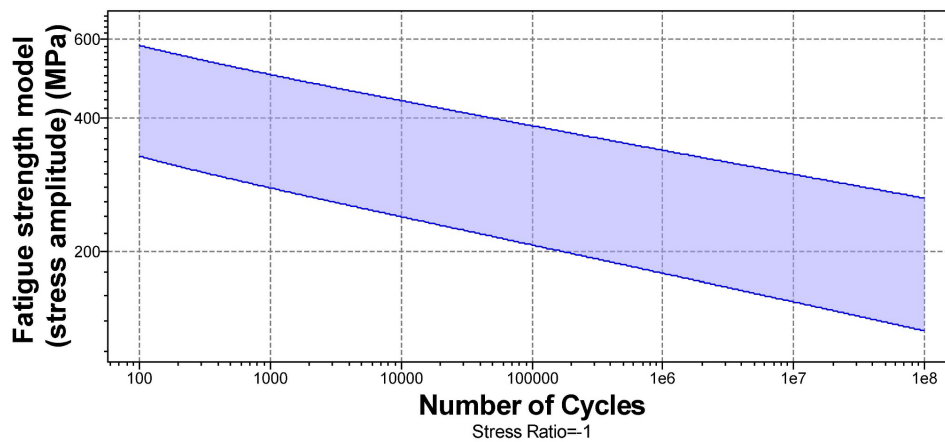
Mechanical properties

Young's modulus	205	-	215	GPa
Specific stiffness	* 26,1	-	27,4	MN.m/kg
Yield strength (elastic limit)	275	-	321	MPa
Notes These values are applicable for minimum thickness for this grade.				
Tensile strength	410	-	580	MPa
Notes These values are applicable for minimum thickness for this grade.				
Specific strength	* 35	-	40,9	kN.m/kg
Elongation	15	-	23	% strain
Tangent modulus	1,41e3			MPa
Compressive modulus	* 205	-	215	GPa
Compressive strength	* 275	-	321	MPa

Values marked * are estimates.
ANSYS, Inc. provides no warranty for this data.

Flexural modulus	* 205	- 215	GPa
Flexural strength (modulus of rupture)	* 266	- 376	MPa
Shear modulus	* 78,9	- 82,7	GPa
Shear strength	* 159	- 185	MPa
Bulk modulus	* 171	- 179	GPa
Poisson's ratio	0,3		
Shape factor	61		
Hardness - Vickers	* 127	- 162	HV
Hardness - Brinell	121	- 163	HB
Elastic stored energy (springs)	* 181	- 244	kJ/m ³
Fatigue strength at 10 ⁷ cycles	* 199	- 232	MPa
Fatigue strength model (stress amplitude)	* 155	- 299	MPa

Parameters: Stress Ratio = -1, Number of Cycles = 1e7cycles



Impact & fracture properties

Fracture toughness	* 52,9	- 64	MPa.m ^{0.5}
Toughness (G)	* 13,4	- 19,4	kJ/m ²

Thermal properties

Melting point	1,48e3	- 1,53e3	°C
Maximum service temperature	* 473	- 519	°C
Minimum service temperature	* -54	- -44	°C
Thermal conductivity	40	- 53,4	W/m.°C
Specific heat capacity	460	- 480	J/kg.°C
Thermal expansion coefficient	11	- 13	µstrain/°C
Thermal shock resistance	* 106	- 133	°C
Thermal distortion resistance	* 3,28	- 4,55	MW/m
Latent heat of fusion	* 343	- 364	kJ/kg

Electrical properties

Electrical resistivity	19,7		µhm.cm
Electrical conductivity	8,75		%IACS

Values marked * are estimates.
ANSYS, Inc. provides no warranty for this data.

Galvanic potential	* -0,52	-	-0,44	V
--------------------	---------	---	-------	---

Magnetic properties

Magnetic type	Magnetic
---------------	----------

Optical, aesthetic and acoustic properties

Transparency	Opaque
Acoustic velocity	* 5,11e3 - 5,23e3 m/s
Mechanical loss coefficient (tan delta)	* 2,2e-4 - 9,3e-4

Restricted substances risk indicators

SIN List indicator (0-1, 1 = high risk)	0
---	---

Critical materials risk

Contains >5wt% critical elements?	No
-----------------------------------	----

Processing properties

Metal casting	Unsuitable
Metal cold forming	Acceptable
Metal hot forming	Excellent
Metal press forming	Acceptable
Metal deep drawing	Limited use
Machining speed	36,3 m/min
Weldability	Good
Notes	Preheating and post weld heat treatments may be required
Carbon equivalency	* 0 - 0,323

Durability

Water (fresh)	Acceptable
Water (salt)	Limited use
Weak acids	Limited use
Strong acids	Unacceptable
Weak alkalis	Acceptable
Strong alkalis	Limited use
Organic solvents	Excellent
Oxidation at 500C	Acceptable
UV radiation (sunlight)	Excellent
Galling resistance (adhesive wear)	Acceptable

Notes
Aluminum bronze is the most suitable mating material to minimize galling.

Flammability	Non-flammable
--------------	---------------

Corrosion resistance of metals

Stress corrosion cracking	Slightly susceptible
Notes	Rated in chloride; Other susceptible environments: Nitrate, hydroxide, carbonate, ammonia

Primary production energy, CO2 and water

Embodied energy, primary production (virgin grade)	* 26,3 - 29 MJ/kg
--	-------------------

Sources
Estimated from sources including Hammond and Jones, 2008; Ecoinvent v3.7.1

Values marked * are estimates.
ANSYS, Inc. provides no warranty for this data.

Embodied energy, primary production (typical grade)	* 16,3	- 19,2	MJ/kg
CO2 footprint, primary production (virgin grade)	* 2,85	- 3,14	kg/kg
Sources			
Estimated from sources including Voet, van der and Oers, van, 2003; Hammond and Jones, 2008; Ecoinvent v3.7.1			
CO2 footprint, primary production (typical grade)	* 1,64	- 1,94	kg/kg

Processing energy, CO2 footprint & water

Roll forming, forging energy	* 2,69	- 2,96	MJ/kg
Roll forming, forging CO2	* 0,202	- 0,222	kg/kg
Extrusion, foil rolling energy	* 5,09	- 5,61	MJ/kg
Extrusion, foil rolling CO2	* 0,382	- 0,421	kg/kg
Wire drawing energy	* 18,3	- 20,2	MJ/kg
Wire drawing CO2	* 1,37	- 1,51	kg/kg
Metal powder forming energy	* 38,4	- 42,4	MJ/kg
Metal powder forming CO2	* 2,88	- 3,18	kg/kg
Metal powder forming water	* 43,5	- 62,7	l/kg
Vaporization energy	* 1,41e4	- 1,56e4	MJ/kg
Vaporization CO2	* 1,06e3	- 1,17e3	kg/kg
Vaporization water	* 6,12e3	- 8,81e3	l/kg
Coarse machining energy (per unit wt removed)	* 0,837	- 0,922	MJ/kg
Coarse machining CO2 (per unit wt removed)	* 0,0627	- 0,0692	kg/kg
Fine machining energy (per unit wt removed)	* 4,08	- 4,5	MJ/kg
Fine machining CO2 (per unit wt removed)	* 0,306	- 0,337	kg/kg
Grinding energy (per unit wt removed)	* 7,69	- 8,47	MJ/kg
Grinding CO2 (per unit wt removed)	* 0,576	- 0,636	kg/kg
Non-conventional machining energy (per unit wt removed)	* 141	- 156	MJ/kg
Non-conventional machining CO2 (per unit wt removed)	* 10,6	- 11,7	kg/kg

Recycling and end of life

Recycle	✓		
Embodied energy, recycling	7,2	- 8	MJ/kg
CO2 footprint, recycling	0,566	- 0,626	kg/kg
Recycle fraction in current supply	49,4	- 54,6	%
Downcycle	✓		
Combust for energy recovery	✗		
Landfill	✓		
Biodegrade	✗		

Notes

Other notes

The values shown in the datasheet are valid for the minimum thickness for this grade.
S275J is a popular low carbon manganese steel with good machinability. It is readily weldable and possesses good impact resistance including at sub-zero temperatures.
The sub-grades JR, J0 and J2 define the structural steel's ability to behave in a ductile manner and thus avoid brittle fracture: the J corresponds to a minimum impact energy of 27J that the specimen must withstand at the test temperatures. The test temperatures are room temperature (+20°C) [JR], 0°C [J0] and -20°C [J2].

Keywords

Values marked * are estimates.
ANSYS, Inc. provides no warranty for this data.

General information

Designation

Structural steel, S355J, wrought	
Condition	Hot rolled
US name	A572 Grade 50
EN name	S355JR, S355J0, S355J2
EN number	1.0045, 1.0553, 1.0577

Typical uses

Welded, bolted and riveted structures, construction, power plants, yellow goods, oil rigs, offshore structures, tanks, rail, energy, mining, wind tower components.

Included in Materials Data for Simulation	✓
Materials Data for Simulation name	Structural steel, S355J

Composition overview

Compositional summary

Fe97-100 (impurities: Mn<1.6, Cu<0.55, C<0.24, P<0.035, S<0.035, N<0.012)	
Material family	Metal (ferrous)
Base material	Fe (Iron)

Composition detail (metals, ceramics and glasses)

C (carbon)	0	-	0,24	%
Cu (copper)	0	-	0,55	%
Fe (iron)	* 97	-	100	%
Mn (manganese)	0	-	1,6	%
N (nitrogen)	0	-	0,012	%
P (phosphorus)	0	-	0,035	%
S (sulfur)	0	-	0,035	%
Si (silicon)	0	-	0,55	%

Price

Price	* 0,649	-	0,852	EUR/kg
Price per unit volume	* 5,08e3	-	6,68e3	EUR/m ³

Physical properties

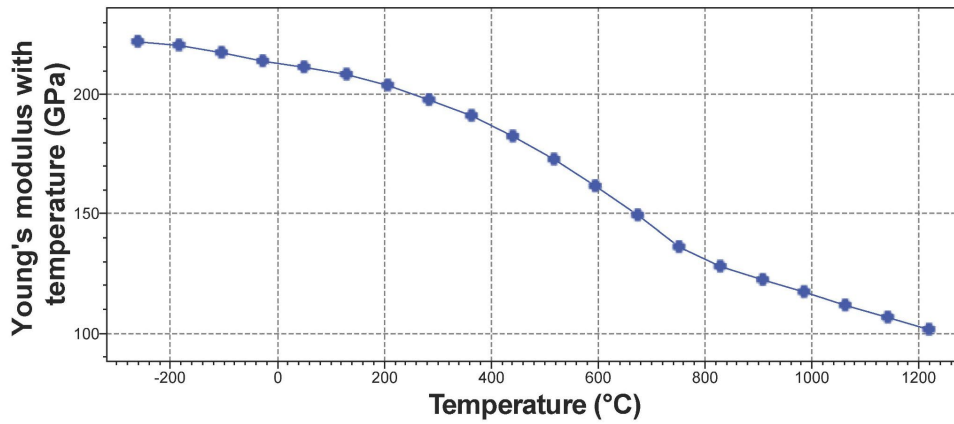
Density	7,83e3	-	7,84e3	kg/m ³
---------	--------	---	--------	-------------------

Mechanical properties

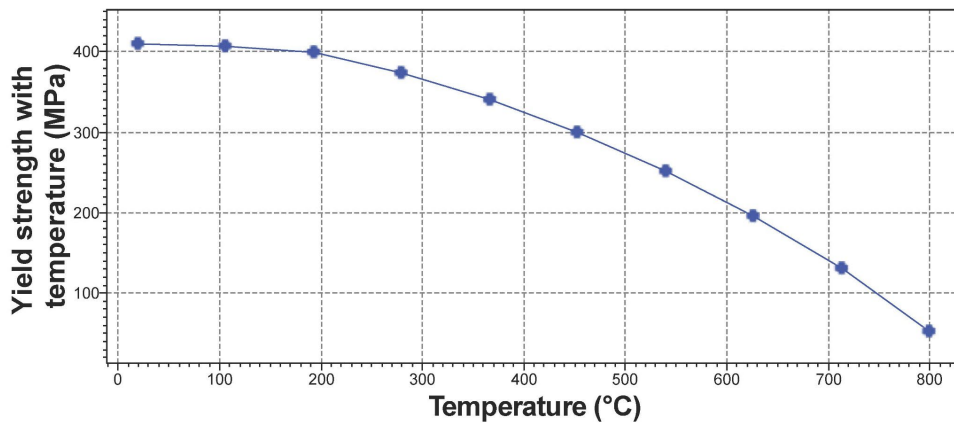
Young's modulus	205	-	215	GPa
Young's modulus with temperature	212	-	212	GPa

[Parameters:](#) Temperature = 23°C

Values marked * are estimates.
ANSYS, Inc. provides no warranty for this data.



Specific stiffness	* 26,2	- 27,4	MN.m/kg
Yield strength (elastic limit)	355	- 414	MPa
Notes	These values are applicable for minimum thickness for this grade.		
Yield strength with temperature	409	- 409	MPa
Parameters:	Temperature = 23°C		

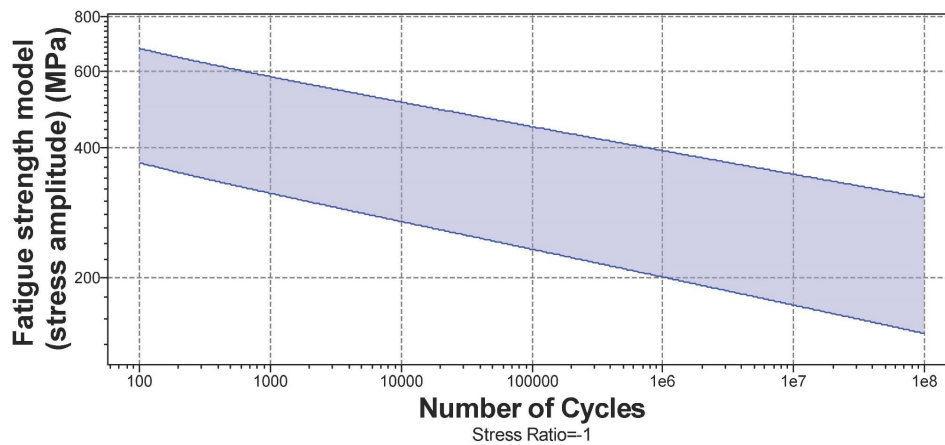


Tensile strength	470	- 680	MPa
Notes	These values are applicable for minimum thickness for this grade.		
Specific strength	* 45,3	- 52,8	kN.m/kg
Elongation	14	- 22	% strain
Tangent modulus	1,48e3		MPa
Compressive modulus	* 205	- 215	GPa
Compressive strength	* 355	- 414	MPa
Flexural modulus	* 205	- 215	GPa
Flexural strength (modulus of rupture)	* 315	- 455	MPa
Shear modulus	* 78,9	- 82,7	GPa

Values marked * are estimates.
ANSYS, Inc. provides no warranty for this data.

Shear strength	* 205	- 239	MPa
Bulk modulus	* 171	- 179	GPa
Poisson's ratio	0,3		
Shape factor	56		
Hardness - Vickers	* 147	- 185	HV
Hardness - Brinell	146	- 187	HB
Elastic stored energy (springs)	* 301	- 407	kJ/m ³
Fatigue strength at 10 ⁷ cycles	* 226	- 264	MPa
Fatigue strength model (stress amplitude)	* 172	- 346	MPa

Parameters: Stress Ratio = -1, Number of Cycles = 1e7cycles



Impact & fracture properties

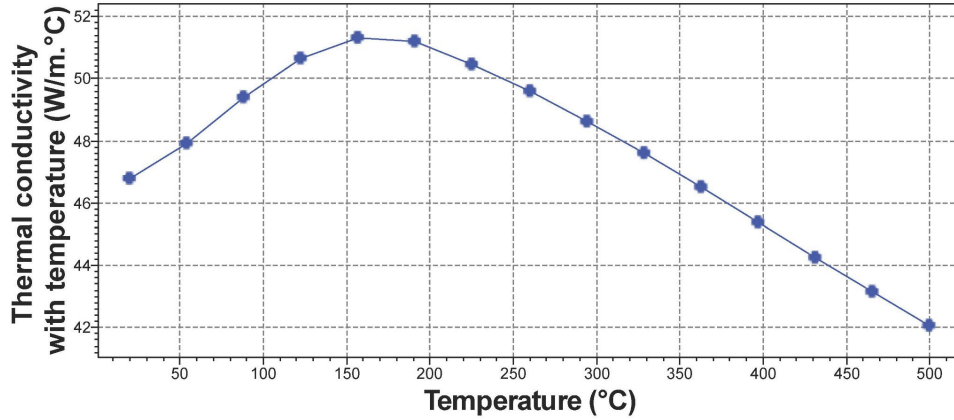
Fracture toughness	* 68,6	- 83	MPa.m ^{0,5}
Toughness (G)	* 22,6	- 32,6	kJ/m ²

Thermal properties

Melting point	1,48e3	- 1,53e3	°C
Maximum service temperature	* 473	- 519	°C
Minimum service temperature	* -50,3	- -40,3	°C
Thermal conductivity	40	- 46,5	W/m.°C
Thermal conductivity with temperature	46,9	- 46,9	W/m.°C

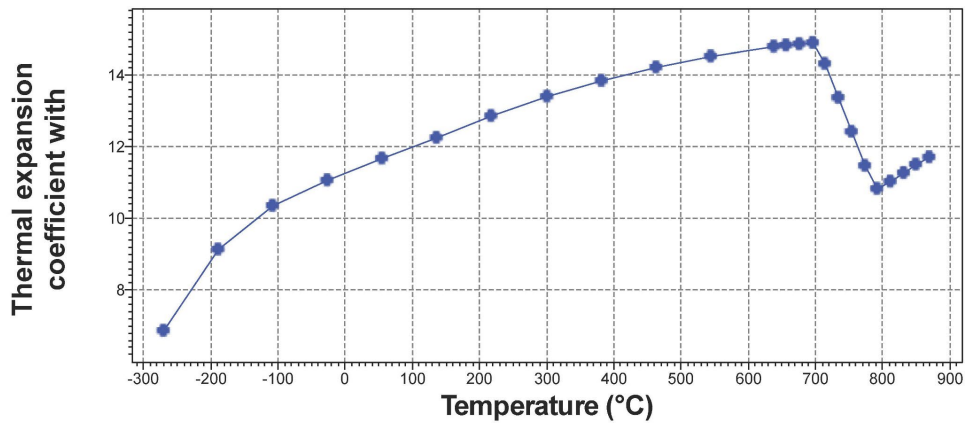
Parameters: Temperature = 23°C

Values marked * are estimates.
ANSYS, Inc. provides no warranty for this data.



Specific heat capacity	460	-	480	J/kg.°C
Thermal expansion coefficient	11,5	-	13	µstrain/°C
Thermal expansion coefficient with temperature	11,4	-	11,4	µstrain/°C

[Parameters:](#) Temperature = 23°C



Reference temp	20		°C
Thermal shock resistance	* 135	-	165 °C
Thermal distortion resistance	* 3,2	-	3,88 MW/m
Latent heat of fusion	* 343	-	364 kJ/kg

Electrical properties

Electrical resistivity	20	-	24,9 µohm.cm
Electrical conductivity	6,92	-	8,62 %IACS
Galvanic potential	* -0,52	-	-0,44 V

Magnetic properties

Magnetic type	Magnetic
---------------	----------

Values marked * are estimates.
ANSYS, Inc. provides no warranty for this data.

Optical, aesthetic and acoustic properties

Transparency	Opaque		
Acoustic velocity	* 5,11e3	-	5,24e3 m/s
Mechanical loss coefficient (tan delta)	* 2,2e-4	-	9,3e-4

Restricted substances risk indicators

SIN List indicator (0-1, 1 = high risk)	0
---	---

Critical materials risk

Contains >5wt% critical elements?	No
-----------------------------------	----

Processing properties

Metal casting	Unsuitable
Metal cold forming	Acceptable
Metal hot forming	Excellent
Metal press forming	Acceptable
Metal deep drawing	Limited use
Machining speed	31,4 m/min
Weldability	Good
Notes	Preheating and post weld heat treatments may be required
Carbon equivalency	* 0 - 0,635

Durability

Water (fresh)	Acceptable
Water (salt)	Limited use
Weak acids	Limited use
Strong acids	Unacceptable
Weak alkalis	Acceptable
Strong alkalis	Limited use
Organic solvents	Excellent
Oxidation at 500C	Acceptable
UV radiation (sunlight)	Excellent
Galling resistance (adhesive wear)	Acceptable
Notes	Aluminum bronze is the most suitable mating material to minimize galling.
Flammability	Non-flammable

Corrosion resistance of metals

Stress corrosion cracking	Slightly susceptible
Notes	Rated in chloride; Other susceptible environments: Nitrate, hydroxide, carbonate, ammonia

Primary production energy, CO2 and water

Embodied energy, primary production (virgin grade)	* 26,3	-	29	MJ/kg
Sources	Estimated from sources including Hammond and Jones, 2008; Ecoinvent v3.7.1			
Embodied energy, primary production (typical grade)	* 18,3	-	21,1	MJ/kg
CO2 footprint, primary production (virgin grade)	* 2,85	-	3,14	kg/kg
Sources	Estimated from sources including Voet, van der and Oers, van, 2003; Hammond and Jones, 2008; Ecoinvent v3.7.1			
CO2 footprint, primary production (typical grade)	* 1,88	-	2,17	kg/kg

Values marked * are estimates.
ANSYS, Inc. provides no warranty for this data.

Processing energy, CO2 footprint & water

Roll forming, forging energy	* 3,39	-	3,74	MJ/kg
Roll forming, forging CO2	* 0,254	-	0,28	kg/kg
Extrusion, foil rolling energy	* 6,5	-	7,17	MJ/kg
Extrusion, foil rolling CO2	* 0,488	-	0,538	kg/kg
Wire drawing energy	* 23,6	-	26	MJ/kg
Wire drawing CO2	* 1,77	-	1,95	kg/kg
Metal powder forming energy	* 38,4	-	42,4	MJ/kg
Metal powder forming CO2	* 2,88	-	3,18	kg/kg
Metal powder forming water	* 43,5	-	62,7	l/kg
Vaporization energy	* 1,41e4	-	1,56e4	MJ/kg
Vaporization CO2	* 1,06e3	-	1,17e3	kg/kg
Vaporization water	* 6,12e3	-	8,81e3	l/kg
Coarse machining energy (per unit wt removed)	* 0,942	-	1,04	MJ/kg
Coarse machining CO2 (per unit wt removed)	* 0,0707	-	0,0779	kg/kg
Fine machining energy (per unit wt removed)	* 5,14	-	5,66	MJ/kg
Fine machining CO2 (per unit wt removed)	* 0,385	-	0,425	kg/kg
Grinding energy (per unit wt removed)	* 9,8	-	10,8	MJ/kg
Grinding CO2 (per unit wt removed)	* 0,735	-	0,81	kg/kg
Non-conventional machining energy (per unit wt removed)	* 141	-	156	MJ/kg
Non-conventional machining CO2 (per unit wt removed)	* 10,6	-	11,7	kg/kg

Recycling and end of life

Recycle	✓			
Embodied energy, recycling	7,2	-	8	MJ/kg
CO2 footprint, recycling	0,566	-	0,626	kg/kg
Recycle fraction in current supply	* 40	-	44	%
Downcycle	✓			
Combust for energy recovery	✗			
Landfill	✓			
Biodegrade	✗			

Notes

Other notes

The values shown in the datasheet are valid for the minimum thickness for this grade. S355J is a medium tensile, micro-alloyed carbon steel which is readily weldable and possesses good impact resistance including at sub-zero temperatures. It is often used where applications require improved mechanical properties than S275J.

The sub-grades JR, J0 and J2 define the structural steel's ability to behave in a ductile manner and thus avoid brittle fracture: the J corresponds to a minimum impact energy of 27J that the specimen must withstand at the test temperatures. The test temperatures are room temperature (+20°C) [JR], 0°C [J0] and -20°C [J2].

Keywords

Q345R; SA/GB 713; UNE 36087 A52RAII; A52RBII; A52RCII

Standards with similar compositions

Q345R, SA/GB 713, UNE 36087 A52RAII, A52RBII, A52RCII

Links

Values marked * are estimates.
ANSYS, Inc. provides no warranty for this data.

General information

Designation

Stainless steel, austenitic, AISI 308L, annealed, wrought	
Condition	Solution annealed
UNS number	S30800
US name	AISI 308L

Typical uses

Processing of potentially corrosive liquids e.g. chemicals/oil/beverages/sewage, structural uses in corrosive environments, e.g. nuclear plants, ships, offshore oil installations, underwater cables and pipes

Composition overview

Compositional summary

Fe64-72 / Cr19-21 / Ni9-12 (impurities: Mn<2, Si<1, C<0.03, P<0.02, S<0.01)	
Material family	Metal (ferrous)
Base material	Fe (Iron)

Composition detail (metals, ceramics and glasses)

C (carbon)	0	-	0,03	%
Cr (chromium)	19	-	21	%
Fe (iron)	* 63,9	-	72	%
Mn (manganese)	0	-	2	%
Ni (nickel)	9	-	12	%
P (phosphorus)	0	-	0,02	%
S (sulfur)	0	-	0,01	%
Si (silicon)	0	-	1	%

Price

Price	* 2,7	-	3,43	EUR/kg
Price per unit volume	* 2,11e4	-	2,75e4	EUR/m ³

Physical properties

Density	7,8e3	-	8,01e3	kg/m ³
---------	-------	---	--------	-------------------

Mechanical properties

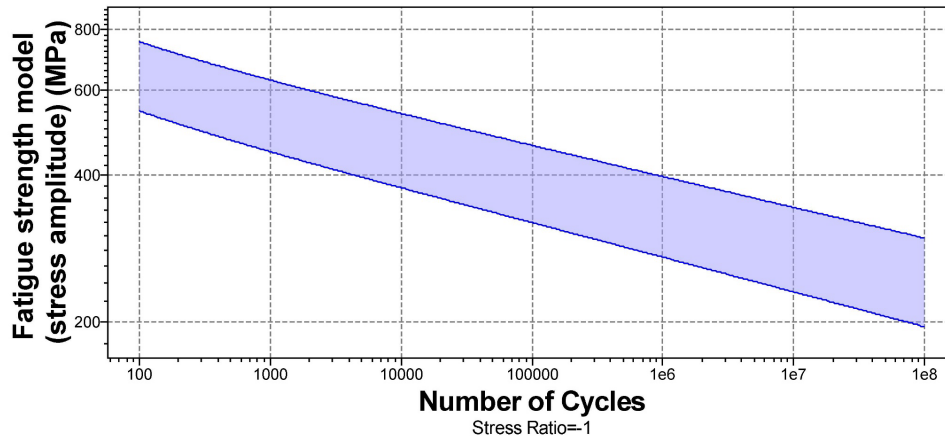
Young's modulus	* 189	-	197	GPa
Specific stiffness	* 23,8	-	25	MN.m/kg
Yield strength (elastic limit)	187	-	227	MPa
Tensile strength	500	-	600	MPa
Specific strength	* 23,6	-	28,7	kN.m/kg
Elongation	50	-	70	% strain
Compressive strength	* 187	-	227	MPa
Flexural modulus	* 189	-	197	GPa
Flexural strength (modulus of rupture)	187	-	227	MPa
Shear modulus	* 74	-	78	GPa
Bulk modulus	* 134	-	146	GPa
Poisson's ratio	0,265	-	0,275	
Shape factor	64			

Values marked * are estimates.
ANSYS, Inc. provides no warranty for this data.

GRANTA EDUPACK

Hardness - Vickers	* 160	- 200	HV
Hardness - Rockwell B	* 82	- 92	HRB
Hardness - Rockwell C	* 0	- 12	HRC
Hardness - Brinell	* 135	- 193	HB
Elastic stored energy (springs)	* 109	- 232	kJ/m ³
Fatigue strength at 10 ⁷ cycles	* 263	- 300	MPa
Fatigue strength model (stress amplitude)	* 230	- 343	MPa

Parameters: Stress Ratio = -1, Number of Cycles = 1e7cycles



Impact & fracture properties

Fracture toughness	* 164	- 243	MPa.m ^{0.5}
Toughness (G)	* 144	- 296	kJ/m ²

Thermal properties

Melting point	* 1,4e3	- 1,42e3	°C
Maximum service temperature	* 880	- 980	°C
Minimum service temperature	-200		°C
Thermal conductivity	* 14	- 17	W/m.°C
Specific heat capacity	490	- 530	J/kg.°C
Thermal expansion coefficient	* 15	- 19	µstrain/°C
Thermal shock resistance	* 54,4	- 73,6	°C
Thermal distortion resistance	* 0,787	- 1,06	MW/m
Latent heat of fusion	* 260	- 285	kJ/kg

Electrical properties

Electrical resistivity	* 65	- 77	µohm.cm
Electrical conductivity	* 2,24	- 2,65	%IACS
Galvanic potential	* -0,27	- -0,19	V

Magnetic properties

Magnetic type	Non-magnetic
---------------	--------------

Optical, aesthetic and acoustic properties

Values marked * are estimates.
ANSYS, Inc. provides no warranty for this data.

Transparency	Opaque		
Acoustic velocity	* 4,88e3	- 5e3	m/s
Mechanical loss coefficient (tan delta)	* 0,00113	- 0,00138	

Restricted substances risk indicators

SIN List indicator (0-1, 1 = high risk)	0
---	---

Critical materials risk

Contains >5wt% critical elements?	Yes
-----------------------------------	-----

Processing properties

Metal casting	Unsuitable
Metal cold forming	Acceptable
Metal hot forming	Acceptable
Metal press forming	Acceptable
Metal deep drawing	Limited use
Machining speed	24,7 m/min
Weldability	Excellent
Notes	Preheating and post weld heat treatments are not required
Weldability - MIG	Excellent
Weldability - plasma	Excellent
Weldability - SAW	Excellent
Weldability - TIG	Excellent
Brazeability	Good
Carbon equivalency	1,1 - 1,41

Durability

Water (fresh)	Excellent
Water (salt)	Excellent
Weak acids	Excellent
Strong acids	Acceptable
Weak alkalis	Excellent
Strong alkalis	Excellent
Organic solvents	Excellent
Oxidation at 500C	Excellent
UV radiation (sunlight)	Excellent
Galling resistance (adhesive wear)	Limited use
Notes	Aluminum bronze is the most suitable mating material to minimize galling.
Flammability	Non-flammable

Corrosion resistance of metals

Pitting resistance equivalent number (PREN)	19 - 21
Pitting and crevice corrosion resistance	Medium (20-30)
Stress corrosion cracking	Slightly susceptible
Notes	Rated in chloride; Other susceptible environments: Hydrogen sulfide
Intergranular (weld line) corrosion resistance	Good
Inorganic acids	Moderate
Organic acids	Moderate

Values marked * are estimates.
ANSYS, Inc. provides no warranty for this data.

Alkalis	Moderate
Humidity / water	Excellent
Sea water	Moderate
Sour oil and gas	Moderate

Primary production energy, CO2 and water

Embodied energy, primary production (virgin grade)	* 69,6	- 76,7	MJ/kg
--	--------	--------	-------

Sources

Estimated from sources including Ecoinvent v3.7.1; Hammond and Jones, 2008; Norgate, Jahanshahi, Rankin, 2007; Sullivan and Gaines, 2010; Nickel Institute, 2003

Embodied energy, primary production (typical grade)	* 39,7	- 46,9	MJ/kg
---	--------	--------	-------

CO2 footprint, primary production (virgin grade)	* 5,96	- 6,57	kg/kg
--	--------	--------	-------

Sources

Estimated from sources including Ecoinvent v3.7.1; Voet, van der and Oers, van, 2003; Hammond and Jones, 2008; Norgate, Jahanshahi, Rankin, 2007; Nickel Institute, 2003

CO2 footprint, primary production (typical grade)	* 3,34	- 3,96	kg/kg
---	--------	--------	-------

Water usage	* 146	- 161	l/kg
-------------	-------	-------	------

Processing energy, CO2 footprint & water

Roll forming, forging energy	* 1,94	- 2,14	MJ/kg
------------------------------	--------	--------	-------

Roll forming, forging CO2	* 0,145	- 0,16	kg/kg
---------------------------	---------	--------	-------

Roll forming, forging water	* 2,38	- 3,57	l/kg
-----------------------------	--------	--------	------

Extrusion, foil rolling energy	* 3,59	- 3,96	MJ/kg
--------------------------------	--------	--------	-------

Extrusion, foil rolling CO2	* 0,269	- 0,297	kg/kg
-----------------------------	---------	---------	-------

Extrusion, foil rolling water	* 3,08	- 4,63	l/kg
-------------------------------	--------	--------	------

Wire drawing energy	* 12,7	- 14	MJ/kg
---------------------	--------	------	-------

Wire drawing CO2	* 0,95	- 1,05	kg/kg
------------------	--------	--------	-------

Wire drawing water	* 4,77	- 7,16	l/kg
--------------------	--------	--------	------

Metal powder forming energy	* 37,5	- 41,4	MJ/kg
-----------------------------	--------	--------	-------

Metal powder forming CO2	* 3	- 3,32	kg/kg
--------------------------	-----	--------	-------

Metal powder forming water	* 40,9	- 61,4	l/kg
----------------------------	--------	--------	------

Vaporization energy	* 1,09e4	- 1,2e4	MJ/kg
---------------------	----------	---------	-------

Vaporization CO2	* 815	- 900	kg/kg
------------------	-------	-------	-------

Vaporization water	* 4,53e3	- 6,79e3	l/kg
--------------------	----------	----------	------

Coarse machining energy (per unit wt removed)	* 0,723	- 0,799	MJ/kg
---	---------	---------	-------

Coarse machining CO2 (per unit wt removed)	* 0,0542	- 0,0599	kg/kg
--	----------	----------	-------

Fine machining energy (per unit wt removed)	* 2,95	- 3,26	MJ/kg
---	--------	--------	-------

Fine machining CO2 (per unit wt removed)	* 0,221	- 0,245	kg/kg
--	---------	---------	-------

Grinding energy (per unit wt removed)	* 5,43	- 6	MJ/kg
---------------------------------------	--------	-----	-------

Grinding CO2 (per unit wt removed)	* 0,407	- 0,45	kg/kg
------------------------------------	---------	--------	-------

Non-conventional machining energy (per unit wt removed)	* 109	- 120	MJ/kg
---	-------	-------	-------

Non-conventional machining CO2 (per unit wt removed)	* 8,15	- 9	kg/kg
--	--------	-----	-------

Recycling and end of life

Recycle	✓		
---------	---	--	--

Embodied energy, recycling	15,1	- 16,6	MJ/kg
----------------------------	------	--------	-------

CO2 footprint, recycling	1,18	- 1,31	kg/kg
--------------------------	------	--------	-------

Recycle fraction in current supply	49,4	- 54,6	%
------------------------------------	------	--------	---

Downcycle	✓		
-----------	---	--	--

Combust for energy recovery	✗		
-----------------------------	---	--	--

Values marked * are estimates.
ANSYS, Inc. provides no warranty for this data.

Landfill	✓
Biodegrade	✗

Notes

Keywords

RDN 260, Roldan S.A. (SPAIN); RDN 240, Roldan S.A. (SPAIN); RDN 210, Roldan S.A. (SPAIN); RDN 340, Roldan S.A. (SPAIN); ARGESTE 4306 LA/LF/SBVC, Stahlwerk Ergste Westig GmbH (GERMANY); STAINWELD 308-15, Lincoln Electric Co. (USA); STAINWELD 308-16, Lincoln Electric Co. (USA); EASTERN STAINLESS TYPE 304L, Eastern Stainless Corp. (USA); PROJECT 7000 STAINLESS TYPE 304L, Carpenter Technology Corp. (USA); PROJECT 70 STAINLESS TYPE 304L, Carpenter Technology Corp. (USA); RDN 205, Roldan S.A. (SPAIN); EASTERN STAINLESS TYPE 304, Eastern Stainless Corp. (USA); PRODEC STAINLESS TYPE 304, Avesta Sheffield, Inc. (USA); PROJECT 70 STAINLESS TYPE 304, Carpenter Technology Corp. (USA); PROJECT 7000 STAINLESS TYPE 304, Carpenter Technology Corp. (USA); EMPIRE TYPE 304EZ, Empire Specialty Steel Inc. (USA); PRODEC STAINLESS TYPE 316L, Avesta Sheffield, Inc. (USA); RDN 200, Roldan S.A. (SPAIN); SANDVIK 2R17, Sandvik Steel Co. (USA); SANDVIK 2R16, Sandvik Steel Co. (USA);

Standards with similar compositions

- Austria:
X2CrNi1911KKW to ONORM M3121
- Hungary:
KO41LC to MSZ 4360
- International:
X2CrNi19-11 to ISO 16143-1, X2CrNi19-11 to ISO 16143-2, X2CrNi19-11 to ISO 16143-3, X2CrNi19-11 to ISO 9328-7
- Japan:
SUS304L to JIS G3459, SUS304L to JIS G4303, SUS304L to JIS G4304, SUS304L to JIS G4305, SUS304L to JIS G4306, SUS304L to JIS G4307, SUS304L to JIS G4308, SUS304L to JIS G4309, SUS304L to JIS G4317, SUS304LFB to JIS G4319, SUS304LTB to JIS G3463, SUS304LTBS to JIS G3447, SUS304LTP to JIS G3459, SUS304LTPY to JIS G3468, SUS304L-WSA to JIS G4315, SUS304L-WSB to JIS G4315, SUSF304L to JIS G3214
- Romania:
2NiCr185 to STAS 3583
- South Korea:
STS 304L to KS D 3706, STS 304L-W1 to KS D 3703, STS 304L-WSA to KS D 3697, STS F 304L to KS D 4115, STS304L to KS D 3692, STS304L to KS D 3698, STS304L to KS D 3705, STS304LFB to KS D 3691, STS304LTPY to KS D 3588
- UK:
X2CrNi19-11 to BS EN 10088-1, X2CrNi19-11 to BS EN 10088-2, X2CrNi19-11 to BS EN 10088-3, X2CrNi19-11 to BS EN 10216-5, X2CrNi19-11 to BS EN 10250-4, X2CrNi19-11 to BS EN 10272, X2CrNi19-11 to BS EN 10296-2, X2CrNi19-11 to BS EN 10297-2
- Tradenames:
ARGESTE 4306 LA/LF/SBVC, COR-A-ROSTA 304L, EUTECTRODE E308L-16, IN-FLUX 308L-G/S, IN-FLUX 308L-O, IN-FLUX 347L-O, JOSLYN STAINLESS TYPE 308L, MCKAY 308/308L-15 DC LIME, MCKAY 308/308L-16 STERLING AP, MCKAY 308/308L-17 STERLING, MCKAY 308L, NOVONIT 4302, NOVONIT 4316, OK AUTROD 16.10, OK TUBROD 15.30, PURO 18/8 L SUPRA, SANDVIK 2R16, SANDVIK 308L-15, SANDVIK 308L-16, SOUDINOX 308L, SOUDINOX 308W, UNILOY 308L, VERTAROSTA 304 L

Links

ProcessUniverse
Producers
Reference
Shape

Values marked * are estimates.
ANSYS, Inc. provides no warranty for this data.

In the following graph (figure 51) all generated designs are illustrated with their corresponding objective value. The designs are generated according to the stock from the new production. The red dot indicates the design that was used for the research. In figure 52 the distribution of the emissions is illustrated including the emissions of the nodes and the glass.

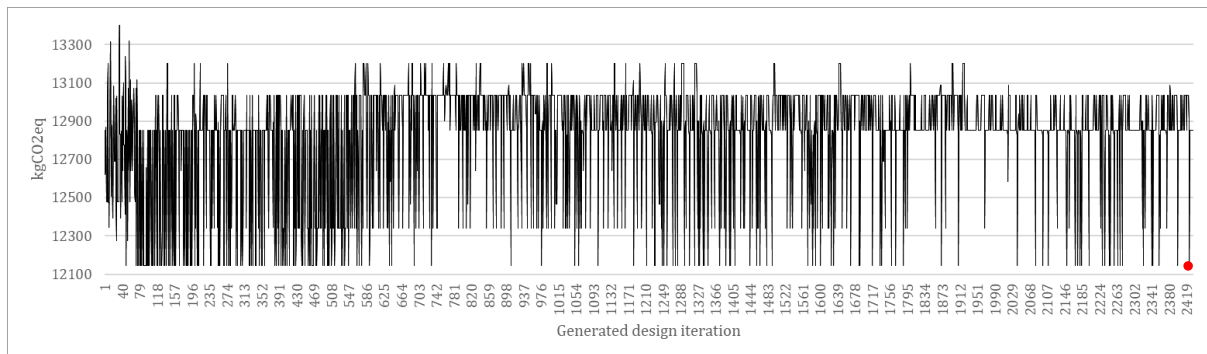


Figure 51 – illustration of the objective of all generated designs for the comparison of scenarios



Figure 52 - top left: distribution of emissions for the single cross-section gridshell, top right: distribution of emissions for the cross-section optimized gridshell all new scenario, bottom left: distribution of emissions for the cross-section optimized gridshell all deconstruction scenario, bottom right: distribution of emissions for the cross-section optimized gridshell all stockpile scenario

8.6 Comparison stock-sizes

The following illustrations illustrate the results from the assignment of small- (fig. 51), medium- (fig. 52) and large stock (fig. 53) for the regular non-node shifted triangulated gridshell. For an overview of all the assigned stock see Appendix '8.12 Overview stock assignment'.

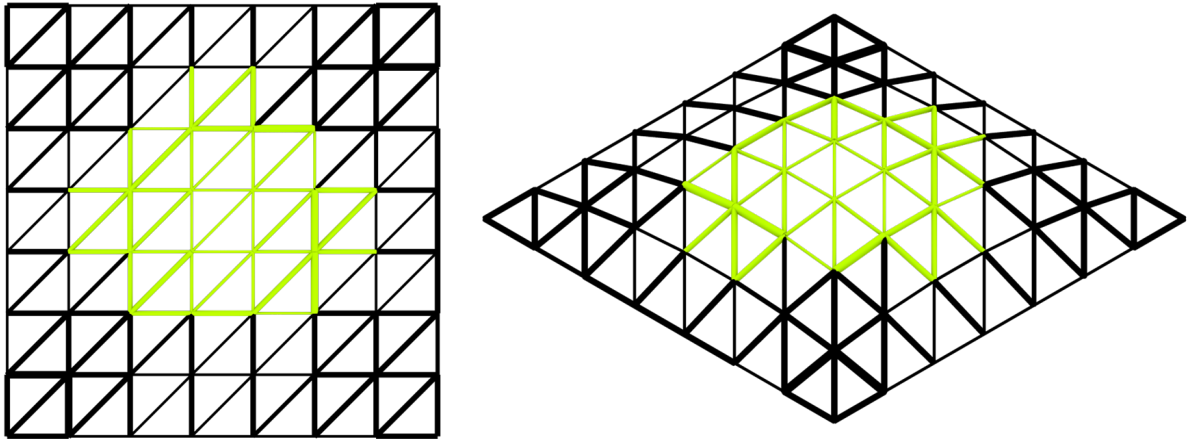


Figure 51 - illustration of a small sized stock assigned to the regular gridshell structure where black indicates new beam members and lime green indicates reused beam members

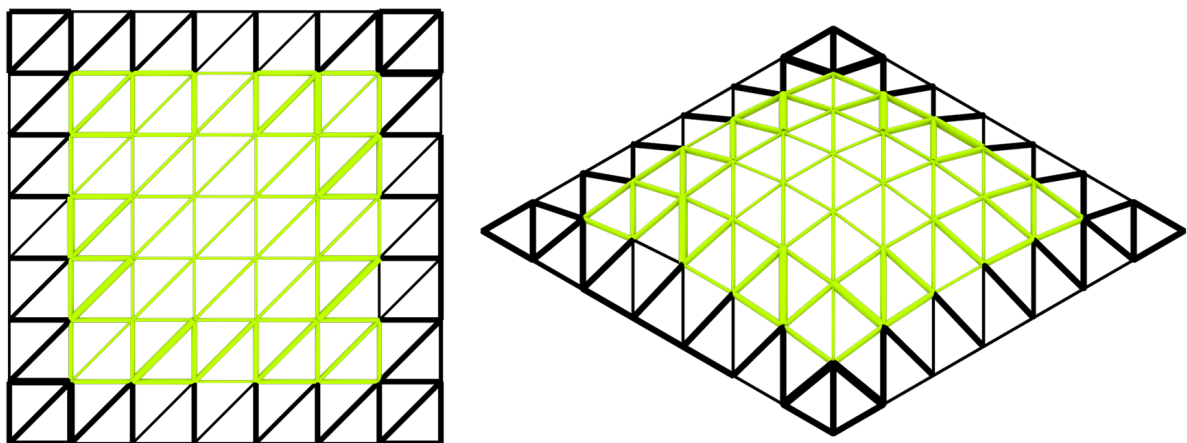


Figure 52 - illustration of a medium sized stock assigned to the regular gridshell structure where black indicates new beam members and lime green indicates reused beam members

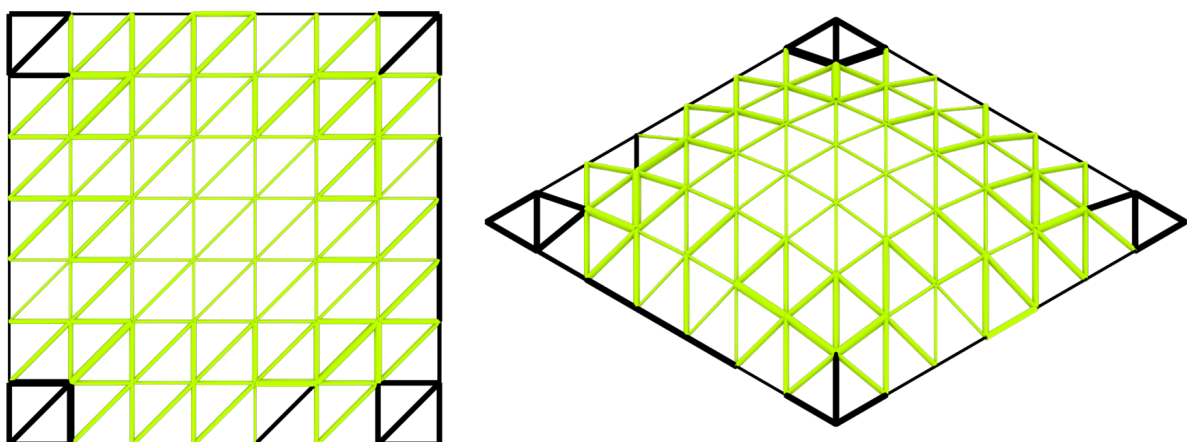


Figure 53 - illustration of a large sized stock assigned to the regular gridshell structure where black indicates new beam members and lime green indicates reused beam members

In the following graphs all generated designs are illustrated with their corresponding objective value. The graphs relate to the optimization sequence of the optimized gridshell. Here again are the designs generated according to a small, medium and large deconstruction stock size. The red dot indicates the design that was used for the research. Below the graph an illustration is made of the gridshell design. Reuse beam members are indicated with lime green and beam members from new production are indicated in black. In case of the small and large stock-size Galapagos couldn't exit the optimization interface. It still did record the last best objective. An optimization was run with this last known best objective. This explains the viewer amount of design iterations. For an overview of all the assigned stock see Appendix '8.12 Overview stock assignment'.

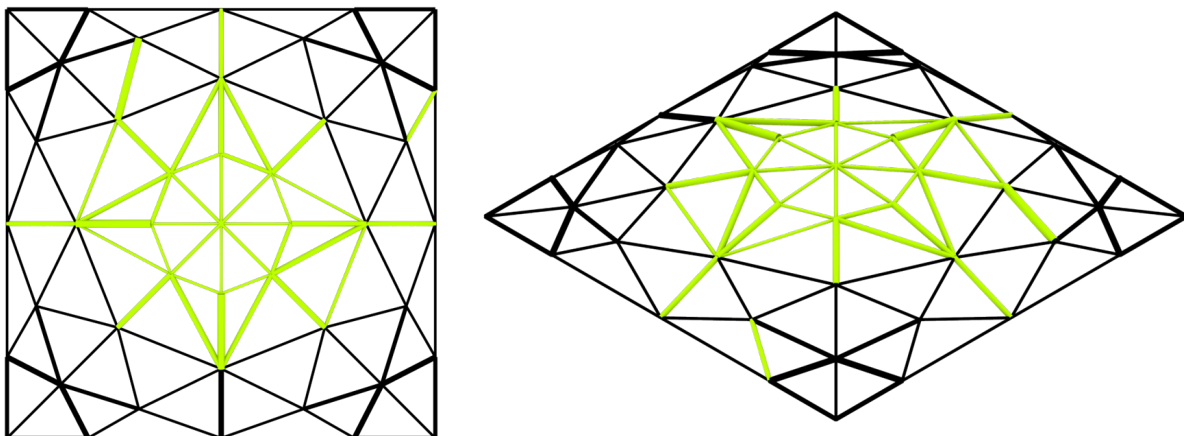
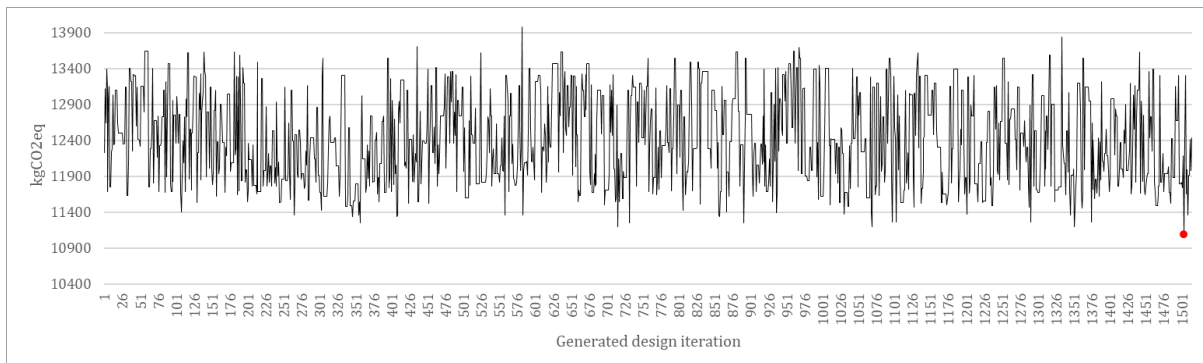


Figure 54 - illustration of the objective of all generated designs for a small stock-size and illustration of stock assigned to the structure where black indicates new beam members and lime green indicates reused beam members

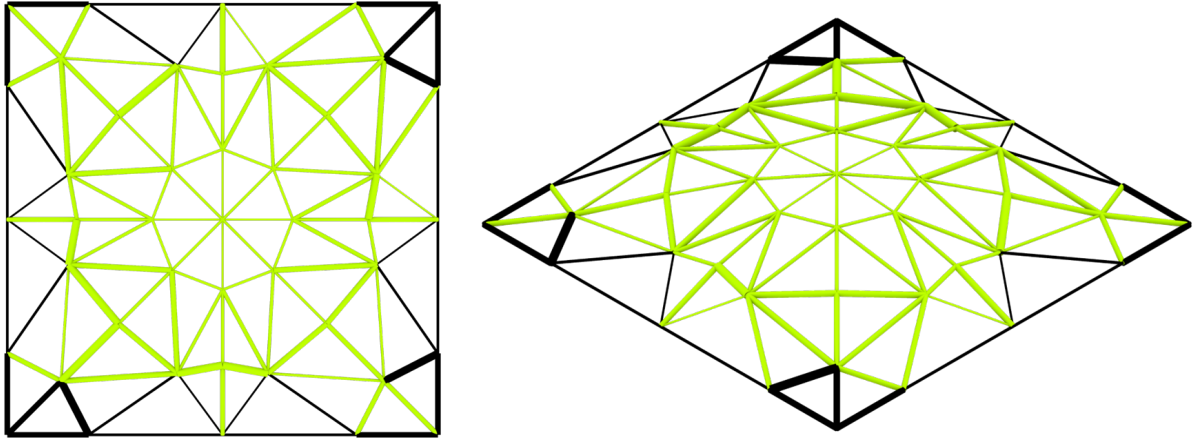
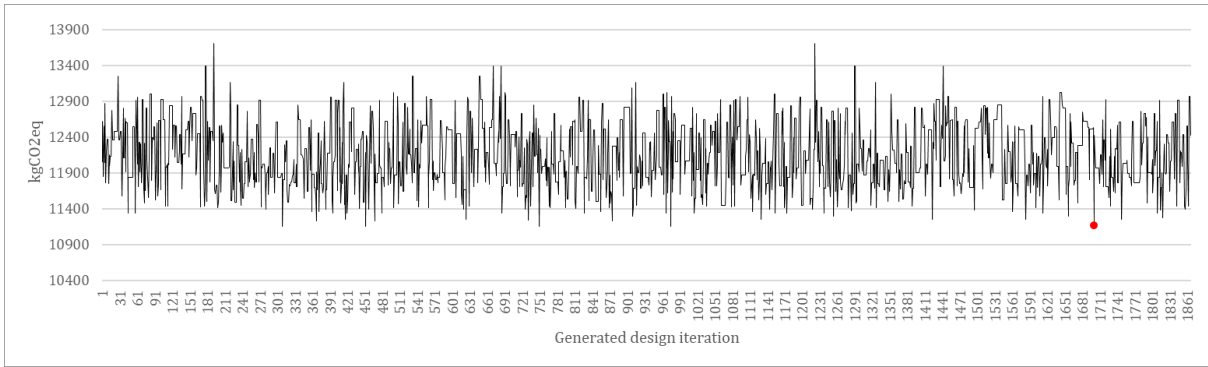


Figure 56 - illustration of the objective of all generated designs for a medium stock-size and illustration of stock assigned to the structure where black indicates new beam members and lime green indicates reused beam members

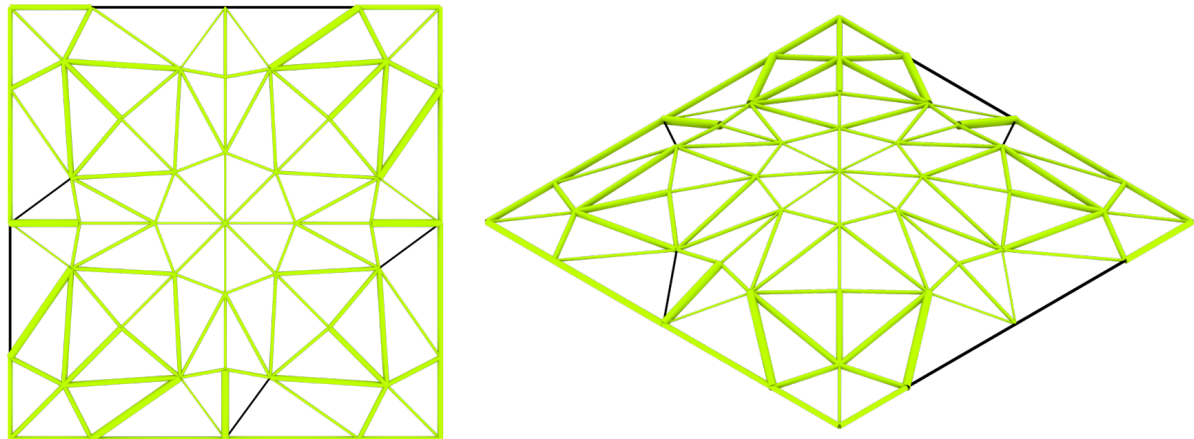
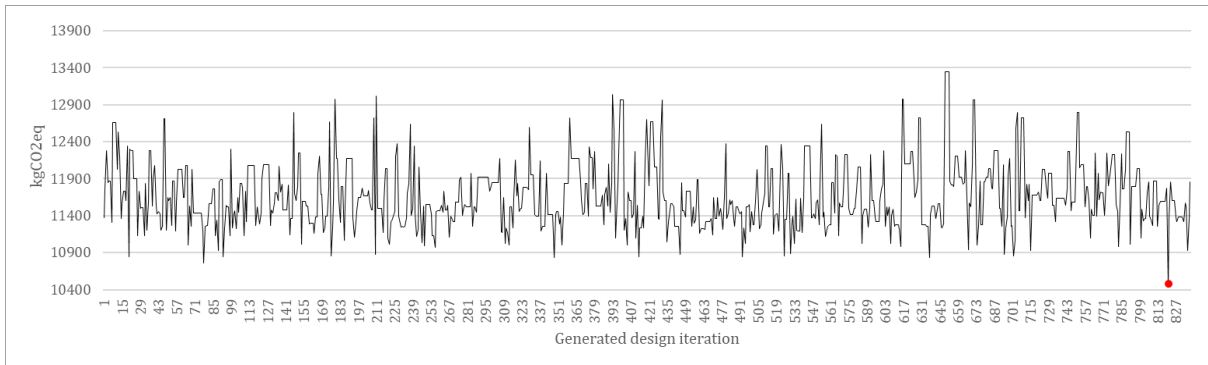


Figure 55 - illustration of the objective of all generated designs for a large stock-size and illustration of stock assigned to the structure where black indicates new beam members and lime green indicates reused beam members

In figure 57 the total distribution of the emissions is illustrated for the different tests with stock sizes. This includes the beam members, nodes and the glass.

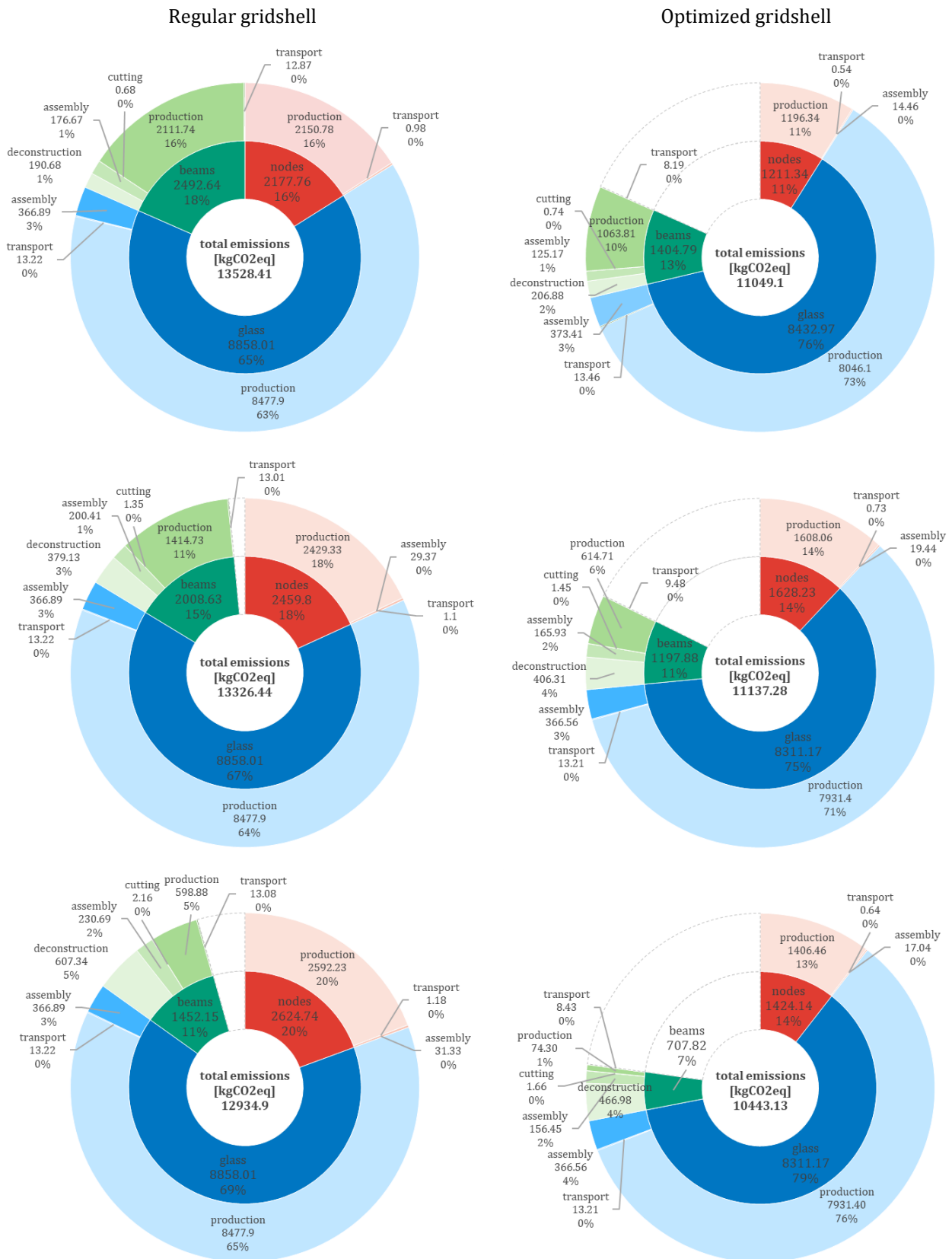


Figure 57 - total distribution of greenhouse gas emissions over the different stock sizes and gridshell structures, from top to bottom: small-, medium- and large stock-size

8.7 Case-study

The following map shows the context used within chapter '4.2 Case-study'. All lines indicate the transport distance and the dots are the destinations: deconstruction site, steel production facility, building site, fabrication workshop, stockpile, node production facility and glass production facility.



Figure 58 – illustration of the context used within the case-study

In figure 59 all design iterations are illustrated with their corresponding objective value. The red dot illustrates the chosen best-performing design. In the illustrations below the graph the assignment of the stock is illustrated. Here black indicates new members, lime green indicates members from the deconstruction scenario and light blue illustrates members from the stockpile scenario. Also in this case Galapagos couldn't exit the optimization interface. The optimization was ran again with a threshold.

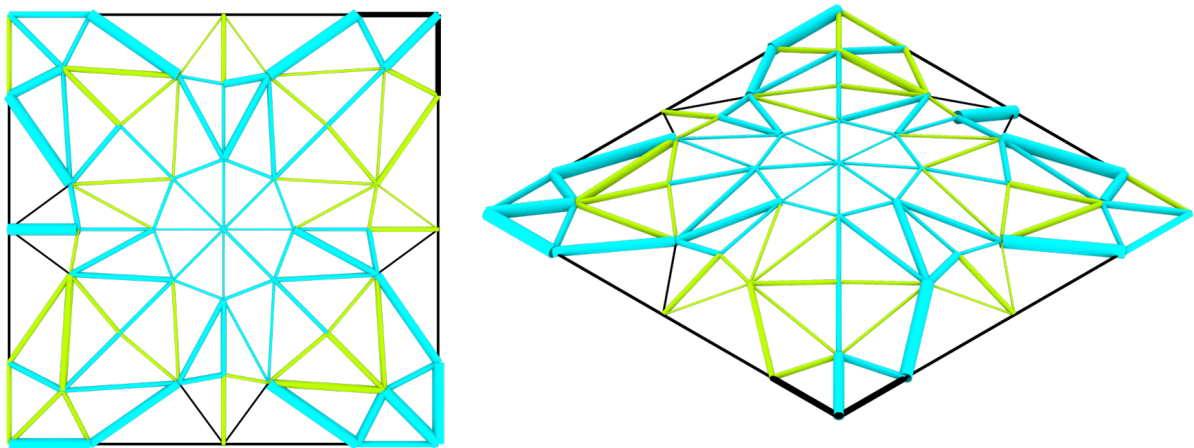
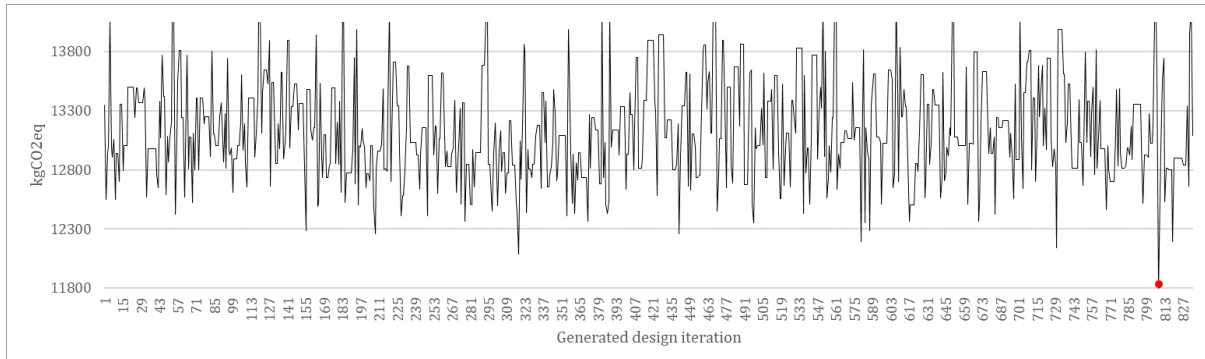


Figure 59 - illustration of the objective of all generated designs for a hybrid stock and illustration of stock assigned to the structure where black indicates new beam members, lime green indicates reused beam members and light blue indicates beam members from stockpile

In figure 60 the total distribution of all emissions are illustrated. This includes the emissions of beam members, nodes and glass.

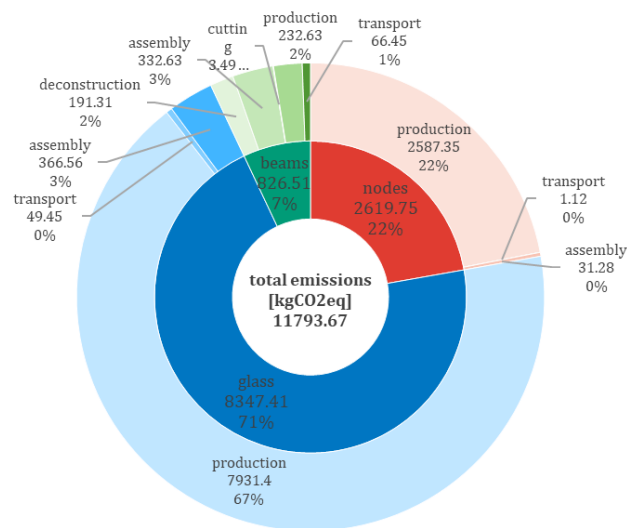


Figure 60 - distribution of the emissions within the gridshell of the case-study

8.8 Benchmark Phoenix3D

The following figure illustrates how the Phoenix3D components are built up in Grasshopper. Indicated with numbers the sub-sections can be described as follows:

1. Here the variables are clustered. In this example variables are related to the geometry of the truss, the assigned load cases and the illustrated output;
2. This part is related to the definition of the geometry of the truss;
3. Here the to-be-analysed model is assembled including initial cross-sections, supports and load cases. Within this sequence also the stock is generated. The stock includes reused- and newly produced beam members.
4. When the model is assembled it can be fed into the optimization algorithms. In this case the algorithms are a Best-Fit and a MILP;
5. In this last step the results are visualized.

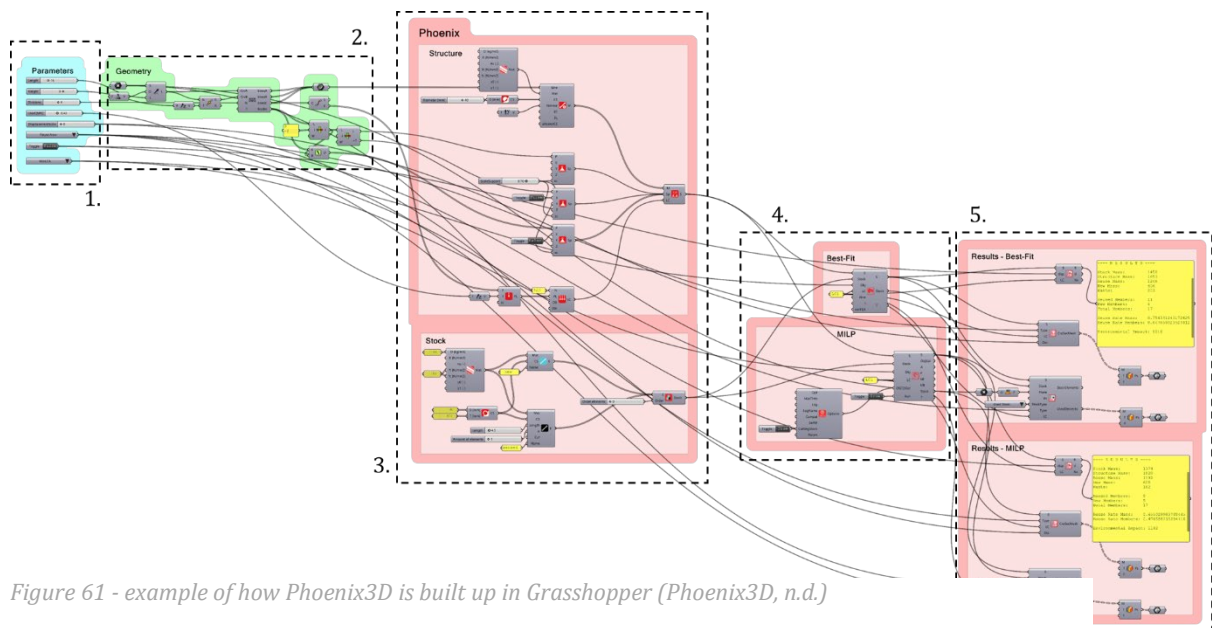
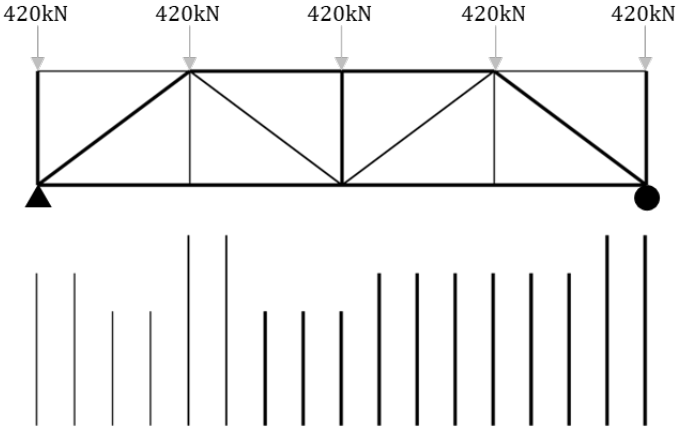
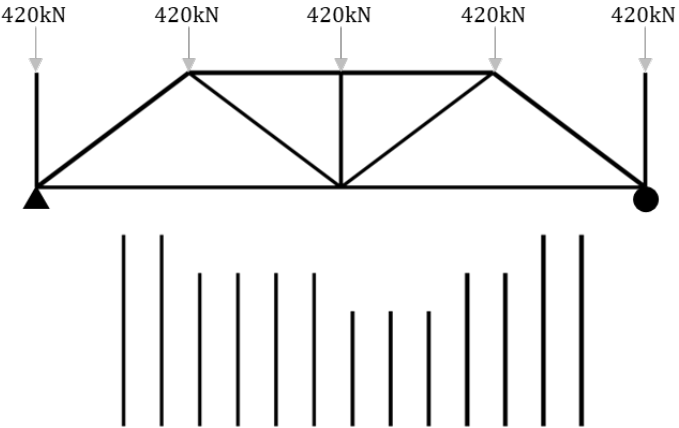
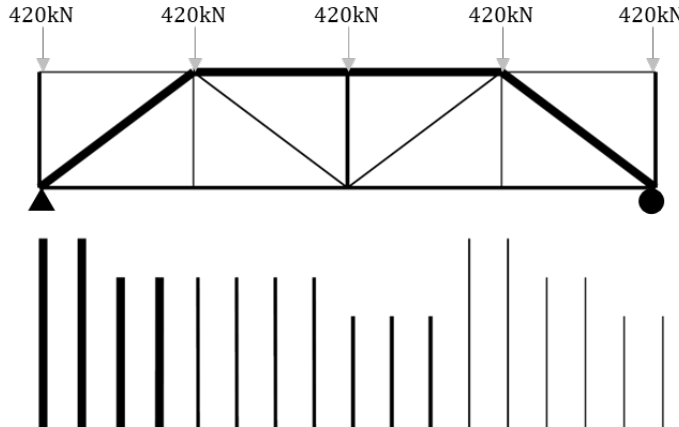
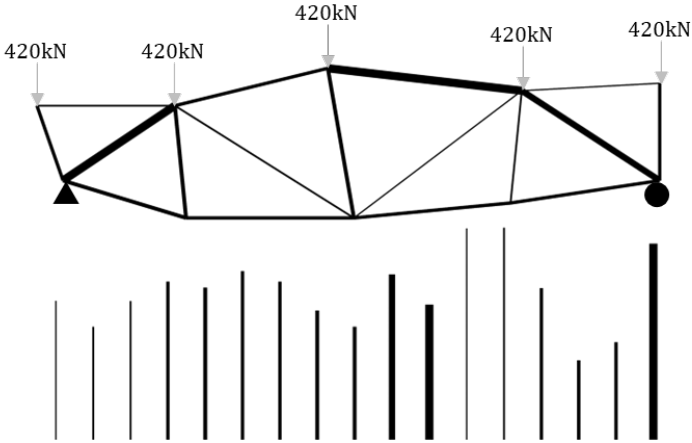
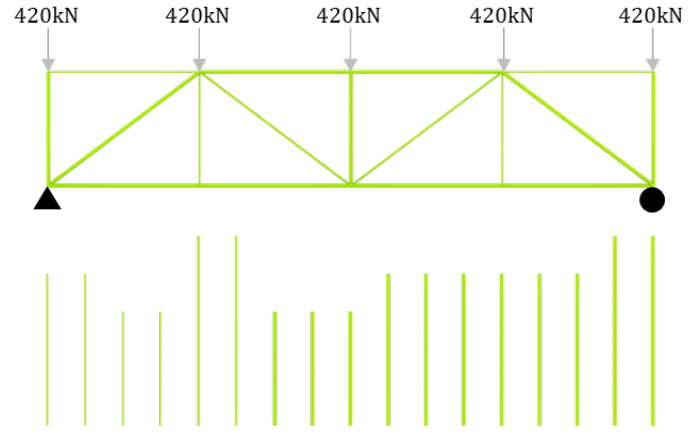
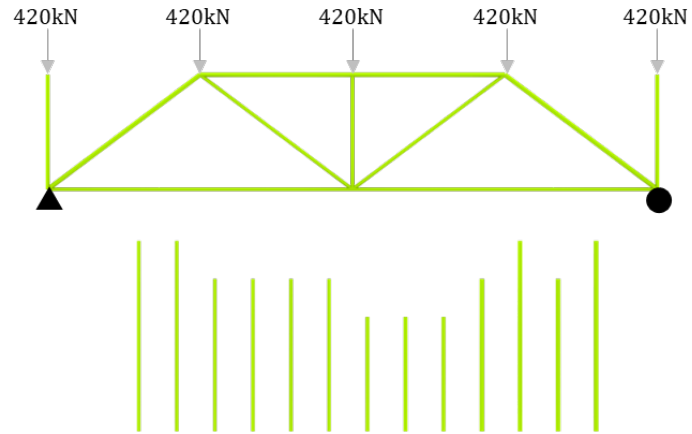


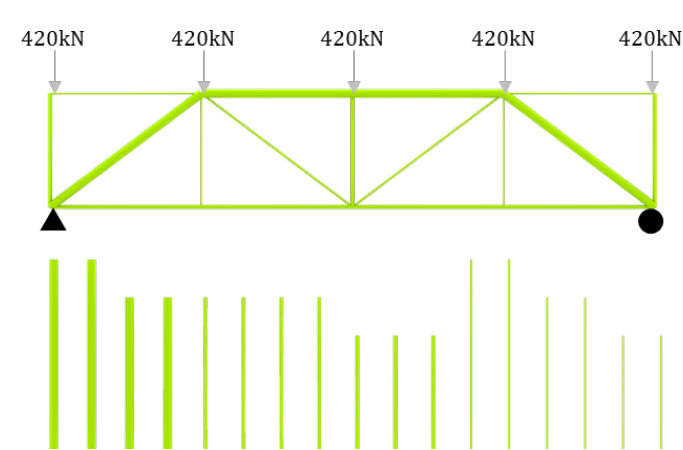
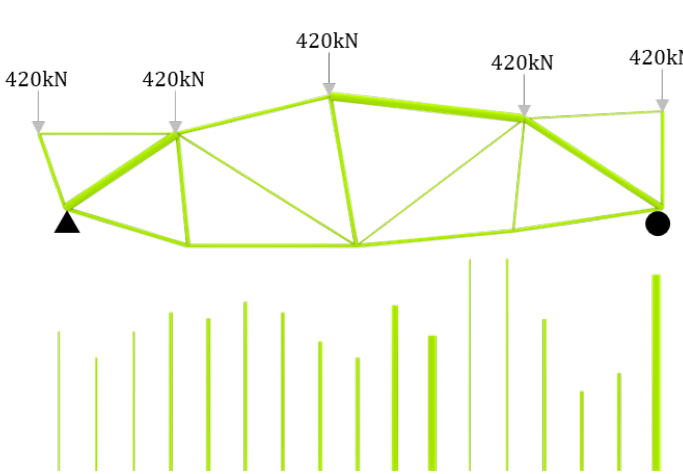
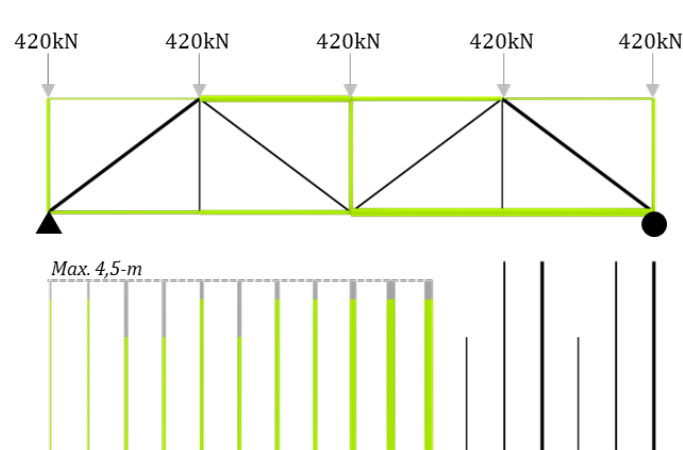
Figure 61 - example of how Phoenix3D is built up in Grasshopper (Phoenix3D, n.d.)

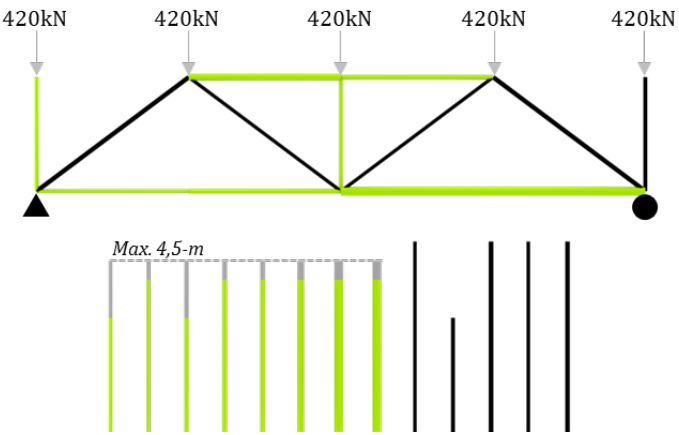
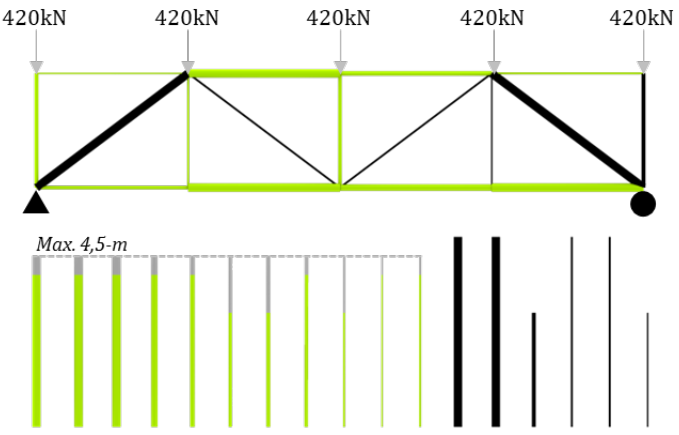
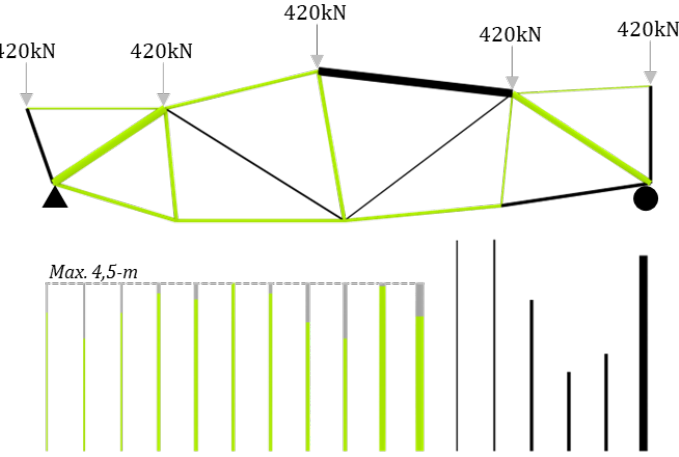
In table 10 all results from the benchmark against Phoenix3D are summarized. For this benchmark different stock is used. Tests were conducted with only new stock, only reused stock and a small-sized (see chapter '4.1.2 Comparison stock sizes) stock in including one unit of 4,5-meter for every unique cross-section from the deconstruction scenario.

Table 10 – all results benchmarked against Phoenix3D and the developed computational tool

Test case	GHG emissions [kgCO _{2eq}]	Reuse-rate	Structure mass [kg]	Illustration
All new stock, Best-Fit	1140	0%	1270	 <p>The diagram shows a truss structure with five 420kN downward loads applied at the top chord. Below the structure is a bar chart representing the weight of each member. The bars vary in height, indicating different member weights.</p>
All new stock, MILP discrete stock	1414	0%	1575	 <p>The diagram shows a truss structure with five 420kN downward loads applied at the top chord. Below the structure is a bar chart representing the weight of each member. The bars vary in height, indicating different member weights.</p>
All new stock, Best-Fit*	1576	0%	1646	 <p>The diagram shows a truss structure with five 420kN downward loads applied at the top chord. Below the structure is a bar chart representing the weight of each member. The bars vary in height, indicating different member weights.</p>

All new stock, Node-shift*	1041	0%	1210	
All reused stock, Best-Fit	686	100%	1270	
All reused stock, MILP discrete stock	839	100%	1575	

All reused stock, Best-Fit*	738	100%	1646	
All reused stock, Node-shift*	542	100%	1210	
Hybrid stock, Best-Fit	1192	66%	1882	

Hybrid stock, MILP discrete stock	1182	65%	1820	
Hybrid stock, Best-Fit*	1193	67%	1889	
Hybrid stock, Node-shift*	763	66%	1210	

*formulation from this research

8.9 Grasshopper script

The following figure illustrates how the components for the computational tool are built up in Grasshopper. Indicated with numbers the sub-sections are described as follows:

1. This section of the script is dedicated to creating the geometry of the gridshell. It also includes the variables that are used by the optimization algorithm;
2. In this part different processes take place. Here the uniformity check is conducted, the loads are calculated and the support points are generated;
3. Here the data loop is created with the use of the plugin Anemone.
4. This section is fully dedicated to performing the finite element analysis with the use of Karamba3D. This analysis is performed for the beam members and the glass;
5. After the finite element analysis the stock is assigned with the use of a Best-Fit algorithm. This algorithm is coded in Python;
6. When the Best-Fit algorithm assigned all members the emissions of glass and nodes are calculated based on this. Here also additional information is calculated such as the reuse rate and the mass of the structure;
7. In combination with another finite element analysis a final check of all constraints is conducted here. When the design does not comply with the constraints penalty score is given to the fitness value. In this way the optimization algorithm can distinguish compatible designs and non-compatible designs;
8. Here all design iterations are recorded;
9. This part is mainly used to export all numerical and visual data for Design Explorer.

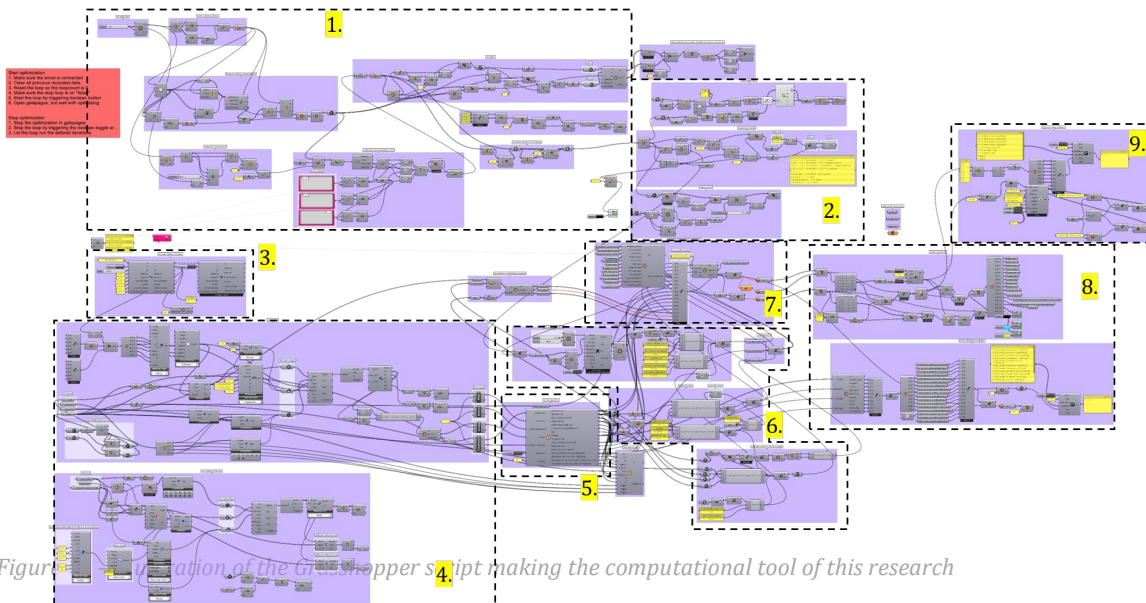


Figure 61: Organization of the Grasshopper script making the computational tool of this research

The following part will zoom in on the parts of the script that are highlighted in figure 61. It will also explain what the input data and the output data are of this particular part.

Part 1 (see fig. 63)

Input:

- Size of 1/4th of the gridshell;
- The number of points (representing the nodes) that need to make 1/4th of the gridshell.

Output:

- Triangulated glass panels in the form of surfaces;
- Information about if the triangles in the grid meet the size constraints for manufacturing of glass;
- Angles of the corners of the glass panes.

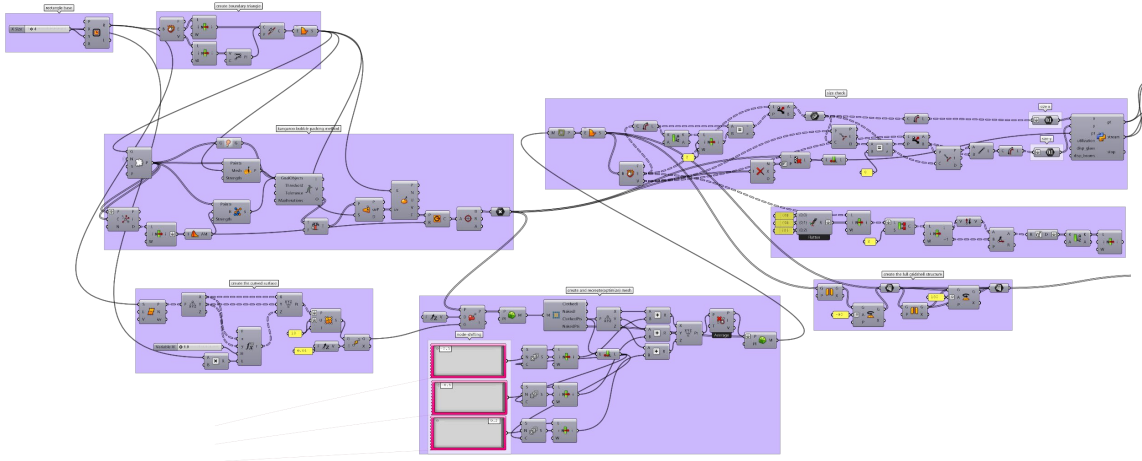


Figure 63 - zoom in on part 1 of the Grasshopper script

Part 2 (see fig. 64)

Input:

- Triangulated glass panes in the form of surfaces;
- Information about if the triangles in the grid meet the sizes for manufacturing of glass.

Output:

- Information about the uniformity of the gridshell;
- Values for the needed loads making the line loads on the beams;
- The points that locate the supports for the gridshell.

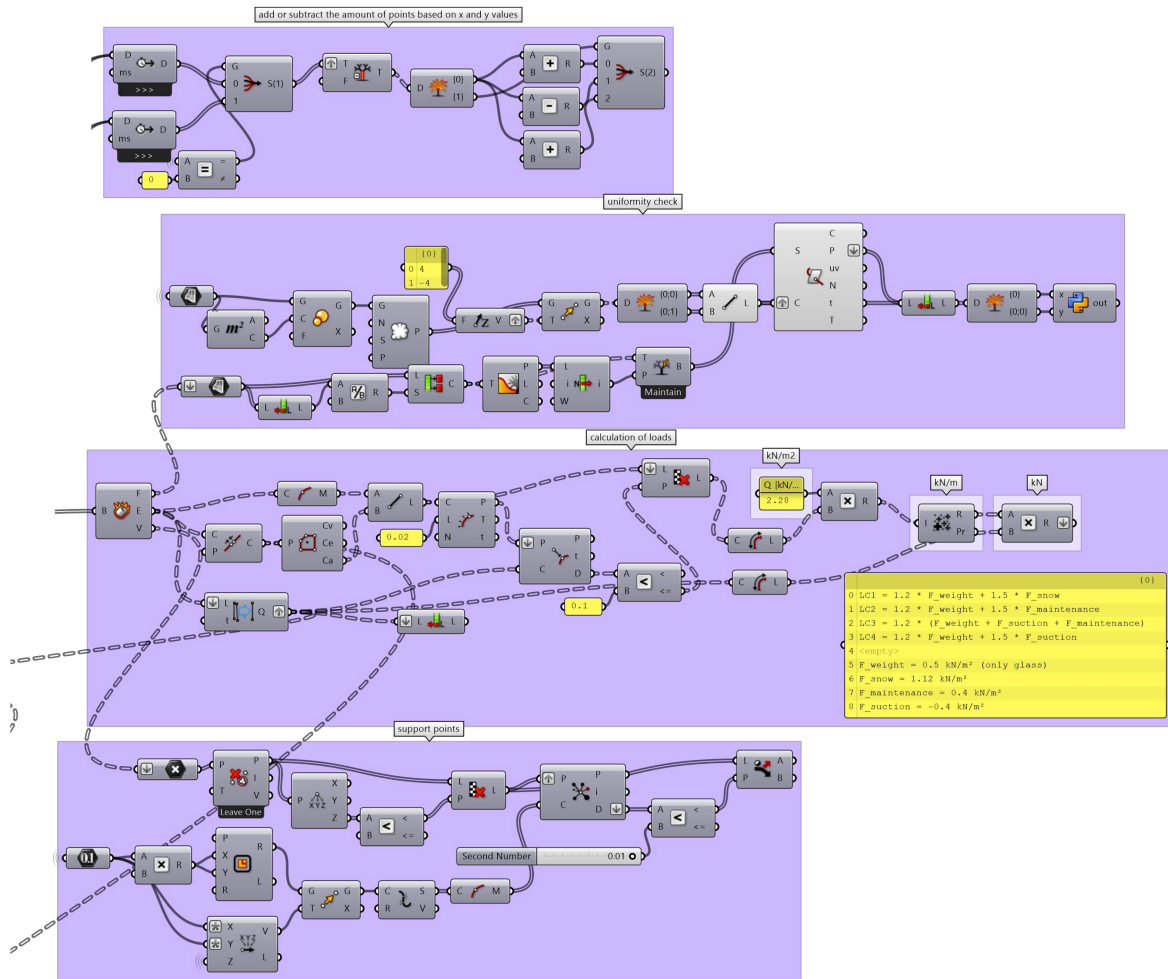


Figure 64 - zoom in on part 2 of the Grasshopper script

Part 3 (see fig. 65)

Input:

- Starting values for the properties of the beam members;
- For Galapagos, the objective in greenhouse gas emissions and the variables to calculate with.

Output:

- Starting values for the properties of the beam members;
- New values for the properties of the beam members calculated by the Best-Fit algorithm;
- For Galapagos, resulting designs with calculated objectives in greenhouse gas emissions.

Part 7 (see fig. 69)

Input:

- Information about the utilization and deflection of both beam members and glass;
- Length of the beam members;
- Information about the uniformity of the structure.

Output:

- All relevant numerical and geometrical data concerning the designed structure.

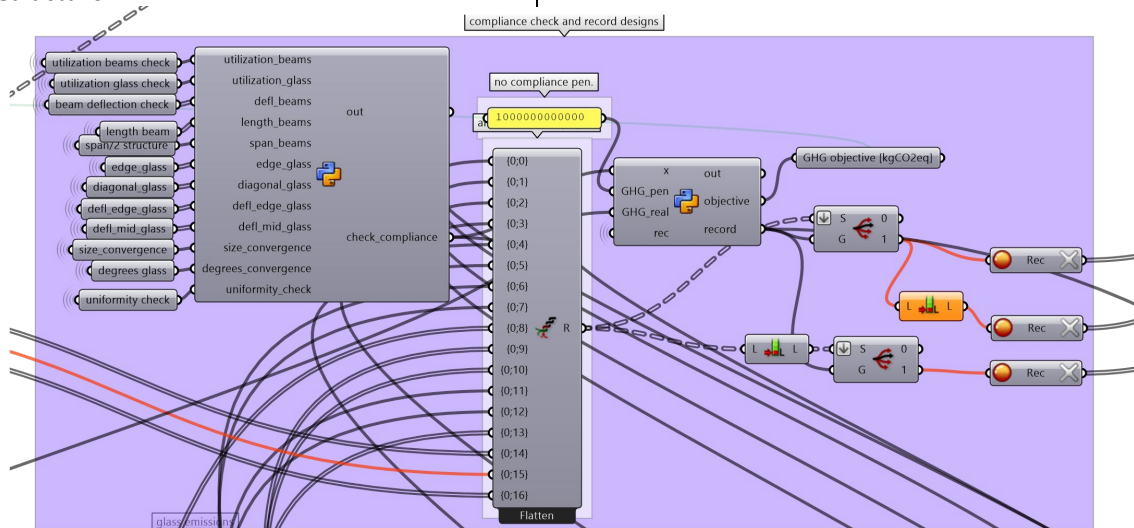


Figure 69 - zoom in on part 7 of the Grasshopper script

Part 8 (see fig. 70)

Input:

- All relevant numerical and geometrical data concerning the designed structure.

Output:

- All relevant numerical and geometrical data concerning all the designed structures that meet the constraints are organized to be exported.

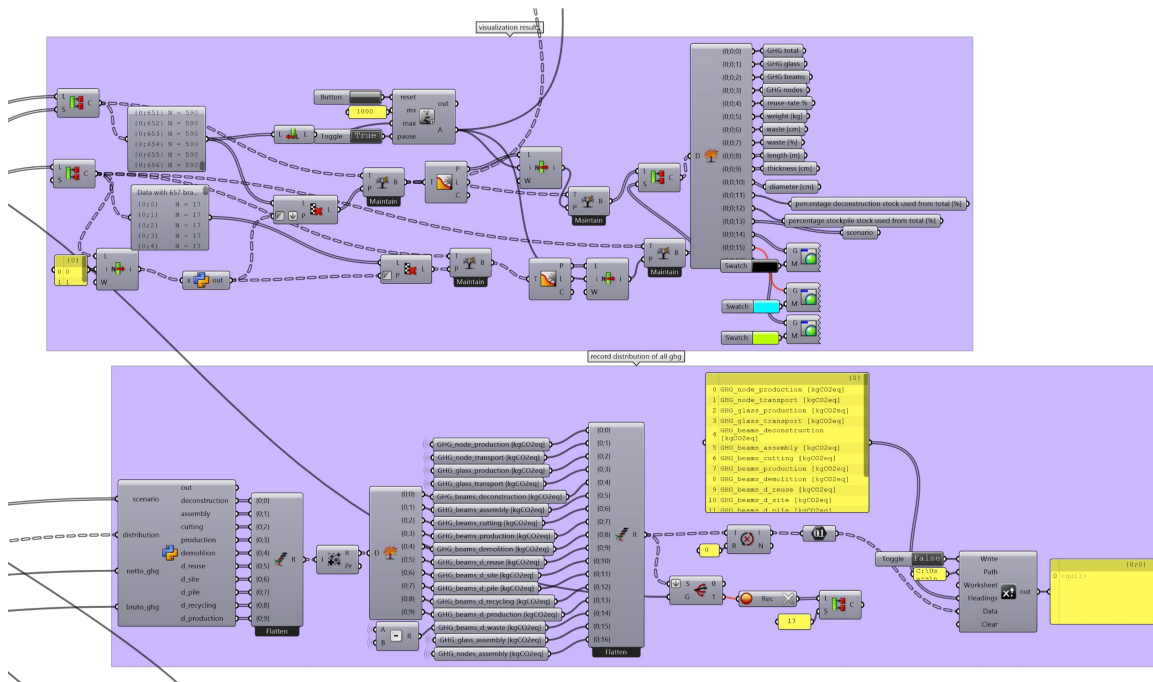


Figure 70 - zoom in on part 8 of the Grasshopper script

Part 9 (see fig. 71)

Input:

- All relevant numerical and geometrical data concerning all the designed structures that meet the constraints are organized to be exported.

Output:

- Data in Excel including exported illustrations of the structure with the assignment of beam members. This is organized in a way that the data can also be used by Design Explorer.

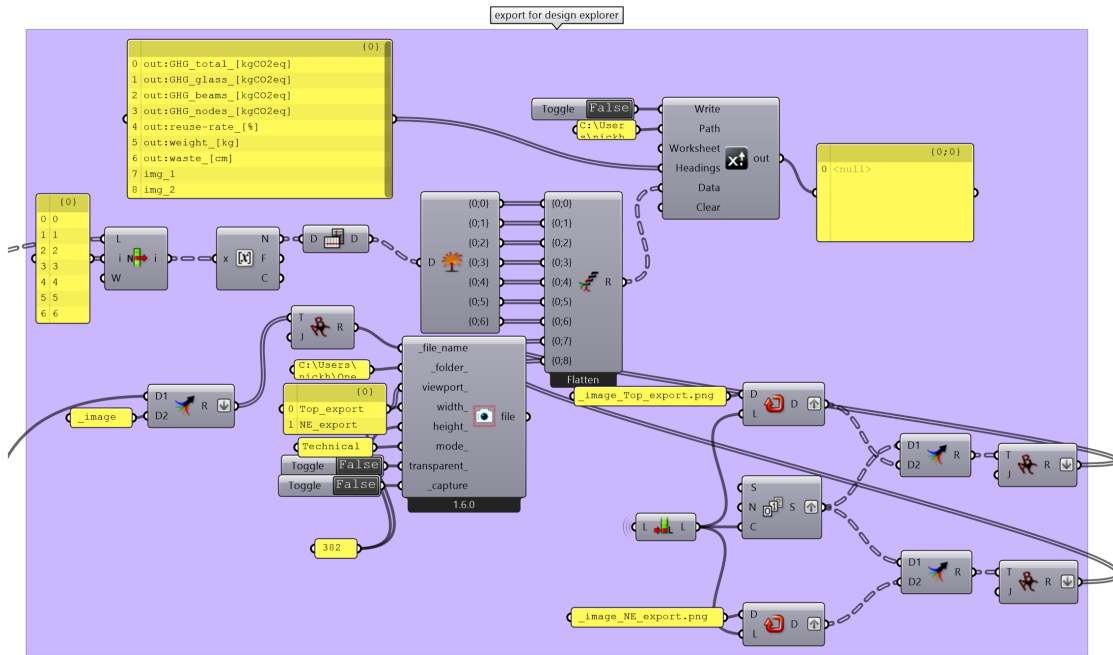


Figure 71 - zoom in on part 9 of the Grasshopper script

8.10 Pseudocode

The following pseudocode is related to the Best-Fit algorithm. The Best-Fit algorithm assigns stock according to their capacity and their objective value in terms of emissions [kgCO_{2eq}].

```
SteelGHG = 0
FOR Member in structure
  BestObjective = +∞
  OptimalAssignment = [0,0]
  FOR Stock in stocklist
    IF MemberLength <= StockLength OR StockType = new
      Calculate CompressionCapacity =  $f_c^c$ 
      Calculate TensionCapacity =  $f_c^t$ 
      Calculate BendingmomentCapacity =  $f_c^{bm}$ 
      Calculate ShearforceCapacity =  $f_c^s$ 
      Get CompressionMember from Karamba =  $f_m^c$ 
      Get TensionMember from Karamba =  $f_m^t$ 
      Get BendingmomentMember from Karamba =  $f_m^{bm}$ 
      Get ShearforceMember from Karamba =  $f_m^s$ 

      IF  $f_c^c \geq f_c^s$  AND  $f_c^t \geq f_m^t$  AND  $f_c^{bm} \geq f_m^{bm}$  AND  $f_c^s \geq f_m^s$ 
        Mass = MemberLength * AreaStock * DensityStock
        IF StockType = reuse
          IF StockScenario = deconstruction
            IF StockLength = MemberLength
              Objective = Mass * (∑ EmissionCoefficients related to deconstruction excl. cutting)
            ELSE
              Objective = Mass * (∑ EmissionCoefficients related to deconstruction incl. cutting)
          ELSE
            Objective = Mass * (∑ EmissionCoefficients related to stockpile)
        ELSE
          Objective = Mass * (∑ EmissionCoefficients related to new production)
        IF Objective < BestObjective
          BestObjective = Objective
          OptimalAssignment = [GroupIndex, MemberIndex]
          Call = OptimalAssignment[1] - 1
    SteelGHG = SteelGHG + BestObjective

MaterialGrade = Grade[Call]
IF OptimalAssignment == [0,0]
  Assignment = Member is infeasible and nothing is assigned
  return AssignedStockProperties
ELIF MaterialGrade = S235 OR MaterialGrade = S275 OR MaterialGrade = S355
  Assignment = Member is assigned
  return AssignedStockProperties
ELSE
  Assignment = Member is assigned but steel grade is not added to code
  return AssignedStockProperties
IF StockType[Call] = reuse
  StockLength[Call] = StockLength[Call] - MemberLength[Call]
  TotalStockLength.append(StockLength)
  TotalCalledStock.append(initial StockLength)
  WasteSteel = TotalStockLength - TotalCalledStock
```

The following pseudocode is related to the check of all constraints.

```
CheckCompliance = 0
CheckDeflectionGlass = 0
CheckDeflectionBeams = 0

FOR Member in structure
  IF DeflectionMember < LengthMember / 250
    CheckDeflectionBeams = 1
  ELSE
    CheckDeflectionBeams = 0
    break

FOR Glass in structure
  IF DeflectionEdgeGlass <= LengthEdgeGlass / 100 AND DeflectionCentreGlass <= DiagonalGlass / 65
  AND DiagonalGlass / 65 <= 50
    CheckDeflectionGlass = 1
  ELSE
    CheckDeflectionGlass = 0
    break

IF UtilizationMember < 100% AND UtilizationGlass < 100% AND CheckDeflectionBeams = 1
AND CheckDeflectionGlass = 1
  CheckCompliance = 1
ELSE
  CheckCompliance = 0
```

The original code is available upon request. Contact the author by sending an e-mail to:

N.Heijne

8.11 Visualisations gridshell

Here visualizations are made from the results of the different tests that are conducted in this research.

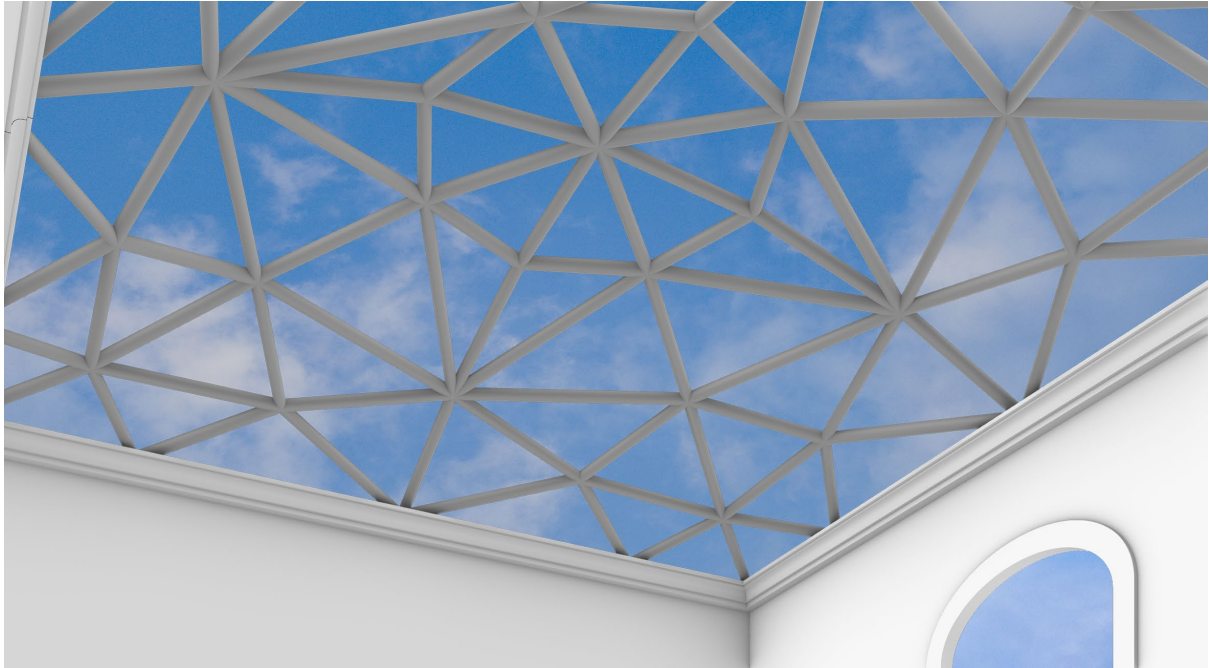


Figure 72 - all new production scenario single cross-section

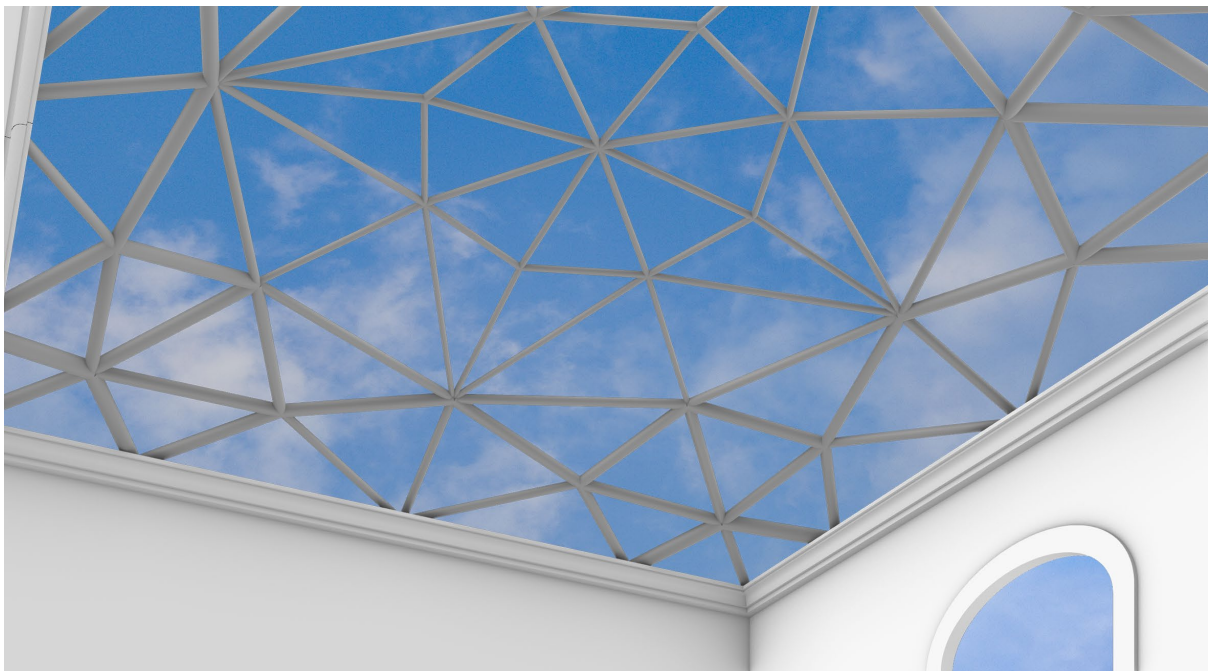


Figure 73 - all new production scenario optimized cross-sections

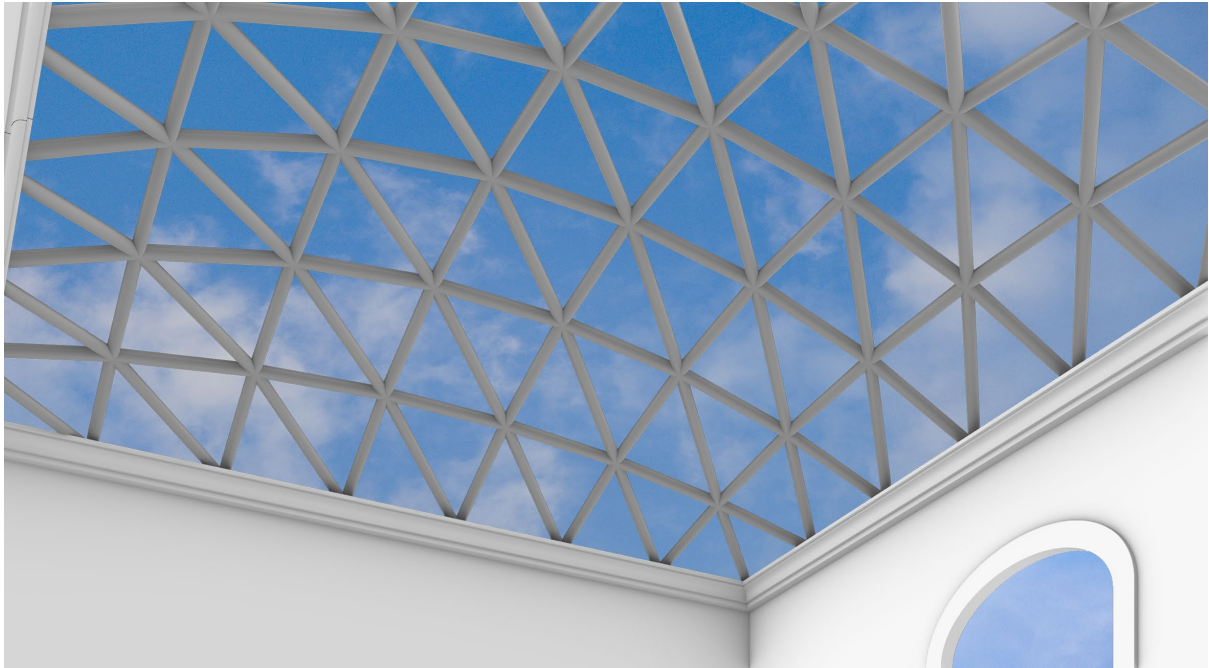


Figure 74 – standardized gridshell pattern single cross-section

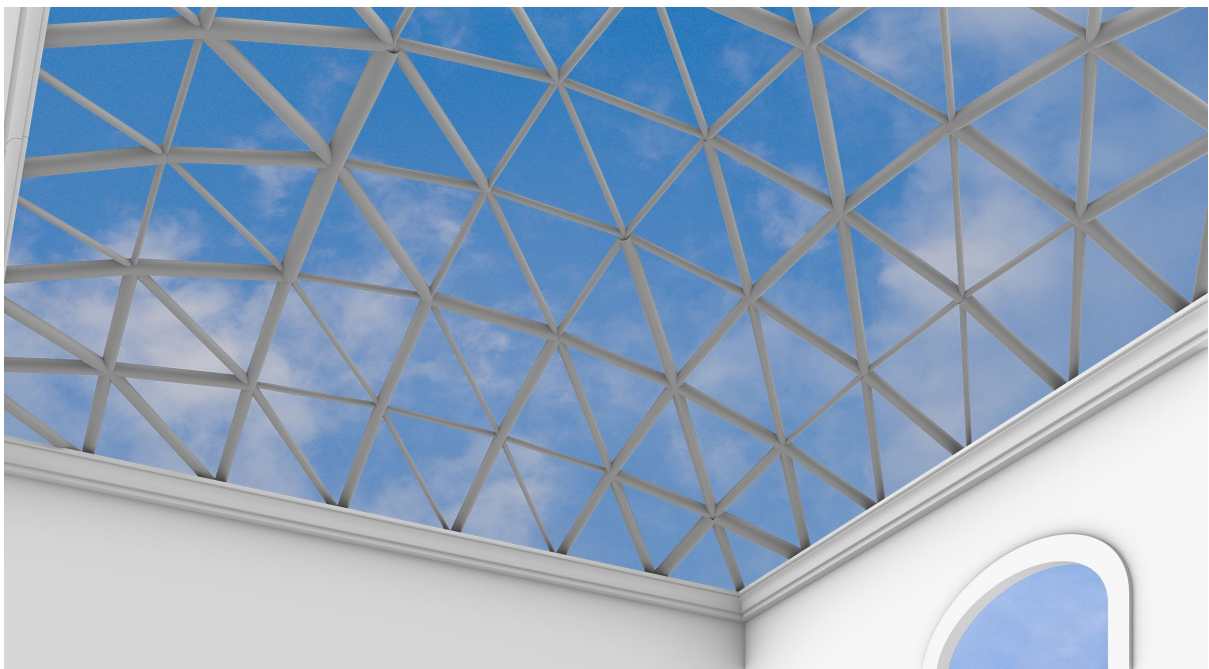


Figure 75 – standardized gridshell pattern assignment small stock



Figure 76 - standardized gridshell pattern assignment medium stock

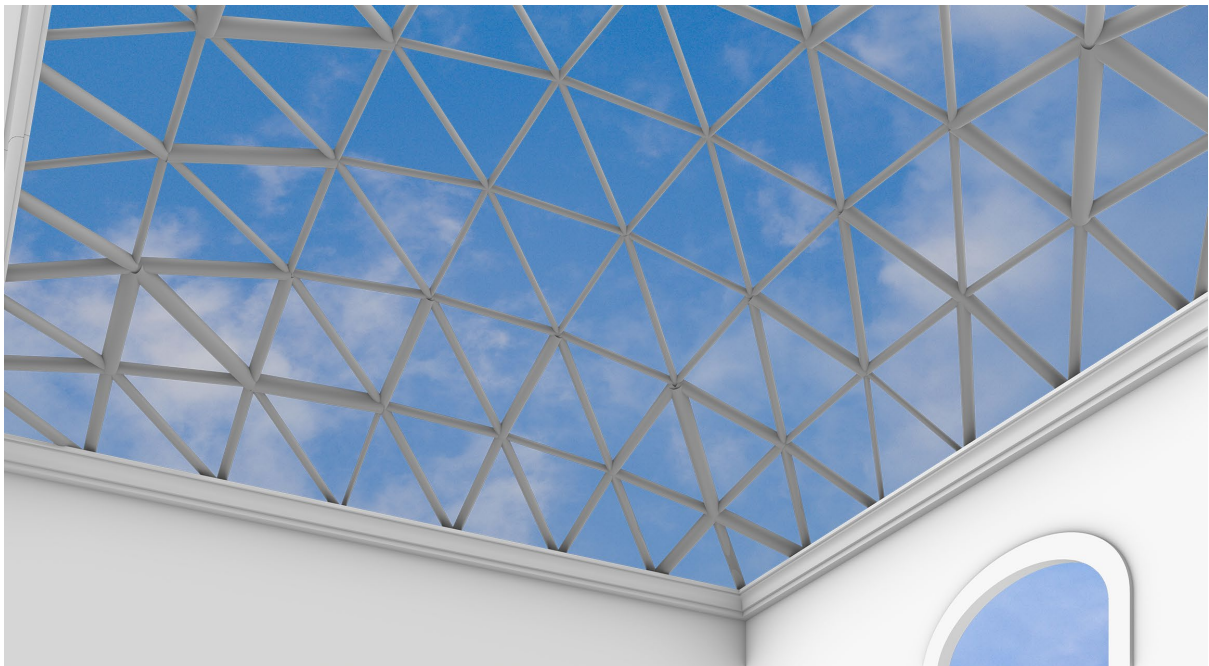


Figure 77 - standardized gridshell pattern assignment large stock

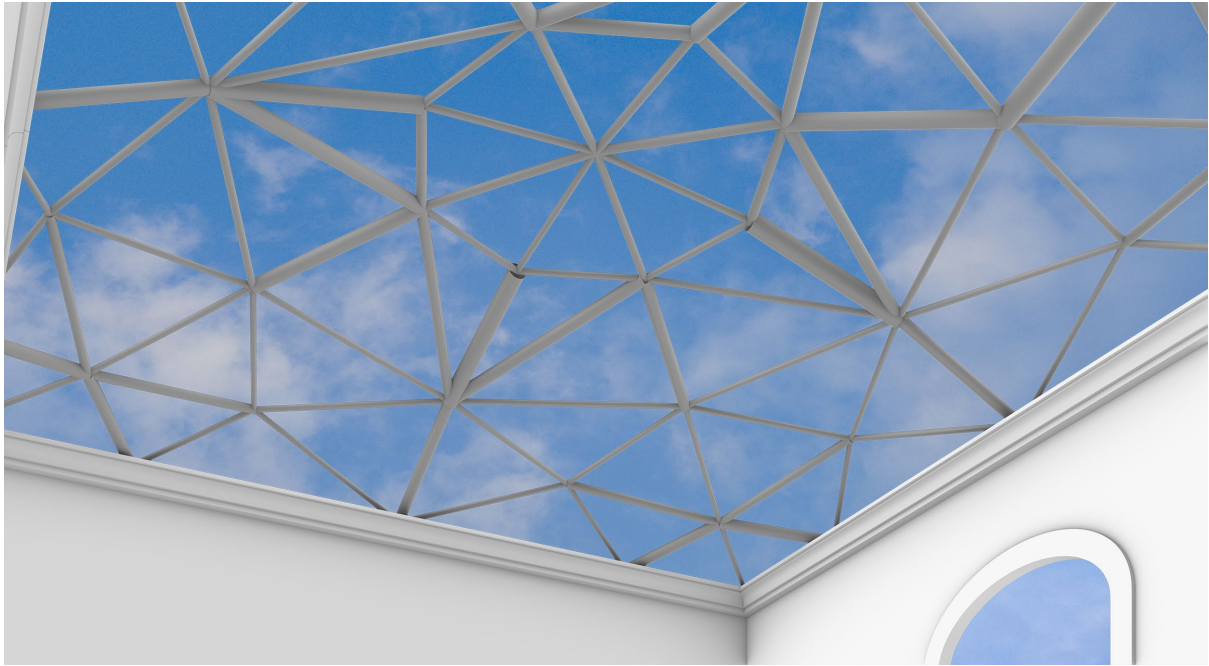


Figure 78 - optimized gridshell pattern assignment small stock

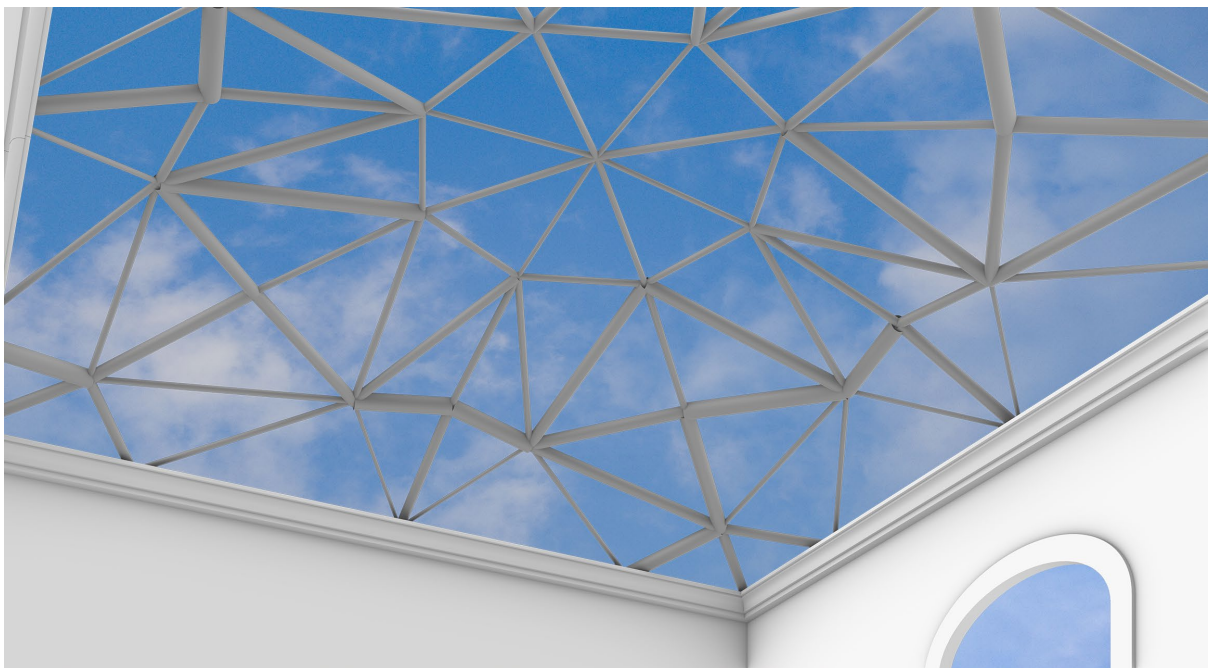


Figure 79 - optimized gridshell pattern assignment medium stock

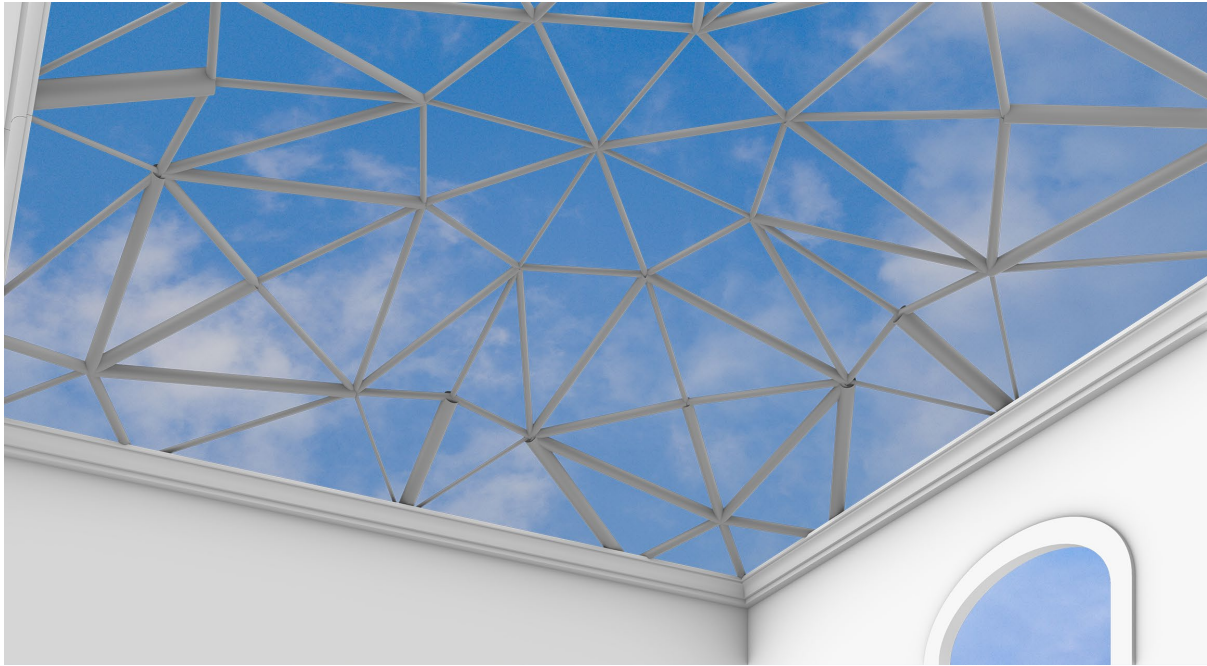


Figure 80 - optimized gridshell pattern assignment large stock

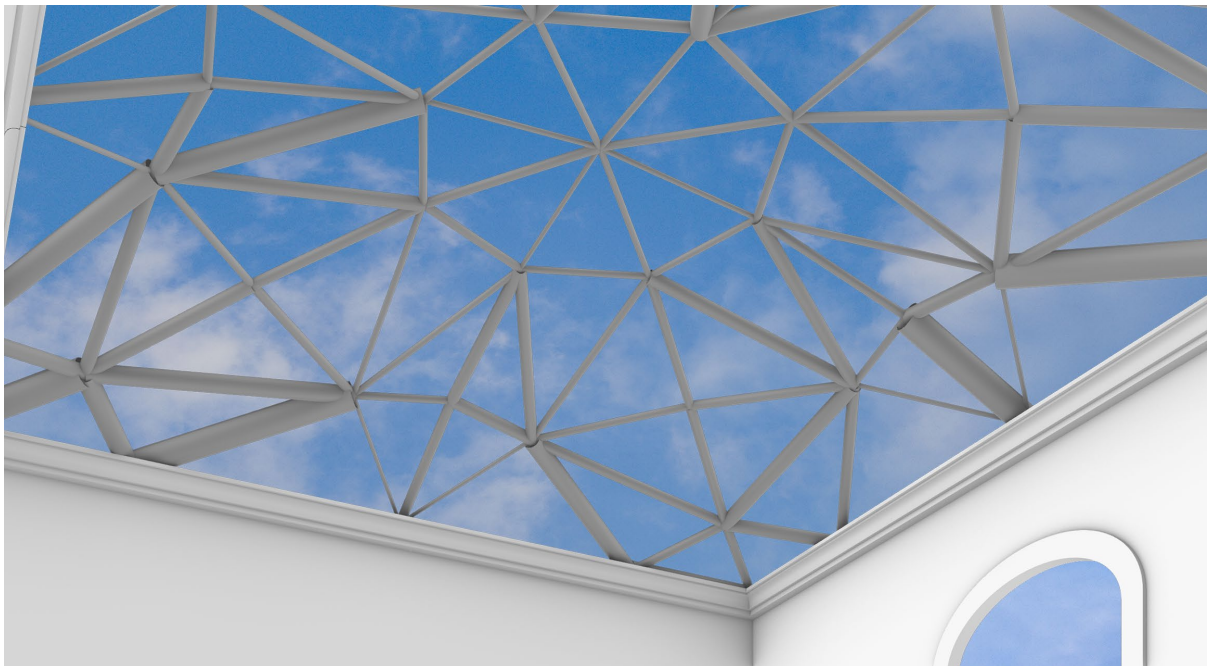


Figure 81 – case-study assignment hybrid stock (all scenarios)

Since it is assumed that aesthetics are subjective no hard conclusions will be drawn within this topic. It can be said that visually the gridshells that are resultant are impacted by the size and composition of the stock. It can be noticed that when the stock size of reuse is bigger the larger cross-sections shift to the edge of the gridshell. This also has to do with the order of members. As seen in the illustrations in some cases the assignment of stock will result in an asymmetrical design. In practice this could be overcome by fine-tuning the symmetry by assigning newly produced members with sufficient structural capacity. Of course this will be at the cost of the embodied carbon of the structure.

8.12 Overview stock assignment

In this part of the Appendix an overview is shown with the assigned stock from the different tests. Some values are marked in red. The reason for this is because this stock exceeds the maximum value due to an error in the Best-Fit algorithm. For the small stock the maximum size is 4,5-meter, for the medium stock the maximum size is 9-meter and for large stock the maximum size is 13,5-meter.

8.12.1 Small stock, optimized gridshell

length [cm]	thickness [cm]	diameter [cm]	scenario
131.03	0.32	4.8	deconstruction
131.03	0.32	4.8	deconstruction
131.03	0.32	4.8	deconstruction
131.03	0.29	6	deconstruction
133.75	0.29	6	deconstruction
133.75	0.29	6	deconstruction
133.75	0.3	6	deconstruction
133.75	0.3	6	deconstruction
101.03	0.25	4.8	deconstruction
101.03	0.25	4.8	deconstruction
101.03	0.25	4.8	deconstruction
101.03	0.25	4.8	deconstruction
101.03	0.3	6	deconstruction
101.03	0.25	7.6	deconstruction
101.03	0.25	7.6	deconstruction
101.03	0.25	7.6	deconstruction
143.71	0.36	10.2	deconstruction
143.71	0.36	10.2	deconstruction
143.71	0.36	10.2	deconstruction
143.71	0.4	10.2	deconstruction
144.45	0.4	10.2	deconstruction
144.45	0.4	10.2	deconstruction
144.45	0.3	14	deconstruction
144.45	0.3	14	deconstruction
203.09	0.9	4.8	deconstruction
203.09	0.9	4.8	deconstruction
203.09	0.6	8.9	deconstruction
203.09	0.6	8.9	deconstruction
203.09	0.6	10.2	deconstruction
203.09	0.6	10.2	deconstruction
203.09	0.76	8.9	deconstruction
203.09	0.76	8.9	deconstruction
208.42	0.32	6	deconstruction
208.42	0.32	6	deconstruction
208.42	0.25	4.8	new_production
208.42	0.25	4.8	new_production
208.42	0.25	4.8	new_production
208.42	0.25	4.8	new_production
208.42	0.25	4.8	new_production

208.42	0.25	4.8	new_production
157.81	0.3	14	deconstruction
157.81	0.32	4.8	new_production
157.81	0.32	4.8	new_production
157.81	0.32	4.8	new_production
157.81	0.32	4.8	new_production
157.81	0.32	4.8	new_production
157.81	0.32	4.8	new_production
157.81	0.32	4.8	new_production
157.81	0.32	4.8	new_production
171.33	0.32	4.8	new_production
171.33	0.32	4.8	new_production
171.33	0.32	4.8	new_production
171.33	0.32	4.8	new_production
171.33	0.32	4.8	new_production
171.33	0.32	4.8	new_production
171.33	0.32	4.8	new_production
171.33	0.32	4.8	new_production
171.33	0.32	4.8	new_production
155.67	0.25	4.8	new_production
155.67	0.25	4.8	new_production
155.67	0.25	4.8	new_production
155.67	0.25	4.8	new_production
155.6	0.25	7.6	new_production
155.6	0.25	7.6	new_production
155.6	0.25	7.6	new_production
155.6	0.25	7.6	new_production
155.6	0.25	7.6	new_production
155.6	0.25	7.6	new_production
155.6	0.25	7.6	new_production
155.6	0.25	7.6	new_production
155.6	0.25	7.6	new_production
140.19	1.75	8.9	deconstruction
140.19	1.75	8.9	deconstruction
140.19	1.75	8.9	deconstruction
140.19	0.36	10.2	new_production
118.74	0.25	7.6	deconstruction
118.74	0.32	4.8	new_production
118.74	0.32	4.8	new_production
169.51	0.32	4.8	new_production
169.51	0.32	4.8	new_production
118.74	0.32	4.8	new_production
169.51	0.32	4.8	new_production
169.51	0.32	4.8	new_production
118.74	0.32	4.8	new_production
169.51	0.32	4.8	new_production
169.51	0.32	4.8	new_production
169.51	0.32	4.8	new_production
169.51	0.32	4.8	new_production
118.74	0.32	4.8	new_production

118.74	0.32	4.8	new_production
118.74	0.32	4.8	new_production
113.95	0.36	10.2	new_production
113.95	0.36	10.2	new_production
142.66	0.32	4.8	new_production
142.66	0.32	4.8	new_production
113.95	0.36	10.2	new_production
113.95	0.36	10.2	new_production
113.95	0.36	10.2	new_production
113.95	0.36	10.2	new_production
113.95	0.36	10.2	new_production
142.66	0.32	4.8	new_production
142.66	0.32	4.8	new_production
248.78	0.32	4.8	new_production
151.22	0.25	7.6	new_production
151.22	0.25	7.6	new_production
248.78	0.32	4.8	new_production
248.78	0.32	4.8	new_production
248.78	0.32	4.8	new_production
151.22	0.25	7.6	new_production
151.22	0.25	7.6	new_production
248.78	0.32	4.8	new_production
151.22	0.25	7.6	new_production
248.78	0.32	4.8	new_production
151.22	0.25	7.6	new_production
248.78	0.32	4.8	new_production
151.22	0.25	7.6	new_production
248.78	0.32	4.8	new_production
151.22	0.25	7.6	new_production
248.78	0.32	4.8	new_production
151.22	0.25	7.6	new_production

8.12.2 Medium stock, optimized gridshell

length [cm]	thickness [cm]	diameter [cm]	scenario
131.03	0.25	3.4	deconstruction
131.03	0.25	3.4	deconstruction
131.03	0.25	3.4	deconstruction
131.03	0.25	3.4	deconstruction
133.75	0.32	4.8	deconstruction
133.75	0.32	4.8	deconstruction
133.75	0.32	4.8	deconstruction
133.75	0.32	4.8	deconstruction
101.03	0.25	4.8	deconstruction
101.03	0.25	4.8	deconstruction
101.03	0.25	4.8	deconstruction
101.03	0.25	4.8	deconstruction
101.03	0.25	4.8	deconstruction

101.03	0.25	4.8	deconstruction
101.03	0.25	4.8	deconstruction
101.03	0.25	4.8	deconstruction
143.71	0.32	4.8	deconstruction
143.71	0.32	4.8	deconstruction
143.71	0.29	6	deconstruction
143.71	0.29	6	deconstruction
144.45	0.29	6	deconstruction
144.45	0.29	6	deconstruction
144.45	0.29	6	deconstruction
144.45	0.29	6	deconstruction
181.55	0.3	6	deconstruction
181.55	0.3	6	deconstruction
181.55	0.3	6	deconstruction
181.55	0.3	6	deconstruction
181.55	0.25	7.6	deconstruction
181.55	0.25	7.6	deconstruction
181.55	0.25	7.6	deconstruction
181.55	0.25	7.6	deconstruction
196.55	0.32	6	deconstruction
196.55	0.32	6	deconstruction
196.55	0.32	6	deconstruction
196.55	0.32	6	deconstruction
196.55	0.36	10.2	deconstruction
196.55	0.36	10.2	deconstruction
196.55	0.36	10.2	deconstruction
196.55	0.36	10.2	deconstruction
143.89	0.4	10.2	deconstruction
143.89	0.4	10.2	deconstruction
143.89	0.4	10.2	deconstruction
143.89	0.4	10.2	deconstruction
143.89	0.4	10.2	deconstruction
143.89	0.3	14	deconstruction
143.89	0.3	14	deconstruction
85.52	0.3	6	deconstruction
85.52	0.3	6	deconstruction
85.52	0.25	7.6	deconstruction
85.52	0.25	7.6	deconstruction
85.52	0.3	14	deconstruction
85.52	0.3	14	deconstruction
85.52	0.3	14	deconstruction
85.52	0.3	14	deconstruction
155.67	0.3	14	deconstruction
155.67	0.6	8.9	deconstruction
155.67	0.6	8.9	deconstruction
155.67	0.6	8.9	deconstruction

218.39	0.9	4.8	deconstruction
218.39	0.9	4.8	deconstruction
218.39	0.9	4.8	deconstruction
218.39	0.9	4.8	deconstruction
218.39	0.6	8.9	deconstruction
218.39	0.6	10.2	deconstruction
218.39	0.6	10.2	deconstruction
218.39	0.6	10.2	deconstruction
140.19	0.6	10.2	deconstruction
140.19	0.76	8.9	deconstruction
140.19	0.76	8.9	deconstruction
140.19	0.76	8.9	deconstruction
205.92	0.76	8.9	deconstruction
205.92	0.76	8.9	deconstruction
149.02	0.25	3.4	deconstruction
149.02	0.25	3.4	deconstruction
149.02	0.25	3.4	new_production
149.02	0.25	3.4	new_production
205.92	0.32	4.8	new_production
149.02	0.25	3.4	new_production
205.92	0.32	4.8	new_production
149.02	0.25	3.4	new_production
205.92	0.32	4.8	new_production
149.02	0.25	3.4	new_production
205.92	0.32	4.8	new_production
149.02	0.25	3.4	new_production
205.92	0.32	4.8	new_production
205.92	0.32	4.8	new_production
113.95	0.6	8.9	deconstruction
142.66	1.75	8.9	deconstruction
113.95	1.75	8.9	deconstruction
113.95	1.75	8.9	deconstruction
142.66	1.75	8.9	deconstruction
113.95	1.75	8.9	deconstruction
113.95	1.75	8.9	deconstruction
142.66	0.36	10.2	new_production
113.95	0.3	14	new_production
142.66	0.36	10.2	new_production
113.95	0.3	14	new_production
113.95	0.3	14	new_production
151.22	0.36	10.2	new_production
151.22	0.36	10.2	new_production
248.78	0.32	4.8	new_production
248.78	0.32	4.8	new_production
151.22	0.36	10.2	new_production
151.22	0.36	10.2	new_production
248.78	0.32	4.8	new_production

248.78	0.32	4.8	new_production
151.22	0.36	10.2	new_production
248.78	0.32	4.8	new_production
248.78	0.32	4.8	new_production
151.22	0.36	10.2	new_production
248.78	0.32	4.8	new_production
151.22	0.36	10.2	new_production
248.78	0.32	4.8	new_production
151.22	0.36	10.2	new_production

8.12.3 Large stock, optimized gridshell

length [cm]	thickness [cm]	diameter [cm]	scenario
131.03	0.25	3.4	deconstruction
131.03	0.25	3.4	deconstruction
131.03	0.25	3.4	deconstruction
131.03	0.25	3.4	deconstruction
133.75	0.32	4.8	deconstruction
133.75	0.32	4.8	deconstruction
133.75	0.32	4.8	deconstruction
133.75	0.32	4.8	deconstruction
101.03	0.25	4.8	deconstruction
101.03	0.25	4.8	deconstruction
101.03	0.25	4.8	deconstruction
101.03	0.25	4.8	deconstruction
101.03	0.25	4.8	deconstruction
101.03	0.25	4.8	deconstruction
101.03	0.25	4.8	deconstruction
101.03	0.25	4.8	deconstruction
101.03	0.25	4.8	deconstruction
143.71	0.32	4.8	deconstruction
143.71	0.32	4.8	deconstruction
143.71	0.32	4.8	deconstruction
143.71	0.32	4.8	deconstruction
144.45	0.25	4.8	deconstruction
144.45	0.25	4.8	deconstruction
144.45	0.25	4.8	deconstruction
144.45	0.32	4.8	deconstruction
181.55	0.29	6	deconstruction
181.55	0.29	6	deconstruction
181.55	0.29	6	deconstruction
181.55	0.29	6	deconstruction
181.55	0.29	6	deconstruction
181.55	0.3	6	deconstruction
181.55	0.3	6	deconstruction
196.55	0.3	6	deconstruction
196.55	0.3	6	deconstruction

196.55	0.3	6	deconstruction
196.55	0.3	6	deconstruction
196.55	0.25	7.6	deconstruction
196.55	0.25	7.6	deconstruction
196.55	0.25	7.6	deconstruction
196.55	0.25	7.6	deconstruction
143.89	0.25	7.6	deconstruction
143.89	0.25	7.6	deconstruction
143.89	0.25	7.6	deconstruction
143.89	0.32	6	deconstruction
143.89	0.32	6	deconstruction
143.89	0.32	6	deconstruction
143.89	0.32	6	deconstruction
143.89	0.32	6	deconstruction
85.52	0.29	6	deconstruction
85.52	0.29	6	deconstruction
85.52	0.29	6	deconstruction
85.52	0.3	6	deconstruction
85.52	0.32	6	deconstruction
85.52	0.32	6	deconstruction
85.52	0.32	6	deconstruction
85.52	0.32	6	deconstruction
155.67	0.36	10.2	deconstruction
155.67	0.36	10.2	deconstruction
155.67	0.36	10.2	deconstruction
155.67	0.36	10.2	deconstruction
218.39	0.36	10.2	deconstruction
218.39	0.36	10.2	deconstruction
218.39	0.4	10.2	deconstruction
218.39	0.4	10.2	deconstruction
218.39	0.4	10.2	deconstruction
218.39	0.4	10.2	deconstruction
218.39	0.4	10.2	deconstruction
218.39	0.4	10.2	deconstruction
140.19	0.32	6	deconstruction
140.19	0.3	14	deconstruction
140.19	0.3	14	deconstruction
140.19	0.3	14	deconstruction
205.92	0.3	14	deconstruction
205.92	0.3	14	deconstruction
149.02	0.25	3.4	deconstruction
149.02	0.25	3.4	deconstruction
149.02	0.25	3.4	deconstruction
149.02	0.25	3.4	deconstruction
205.92	0.3	14	deconstruction
149.02	0.25	3.4	deconstruction
205.92	0.3	14	deconstruction

149.02	0.25	3.4	new_production
205.92	0.9	4.8	deconstruction
149.02	0.25	3.4	new_production
205.92	0.9	4.8	deconstruction
149.02	0.25	3.4	new_production
205.92	0.9	4.8	deconstruction
205.92	0.9	4.8	deconstruction
113.95	0.6	8.9	deconstruction
142.66	0.9	4.8	deconstruction
113.95	0.6	8.9	deconstruction
113.95	0.6	8.9	deconstruction
142.66	0.9	4.8	deconstruction
113.95	0.6	8.9	deconstruction
113.95	0.6	8.9	deconstruction
142.66	0.9	4.8	deconstruction
113.95	0.6	8.9	deconstruction
142.66	0.6	8.9	deconstruction
113.95	0.6	8.9	deconstruction
113.95	0.6	8.9	deconstruction
151.22	0.6	10.2	deconstruction
151.22	0.6	10.2	deconstruction
248.78	0.6	10.2	deconstruction
248.78	0.6	10.2	deconstruction
151.22	0.6	10.2	deconstruction
151.22	0.6	10.2	deconstruction
248.78	0.76	8.9	deconstruction
248.78	0.76	8.9	deconstruction
151.22	0.76	8.9	deconstruction
248.78	0.76	8.9	deconstruction
248.78	0.32	4.8	new_production
151.22	0.76	8.9	deconstruction
248.78	0.32	4.8	new_production
151.22	0.76	8.9	deconstruction
248.78	0.32	4.8	new_production
151.22	1.75	8.9	deconstruction

8.12.4 Small stock, standard gridshell

length [cm]	thickness [cm]	diameter [cm]	scenario
161.62	0.32	4.8	deconstruction
114.29	0.25	4.8	deconstruction
114.29	0.25	4.8	deconstruction
114.29	0.25	4.8	deconstruction
114.29	0.32	4.8	deconstruction
162.41	0.32	4.8	deconstruction
115.4	0.29	6	deconstruction
115.4	0.29	6	deconstruction

115.4	0.29	6	deconstruction
115.4	0.3	6	deconstruction
115.4	0.3	6	deconstruction
115.4	0.3	6	deconstruction
115.4	0.25	7.6	deconstruction
162.41	0.25	7.6	deconstruction
162.41	0.25	7.6	deconstruction
162.41	0.32	6	deconstruction
115.4	0.32	6	deconstruction
164.26	0.32	6	deconstruction
164.26	0.36	10.2	deconstruction
114.29	0.36	10.2	deconstruction
161.62	0.36	10.2	deconstruction
161.62	0.4	10.2	deconstruction
114.29	0.4	10.2	deconstruction
114.29	0.4	10.2	deconstruction
114.29	0.3	14	deconstruction
115.06	0.3	14	deconstruction
115.06	0.3	14	deconstruction
115.06	0.9	4.8	deconstruction
115.06	0.9	4.8	deconstruction
115.06	0.9	4.8	deconstruction
115.06	0.6	8.9	deconstruction
115.06	0.6	8.9	deconstruction
115.06	0.6	8.9	deconstruction
164.76	0.6	10.2	deconstruction
118.68	0.6	10.2	deconstruction
118.68	0.6	10.2	deconstruction
164.76	0.76	8.9	deconstruction
118.68	0.76	8.9	deconstruction
164.76	0.76	8.9	deconstruction
118.68	1.75	8.9	deconstruction
164.76	0.32	4.8	new_production
118.68	1.75	8.9	deconstruction
118.68	1.75	8.9	deconstruction
118.68	0.36	10.2	new_production
118.68	0.36	10.2	new_production
166.5	0.36	10.2	new_production
166.5	0.25	7.6	new_production
166.5	0.25	7.6	new_production
166.5	0.25	7.6	new_production
162.7	0.32	4.8	new_production
162.7	0.32	4.8	new_production
162.7	0.32	4.8	new_production
162.7	0.32	4.8	new_production
117.35	0.36	10.2	new_production
117.35	0.36	10.2	new_production

117.35	0.36	10.2	new_production
117.35	0.36	10.2	new_production
117.35	0.36	10.2	new_production
117.35	0.36	10.2	new_production
117.35	0.36	10.2	new_production
117.35	0.36	10.2	new_production
114.29	0.32	4.8	new_production
114.29	0.32	4.8	new_production
114.29	0.32	4.8	new_production
114.29	0.32	4.8	new_production
167.16	0.36	10.2	new_production
167.16	0.36	10.2	new_production
114.57	0.25	7.6	new_production
114.57	0.32	4.8	new_production
114.57	0.32	4.8	new_production
114.57	0.25	4.8	new_production
114.57	0.32	4.8	new_production
114.57	0.32	4.8	new_production
114.57	0.32	4.8	new_production
114.57	0.32	4.8	new_production
114.57	0.32	4.8	new_production
161.62	0.25	7.6	new_production
161.62	0.25	7.6	new_production
115.4	0.36	10.2	new_production
115.4	0.36	10.2	new_production
115.4	0.36	10.2	new_production
115.4	0.36	10.2	new_production
115.4	0.36	10.2	new_production
115.4	0.36	10.2	new_production
115.4	0.36	10.2	new_production
115.4	0.36	10.2	new_production
123.95	0.36	10.2	new_production
168.6	0.32	4.8	new_production
123.95	0.36	10.2	new_production
168.6	0.25	7.6	new_production
168.6	0.32	4.8	new_production
123.95	0.36	10.2	new_production
123.95	0.36	10.2	new_production
123.95	0.36	10.2	new_production
168.6	0.32	4.8	new_production
168.6	0.32	4.8	new_production
123.95	0.36	10.2	new_production
168.6	0.32	4.8	new_production
168.6	0.32	4.8	new_production
123.95	0.36	10.2	new_production
123.95	0.36	10.2	new_production
168.6	0.32	4.8	new_production
166.5	0.25	7.6	new_production

121.08	0.36	10.2	new_production
121.08	0.36	10.2	new_production
166.5	0.32	4.8	new_production
121.08	0.36	10.2	new_production
121.08	0.36	10.2	new_production
166.5	0.36	10.2	new_production
121.08	0.36	10.2	new_production
166.5	0.36	10.2	new_production
166.5	0.25	7.6	new_production
121.08	0.36	10.2	new_production
121.08	0.36	10.2	new_production
121.08	0.36	10.2	new_production
166.5	0.36	10.2	new_production
166.5	0.25	7.6	new_production
166.5	0.36	10.2	new_production
163.4	0.36	10.2	new_production
163.4	0.36	10.2	new_production
116.78	0.3	14	new_production
116.78	0.3	14	new_production
163.4	0.36	10.2	new_production
163.4	0.36	10.2	new_production
163.4	0.36	10.2	new_production
116.78	0.36	10.2	new_production
116.78	0.36	10.2	new_production
116.78	0.3	14	new_production
116.78	0.3	14	new_production
163.4	0.36	10.2	new_production
116.78	0.36	10.2	new_production
116.78	0.36	10.2	new_production
114.29	0.32	4.8	new_production
114.29	0.36	10.2	new_production
114.29	0.32	4.8	new_production
114.29	0.32	4.8	new_production
114.29	0.36	10.2	new_production
114.29	0.32	4.8	new_production
114.29	0.36	10.2	new_production
114.29	0.32	4.8	new_production
114.29	0.32	4.8	new_production
114.29	0.32	4.8	new_production
114.29	0.32	4.8	new_production
114.29	0.32	4.8	new_production
114.29	0.32	4.8	new_production
114.29	0.32	4.8	new_production
114.29	0.25	4.8	new_production
114.29	0.32	4.8	new_production
114.29	0.32	4.8	new_production
114.29	0.25	4.8	new_production
114.29	0.25	7.6	new_production
114.29	0.32	4.8	new_production

114.29	0.25	4.8	new_production
114.29	0.32	4.8	new_production
114.29	0.36	10.2	new_production
114.29	0.36	10.2	new_production
114.29	0.36	10.2	new_production
114.29	0.36	10.2	new_production
114.29	0.36	10.2	new_production
114.29	0.36	10.2	new_production
114.29	0.36	10.2	new_production
114.29	0.36	10.2	new_production
161.62	0.36	10.2	new_production
161.62	0.36	10.2	new_production

8.12.5 Medium stock, standard gridshell

length [cm]	thickness [cm]	diameter [cm]	scenario
161.62	0.32	4.8	deconstruction
114.29	0.25	4.8	deconstruction
114.29	0.25	4.8	deconstruction
114.29	0.25	4.8	deconstruction
114.29	0.25	4.8	deconstruction
162.41	0.32	4.8	deconstruction
115.4	0.25	4.8	deconstruction
115.4	0.25	4.8	deconstruction
115.4	0.32	4.8	deconstruction
115.4	0.32	4.8	deconstruction
115.4	0.32	4.8	deconstruction
115.4	0.32	4.8	deconstruction
115.4	0.29	6	deconstruction
162.41	0.29	6	deconstruction
162.41	0.29	6	deconstruction
162.41	0.29	6	deconstruction
115.4	0.29	6	deconstruction
164.26	0.29	6	deconstruction
164.26	0.3	6	deconstruction
114.29	0.3	6	deconstruction
161.62	0.3	6	deconstruction
161.62	0.3	6	deconstruction
114.29	0.3	6	deconstruction
114.29	0.3	6	deconstruction
114.29	0.25	7.6	deconstruction
115.06	0.25	7.6	deconstruction
115.06	0.25	7.6	deconstruction
115.06	0.25	7.6	deconstruction
115.06	0.25	7.6	deconstruction
115.06	0.25	7.6	deconstruction
115.06	0.32	6	deconstruction

115.06	0.32	6	deconstruction
115.06	0.32	6	deconstruction
164.76	0.32	6	deconstruction
118.68	0.36	10.2	deconstruction
118.68	0.36	10.2	deconstruction
164.76	0.32	6	deconstruction
118.68	0.36	10.2	deconstruction
164.76	0.36	10.2	deconstruction
118.68	0.36	10.2	deconstruction
164.76	0.36	10.2	deconstruction
118.68	0.4	10.2	deconstruction
118.68	0.4	10.2	deconstruction
118.68	0.4	10.2	deconstruction
118.68	0.4	10.2	deconstruction
166.5	0.4	10.2	deconstruction
166.5	0.3	14	deconstruction
166.5	0.3	14	deconstruction
166.5	0.3	14	deconstruction
162.7	0.4	10.2	deconstruction
162.7	0.3	14	deconstruction
162.7	0.9	4.8	deconstruction
162.7	0.9	4.8	deconstruction
117.35	0.3	14	deconstruction
117.35	0.6	8.9	deconstruction
117.35	0.6	8.9	deconstruction
117.35	0.6	8.9	deconstruction
117.35	0.6	8.9	deconstruction
117.35	0.6	8.9	deconstruction
117.35	0.6	8.9	deconstruction
117.35	0.6	10.2	deconstruction
114.29	0.32	6	deconstruction
114.29	0.3	14	deconstruction
114.29	0.9	4.8	deconstruction
114.29	0.9	4.8	deconstruction
167.16	0.9	4.8	deconstruction
167.16	0.9	4.8	deconstruction
114.57	0.6	10.2	deconstruction
114.57	0.6	10.2	deconstruction
114.57	0.6	10.2	deconstruction
114.57	0.25	4.8	new_production
114.57	0.6	10.2	deconstruction
114.57	0.6	10.2	deconstruction
114.57	0.76	8.9	deconstruction
114.57	0.76	8.9	deconstruction
161.62	0.76	8.9	deconstruction
161.62	0.76	8.9	deconstruction
115.4	0.76	8.9	deconstruction

115.4	0.76	8.9	deconstruction
115.4	1.75	8.9	deconstruction
115.4	1.75	8.9	deconstruction
115.4	1.75	8.9	deconstruction
115.4	1.75	8.9	deconstruction
115.4	1.75	8.9	deconstruction
115.4	1.75	8.9	deconstruction
123.95	0.36	10.2	new_production
168.6	0.32	4.8	new_production
123.95	0.36	10.2	new_production
168.6	0.25	7.6	new_production
168.6	0.32	4.8	new_production
123.95	0.36	10.2	new_production
123.95	0.36	10.2	new_production
123.95	0.36	10.2	new_production
168.6	0.32	4.8	new_production
168.6	0.32	4.8	new_production
123.95	0.36	10.2	new_production
168.6	0.32	4.8	new_production
168.6	0.32	4.8	new_production
123.95	0.36	10.2	new_production
123.95	0.36	10.2	new_production
168.6	0.32	4.8	new_production
166.5	0.25	7.6	new_production
121.08	0.36	10.2	new_production
121.08	0.36	10.2	new_production
166.5	0.32	4.8	new_production
121.08	0.36	10.2	new_production
121.08	0.36	10.2	new_production
166.5	0.36	10.2	new_production
121.08	0.36	10.2	new_production
166.5	0.36	10.2	new_production
166.5	0.25	7.6	new_production
121.08	0.36	10.2	new_production
121.08	0.36	10.2	new_production
121.08	0.36	10.2	new_production
166.5	0.36	10.2	new_production
166.5	0.25	7.6	new_production
166.5	0.36	10.2	new_production
163.4	0.36	10.2	new_production
163.4	0.36	10.2	new_production
116.78	0.3	14	new_production
116.78	0.3	14	new_production
163.4	0.36	10.2	new_production
163.4	0.36	10.2	new_production
163.4	0.36	10.2	new_production
116.78	0.36	10.2	new_production

116.78	0.36	10.2	new_production
116.78	0.3	14	new_production
116.78	0.3	14	new_production
163.4	0.36	10.2	new_production
116.78	0.36	10.2	new_production
116.78	0.36	10.2	new_production
114.29	0.32	4.8	new_production
114.29	0.36	10.2	new_production
114.29	0.32	4.8	new_production
114.29	0.32	4.8	new_production
114.29	0.36	10.2	new_production
114.29	0.32	4.8	new_production
114.29	0.36	10.2	new_production
114.29	0.32	4.8	new_production
114.29	0.32	4.8	new_production
114.29	0.32	4.8	new_production
114.29	0.32	4.8	new_production
114.29	0.32	4.8	new_production
114.29	0.32	4.8	new_production
114.29	0.25	4.8	new_production
114.29	0.32	4.8	new_production
114.29	0.32	4.8	new_production
114.29	0.25	4.8	new_production
114.29	0.25	7.6	new_production
114.29	0.32	4.8	new_production
114.29	0.25	4.8	new_production
114.29	0.32	4.8	new_production
114.29	0.36	10.2	new_production
114.29	0.36	10.2	new_production
114.29	0.36	10.2	new_production
114.29	0.36	10.2	new_production
114.29	0.36	10.2	new_production
114.29	0.36	10.2	new_production
114.29	0.36	10.2	new_production
161.62	0.36	10.2	new_production
161.62	0.36	10.2	new_production

8.12.6 Large stock, standard gridshell

length [cm]	thickness [cm]	diameter [cm]	scenario
161.62	0.32	4.8	deconstruction
114.29	0.25	4.8	deconstruction
114.29	0.25	4.8	deconstruction
114.29	0.25	4.8	deconstruction
114.29	0.25	4.8	deconstruction
162.41	0.32	4.8	deconstruction
115.4	0.25	4.8	deconstruction

115.4	0.25	4.8	deconstruction
115.4	0.25	4.8	deconstruction
115.4	0.25	4.8	deconstruction
115.4	0.32	4.8	deconstruction
115.4	0.25	4.8	deconstruction
115.4	0.32	4.8	deconstruction
162.41	0.32	4.8	deconstruction
162.41	0.32	4.8	deconstruction
162.41	0.32	4.8	deconstruction
115.4	0.32	4.8	deconstruction
164.26	0.32	4.8	deconstruction
164.26	0.29	6	deconstruction
114.29	0.29	6	deconstruction
161.62	0.29	6	deconstruction
161.62	0.29	6	deconstruction
114.29	0.29	6	deconstruction
114.29	0.29	6	deconstruction
114.29	0.29	6	deconstruction
114.29	0.29	6	deconstruction
115.06	0.29	6	deconstruction
115.06	0.29	6	deconstruction
115.06	0.3	6	deconstruction
115.06	0.3	6	deconstruction
115.06	0.3	6	deconstruction
115.06	0.3	6	deconstruction
115.06	0.3	6	deconstruction
115.06	0.3	6	deconstruction
164.76	0.3	6	deconstruction
118.68	0.36	10.2	deconstruction
118.68	0.36	10.2	deconstruction
164.76	0.3	6	deconstruction
118.68	0.36	10.2	deconstruction
164.76	0.25	7.6	deconstruction
118.68	0.36	10.2	deconstruction
164.76	0.25	7.6	deconstruction
118.68	0.36	10.2	deconstruction
118.68	0.36	10.2	deconstruction
118.68	0.36	10.2	deconstruction
118.68	0.36	10.2	deconstruction
118.68	0.36	10.2	deconstruction
166.5	0.36	10.2	deconstruction
166.5	0.25	7.6	deconstruction
166.5	0.25	7.6	deconstruction
166.5	0.25	7.6	deconstruction
162.7	0.25	7.6	deconstruction
162.7	0.32	6	deconstruction
162.7	0.32	6	deconstruction
162.7	0.32	6	deconstruction
117.35	0.4	10.2	deconstruction

117.35	0.4	10.2	deconstruction
117.35	0.4	10.2	deconstruction
117.35	0.4	10.2	deconstruction
117.35	0.4	10.2	deconstruction
117.35	0.4	10.2	deconstruction
117.35	0.4	10.2	deconstruction
117.35	0.4	10.2	deconstruction
114.29	0.3	6	deconstruction
114.29	0.25	7.6	deconstruction
114.29	0.25	7.6	deconstruction
114.29	0.25	7.6	deconstruction
167.16	0.4	10.2	deconstruction
167.16	0.3	14	deconstruction
114.57	0.3	14	deconstruction
114.57	0.32	6	deconstruction
114.57	0.32	6	deconstruction
114.57	0.32	6	deconstruction
114.57	0.32	6	deconstruction
114.57	0.32	6	deconstruction
114.57	0.32	6	deconstruction
114.57	0.3	14	deconstruction
161.62	0.3	14	deconstruction
161.62	0.3	14	deconstruction
115.4	0.3	14	deconstruction
115.4	0.3	14	deconstruction
115.4	0.3	14	deconstruction
115.4	0.3	14	deconstruction
115.4	0.6	8.9	deconstruction
115.4	0.6	8.9	deconstruction
115.4	0.6	8.9	deconstruction
115.4	0.6	8.9	deconstruction
123.95	0.9	4.8	deconstruction
168.6	0.9	4.8	deconstruction
123.95	0.9	4.8	deconstruction
168.6	0.9	4.8	deconstruction
168.6	0.9	4.8	deconstruction
123.95	0.9	4.8	deconstruction
123.95	0.9	4.8	deconstruction
123.95	0.9	4.8	deconstruction
168.6	0.6	8.9	deconstruction
168.6	0.6	8.9	deconstruction
123.95	0.6	8.9	deconstruction
168.6	0.6	8.9	deconstruction
168.6	0.6	10.2	deconstruction
123.95	0.6	10.2	deconstruction
123.95	0.6	10.2	deconstruction
168.6	0.6	10.2	deconstruction

166.5	0.6	10.2	deconstruction
121.08	0.6	10.2	deconstruction
121.08	0.6	10.2	deconstruction
166.5	0.6	10.2	deconstruction
121.08	0.76	8.9	deconstruction
121.08	0.76	8.9	deconstruction
166.5	0.76	8.9	deconstruction
121.08	0.76	8.9	deconstruction
166.5	0.76	8.9	deconstruction
166.5	0.76	8.9	deconstruction
121.08	0.76	8.9	deconstruction
121.08	0.76	8.9	deconstruction
121.08	0.76	8.9	deconstruction
166.5	1.75	8.9	deconstruction
166.5	0.25	7.6	new_production
166.5	1.75	8.9	deconstruction
163.4	1.75	8.9	deconstruction
163.4	1.75	8.9	deconstruction
116.78	1.75	8.9	deconstruction
116.78	1.75	8.9	deconstruction
163.4	1.75	8.9	deconstruction
163.4	1.75	8.9	deconstruction
163.4	0.36	10.2	new_production
116.78	1.75	8.9	deconstruction
116.78	0.36	10.2	new_production
116.78	0.3	14	new_production
116.78	0.3	14	new_production
163.4	0.36	10.2	new_production
116.78	0.36	10.2	new_production
116.78	0.36	10.2	new_production
114.29	0.6	10.2	deconstruction
114.29	0.36	10.2	new_production
114.29	0.32	4.8	new_production
114.29	0.32	4.8	new_production
114.29	0.36	10.2	new_production
114.29	0.32	4.8	new_production
114.29	0.36	10.2	new_production
114.29	0.32	4.8	new_production
114.29	0.32	4.8	new_production
114.29	0.32	4.8	new_production
114.29	0.32	4.8	new_production
114.29	0.32	4.8	new_production
114.29	0.32	4.8	new_production
114.29	0.32	4.8	new_production
114.29	0.25	4.8	new_production
114.29	0.32	4.8	new_production
114.29	0.32	4.8	new_production
114.29	0.25	4.8	new_production
114.29	0.25	7.6	new_production

114.29	0.32	4.8	new_production
114.29	0.25	4.8	new_production
114.29	0.32	4.8	new_production
114.29	0.36	10.2	new_production
114.29	0.36	10.2	new_production
114.29	0.36	10.2	new_production
114.29	0.36	10.2	new_production
114.29	0.36	10.2	new_production
114.29	0.36	10.2	new_production
114.29	0.36	10.2	new_production
114.29	0.36	10.2	new_production
114.29	0.36	10.2	new_production
161.62	0.36	10.2	new_production
161.62	0.36	10.2	new_production

8.12.7 Hybrid (medium) stock, optimized gridshell (case-study)

length [cm]	thickness [cm]	diameter [cm]	scenario
131.03	0.25	3.4	stockpile
131.03	0.25	3.4	stockpile
131.03	0.25	3.4	stockpile
131.03	0.25	4.8	stockpile
133.75	0.32	4.8	stockpile
133.75	0.32	4.8	stockpile
133.75	0.32	4.8	stockpile
133.75	0.29	6	stockpile
101.03	0.25	4.8	stockpile
101.03	0.25	4.8	stockpile
101.03	0.25	4.8	stockpile
101.03	0.29	6	stockpile
101.03	0.29	6	stockpile
101.03	0.29	6	stockpile
101.03	0.3	6	stockpile
101.03	0.3	6	stockpile
143.71	0.3	6	stockpile
143.71	0.25	7.6	stockpile
143.71	0.25	7.6	stockpile
143.71	0.25	7.6	stockpile
144.45	0.32	6	stockpile
144.45	0.32	6	stockpile
144.45	0.32	6	stockpile
144.45	0.36	10.2	stockpile
181.55	0.36	10.2	stockpile
181.55	0.4	10.2	stockpile
181.55	0.4	10.2	stockpile
181.55	0.25	4.8	deconstruction
181.55	0.25	4.8	deconstruction
181.55	0.3	14	stockpile

181.55	0.3	14	stockpile
181.55	0.9	4.8	stockpile
196.55	0.9	4.8	stockpile
196.55	0.32	4.8	deconstruction
196.55	0.32	4.8	deconstruction
196.55	0.6	8.9	stockpile
196.55	0.6	8.9	stockpile
196.55	0.29	6	deconstruction
196.55	0.29	6	deconstruction
196.55	0.6	10.2	stockpile
143.89	0.6	10.2	stockpile
143.89	0.3	6	deconstruction
143.89	0.3	6	deconstruction
143.89	0.3	6	deconstruction
143.89	0.25	7.6	deconstruction
143.89	0.25	7.6	deconstruction
143.89	0.25	7.6	deconstruction
143.89	0.32	6	deconstruction
85.52	0.3	6	stockpile
85.52	0.36	10.2	stockpile
85.52	0.4	10.2	stockpile
85.52	0.3	14	stockpile
85.52	0.6	10.2	stockpile
85.52	0.32	6	deconstruction
85.52	0.32	6	deconstruction
85.52	0.32	6	deconstruction
155.67	0.76	8.9	stockpile
155.67	0.76	8.9	stockpile
155.67	0.36	10.2	deconstruction
155.67	0.36	10.2	deconstruction
218.39	0.4	10.2	deconstruction
218.39	0.4	10.2	deconstruction
218.39	0.3	14	deconstruction
218.39	0.3	14	deconstruction
218.39	0.9	4.8	deconstruction
218.39	0.9	4.8	deconstruction
218.39	1.75	8.9	stockpile
218.39	1.75	8.9	stockpile
140.19	0.6	8.9	deconstruction
140.19	0.6	8.9	deconstruction
140.19	0.6	8.9	deconstruction
140.19	0.95	21.9	stockpile
205.92	0.95	21.9	stockpile
205.92	0.6	10.2	deconstruction
149.02	0.25	3.4	deconstruction
149.02	0.25	3.4	deconstruction
149.02	0.25	3.4	deconstruction

149.02	0.25	3.4	new_production
205.92	0.6	10.2	deconstruction
149.02	0.25	3.4	new_production
205.92	1.27	16.8	stockpile
149.02	0.25	3.4	new_production
205.92	1.27	16.8	stockpile
149.02	0.25	3.4	new_production
205.92	1	21.9	stockpile
149.02	0.25	3.4	new_production
205.92	1	21.9	stockpile
205.92	1	21.9	stockpile
113.95	0.76	8.9	stockpile
142.66	1	21.9	stockpile
113.95	1.9	11.8	stockpile
113.95	1.9	11.8	stockpile
142.66	1.9	11.8	stockpile
113.95	1.27	17.8	stockpile
113.95	1.27	17.8	stockpile
142.66	1.27	17.8	stockpile
113.95	0.76	8.9	deconstruction
142.66	0.76	8.9	deconstruction
113.95	0.76	8.9	deconstruction
113.95	2.22	11.4	stockpile
151.22	2.22	11.4	stockpile
151.22	2.22	11.4	stockpile
248.78	0.32	4.8	new_production
248.78	0.32	4.8	new_production
151.22	1.43	21.9	stockpile
151.22	1.43	21.9	stockpile
248.78	0.32	4.8	new_production
248.78	0.32	4.8	new_production
151.22	1.75	8.9	deconstruction
248.78	0.32	4.8	new_production
248.78	0.32	4.8	new_production
151.22	1.75	8.9	deconstruction
248.78	0.32	4.8	new_production
151.22	0.36	10.2	new_production
248.78	0.32	4.8	new_production
151.22	0.36	10.2	new_production

8.12.8 Benchmark Phoenix3D, optimized truss, Best-Fit formulation

length [cm]	thickness [cm]	diameter [cm]	scenario
400.00	0.95	21.9	deconstruction
400.00	1	21.9	deconstruction
400.00	1	21.9	deconstruction
400.00	1.27	16.8	deconstruction

400.00	1.9	11.8	deconstruction
300.00	0.6	8.9	deconstruction
300.00	0.36	10.2	deconstruction
400.00	0.76	8.9	deconstruction
300.00	0.25	4.8	deconstruction
400.00	0.25	3.4	deconstruction
400.00	0.32	4.8	deconstruction
500.00	0.95	21.9	new_production
500.00	0.95	21.9	new_production
300.00	0.36	10.2	new_production
500.00	0.25	4.8	new_production
500.00	0.25	4.8	new_production
300.00	0.25	3.4	new_production

8.12.9 Benchmark Phoenix3D, optimized truss, Best-Fit + Node shift

length [cm]	thickness [cm]	diameter [cm]	scenario
370.50	0.25	3.4	deconstruction
301.50	0.25	4.8	deconstruction
370.00	0.32	4.8	deconstruction
422.00	0.6	8.9	deconstruction
406.10	0.36	10.2	deconstruction
450.00	0.76	8.9	deconstruction
412.90	1.75	8.9	deconstruction
344.80	0.4	10.2	deconstruction
301.50	0.6	10.2	deconstruction
441.00	1.27	16.8	deconstruction
360.60	0.95	21.9	deconstruction
564.00	0.25	3.4	new_production
566.00	0.25	4.8	new_production
404.50	0.6	8.9	new_production
211.90	0.6	8.9	new_production
260.00	0.6	8.9	new_production
523.50	0.95	21.9	new_production